Nonlinear Dynamics (2026) 114:1012
https://doi.org/10.1007/s11071-026-12814-z

RESEARCH

Computing parameter-dependent invariant manifolds for data-free nonlinear model reduction

Shobhit Jain[1] · **Mingwu Li**[2]

Received: 3 April 2026 / Revised: 29 June 2026 / Accepted: 29 June 2026

Abstract

Invariant manifolds provide a solid foundation for rigorous model reduction and analysis of complex dynamical behavior in high-dimensional nonlinear systems. Their existence and smooth parameter dependence are well established theoretically; yet the practical computation of parameter-dependent invariant manifolds remains challenging, particularly for systems with nontrivial equilibria, large state dimension, or limited access to governing equations. In this work, we develop efficient computational expressions for invariant manifolds and their reduced dynamics that depend smoothly on system parameters, without shifting coordinates or introducing parameters as auxiliary variables. This approach enables formal Taylor and Taylor–Fourier expansions of parameter-dependent equilibria, invariant manifolds, and reduced-order models directly from the governing equations. We show how our expressions can be implemented nonintrusively for systems with affine parameter dependence and up to cubic nonlinearities. We demonstrate the effectiveness of the method on a range of high-fidelity numerical models, where the resulting parameter-dependent reduced-order models enable the analysis of local bifurcations, including buckling, flutter, period-doubling, and internal and parametric resonances, at computational costs far below those of the full system. The framework provides a practical bridge between rigorous invariant manifold theory and large-scale engineering applications, with particular relevance to design and optimization.

Keywords Invariant Manifolds · Spectral Submanifolds · Nonlinear Model Reduction · Reduced-order modelling · Finite element · Parametric Computations

1 Introduction

Invariant manifolds are hypersurfaces in the phase space of a dynamical system that are composed of trajectories of the full system. Their computation has attracted sustained interest due to their central role in rigorous nonlinear model reduction, stability analysis, and bifurcation theory. In particular, modern developments in invariant manifold theory and computation have enabled the systematic construction of invariant manifolds and their reduced dynamics directly from high-dimensional governing equations [1–4]. These advances have facilitated physically meaningful reduced-order models (ROMs) that faithfully capture nonlinear behavior beyond the reach of linearization.

High-fidelity models of physical systems typically depend on geometric, material, and operating parameters. Understanding how invariant manifolds and their associated reduced dynamics vary with respect to such parameters is therefore essential for design, optimization [5–7], and sensitivity analysis [8, 9]. Despite the strong theoretical foundations guaranteeing the existence and smooth parameter dependence of invariant manifolds, practical computational procedures for parameter-dependent manifold calculations remain challenging, especially for large-scale or black-box models. In this work, we focus on alleviating these computational challenges for high-dimensional systems with parametric dependence.

In engineering applications, local approximations of invariant manifolds are often useful for assessing the influence of nonlinearities on a linearized operating point. An advantage of employing such local computations is that they simplify the nonlinear manifold computation into a recursive

✉ Shobhit Jain
shobhit.jain@tudelft.nl

✉ Mingwu Li

[1] Delft Institute of Applied Mathematics, TU Delft, Mekelweg 4, 2628 CD Delft, The Netherlands

[2] Department of Mechanics and Aerospace Engineering, Southern University of Science and Technology, Shenzhen 518055, China

Published online: 06 August 2026

solution of *linear* equations of the same size and sparsity pattern as the full system (see [2] for a discussion on global vs. local techniques). Local computational procedures for approximating invariant manifolds around a fixed point commonly assume that the equilibrium is located at the origin of the phase space [2, 3, 10, 11]. This assumption is mathematically without loss of generality since coordinates may always be shifted to place the equilibrium at the origin. Such a coordinate shift, however, modifies the structure of the nonlinear terms. Explicit knowledge of these transformed nonlinearities is typically required for manifold computations; e.g., see Ref. [1], where the nonlinearity was explicitly transformed before performing center manifold reduction around a nontrivial bifurcating flow. In practice, performing such transformations can be prohibitively difficult or impossible, depending on the modeling framework used, particularly when governing equations are not explicitly available.

A classical approach for computing invariant manifolds that depend on parameters is based on center manifold theory, wherein parameters $\boldsymbol{\mu} \in \mathbb{R}^m$ are treated as auxiliary variables with trivial dynamics $\dot{\boldsymbol{\mu}} = \mathbf{0}$ (see, e.g., [12]). This reformulation embeds the original system into an extended autonomous system, increasing the dimension of the center subspace, and hence of the center manifold, by m. The resulting center manifold can be interpreted as a parameter-dependent extension of the original center manifold. This dummy-variable approach has also been employed for other types of invariant manifolds for which parameter regularity can be rigorously established, including stable and unstable manifolds [13] or spectral submanifolds (SSMs) [14]. Recently, this approach was applied to compute parameter-dependent unstable manifolds in a pipe conveying fluid by constructing a center–unstable manifold of the extended system [15]. While theoretically sound, this approach leads to an increase in the system dimension of the reduced-order model. Furthermore, since this approach mixes the state variables with the parameters, computational implementation becomes difficult even when using open-source modeling software, and it does not allow for independent control of the expansion orders with respect to the parameters and the manifold coordinates.

In this work, we focus on the parameter-dependent computation of invariant manifolds attached to perturbed fixed points around a nominal parameter configuration, using asymptotic Taylor or Taylor-Fourier expansions. Our goal is to develop formal computational procedures for parameter-dependent invariant manifolds and their reduced dynamics around nontrivial steady states and parameter values without shifting coordinates and without introducing parameters as auxiliary variables. To this end, we take the existence and regularity with respect to parameters of the underlying invariant manifold as theoretically established. These theoretical guarantees may be provided by various classical and modern results, including center manifolds, stable (unstable) manifolds, center-stable (unstable) manifolds, pseudo-stable (unstable) manifolds [12, 13, 16–19], subcenter manifolds [20], the parametrization method [21–25], and spectral submanifolds [14, 26, 27].

Related works include equation-driven local approximation of parametric SSMs around trivial fixed points over a finite parameter range [28]. There, the invariance equations are projected onto an orthogonal polynomial basis over the parameter domain, resulting in a coupled nonlinear system for the leading-order coefficients, followed by recursive linear computations for higher-order terms. Parametric SSMs have also been obtained through interpolation of SSM expansion coefficients computed at discrete parameter values in a data-driven setting [29]; such interpolation is also justified among low-order SSM coefficients across Hopf bifurcations [30]. In contrast, our data-free approach constructs Taylor expansions with respect to the parameter perturbation $\boldsymbol{\delta} = \boldsymbol{\mu} - \boldsymbol{\mu}_0$. Hence, our representation remains local in the parameter space, but enables the invariance equations to decouple into nested linear problems, while naturally supporting local sensitivity and bifurcation analysis around nontrivial parameter configurations.

The remainder of the paper is organized as follows. In Sect. 2, we describe the technical setup for autonomous systems with polynomial nonlinearities and develop expressions for computing Taylor expansions of parameter-dependent equilibria $\mathbf{x}^\star(\boldsymbol{\mu})$ about a nominal parameter value $\boldsymbol{\mu}_0$. We then derive expressions for efficient computation of invariant manifolds attached to these equilibria and their parameter-dependent reduced dynamics. In Sect. 3, we extend the methodology to nonautonomous systems with periodic or quasiperiodic time dependence, enabling a local approximation of nonautonomous invariant manifolds to arbitrary polynomial orders in the amplitude and frequency of time-dependent forcing. Section 4 addresses nonintrusive computations, which are particularly relevant when governing equations are accessible only through black-box modeling packages; here we focus on systems with affine parameter dependence and nonlinearities up to cubic order. Numerical and analytical examples are presented in Sect. 5, followed by concluding remarks in Sect. 6.

2 Autonomous systems

We are generally interested in high-dimensional dynamical systems described by ordinary differential equations (ODEs) for the variable $\mathbf{x}(t) \in \mathbb{R}^N$, dependent on some parameter $\boldsymbol{\mu} \in \mathbb{R}^m$ as

$$\mathbf{B}\dot{\mathbf{x}} = \mathbf{F}(\mathbf{x}; \boldsymbol{\mu}), \tag{1}$$

Table 1 Notation

Symbol	Space	Meaning
N	$\mathbb{N}$	Dimension of the full system (1)
$\mathbf{x}$	$\mathbb{R}^N$	State vector of system (1)
$\mathbf{x}^\star$	$\mathbb{R}^N$	Anchor trajectory for the invariant manifold: fixed point of system (1), or periodic/quasiperiodic orbit of system (35)
$\mathcal{E}$	$\mathbb{R}^N$	Invariant subspace of the linear system (11); main subspace for invariant manifold computation
M	$\mathbb{N}$	$\dim(\mathcal{E})$
m	$\mathbb{N}_0$	Number of parameters
$\boldsymbol{\mu}$	$\mathbb{R}^m$	Vector of parameters
$\boldsymbol{\mu}_0$	$\mathbb{R}^m$	Nominal parameter configuration
$\mathbf{x}_0$	$\mathbb{R}^N$	Fixed point of system (1) or system (35) for $\boldsymbol{\mu} = \boldsymbol{\mu}_0$
$\mathcal{W}(\mathcal{E})$	$\mathbb{R}^N$	Parameter-dependent invariant manifold of system (1) or system (35), tangent to $\mathcal{E}$ at the nominal equilibrium configuration $(\mathbf{x}_0, \boldsymbol{\mu}_0)$
$\boldsymbol{\delta}$	$\mathbb{R}^m$	$\boldsymbol{\delta} = \boldsymbol{\mu} - \boldsymbol{\mu}_0$: deviation from the nominal parameter configuration
$\mathbf{p}$	$\mathbb{C}^M$	Parametrization coordinates for $\mathcal{W}(\mathcal{E})$ along $\mathcal{E}$
$\mathbf{z}^{\boldsymbol{d}}$	$\mathbb{C}$	$\mathbf{z}^{\boldsymbol{d}} := z_1^{d_1} z_2^{d_2} \dots z^{d_n}$ for any $\mathbf{z} \in \mathbb{C}^n, \boldsymbol{d} \in \mathbb{N}_0^n$
$\bar{(\bullet)}$		Complex conjugation operation
$\lvert \bullet \rvert$	$\mathbb{N}_0$	$\lvert \boldsymbol{d} \rvert = d_1 + \dots + d_n$ for any $\boldsymbol{d} \in \mathbb{N}_0^n$
f	$\mathbb{N}$	Number of rationally incommensurate frequencies in the nonautonomous system (35): $f = 1$ for periodic and $f > 1$ for quasiperiodic time dependence)
$\boldsymbol{\Omega}$	$\mathbb{R}^f$	Quasiperiodic forcing frequencies
$\mathbf{e}_j$		$[0, \dots, 0, \overset{j-\text{th position}}{\overset{\uparrow}{1}}, 0, \dots, 0]^T$: vector aligned along the $j-$th coordinate axis in the corresponding Euclidean space
i		imaginary unit

where, $\mathbf{F} : \mathbb{R}^N \times \mathbb{R}^m \to \mathbb{R}^N$ is an arbitrary polynomial in terms of $\mathbf{x}$ and $\boldsymbol{\mu}$. Such systems typically arise upon spatial discretization of partial differential equations (PDEs) that represent continuum models of physical phenomena. Various numerical techniques, such as finite differences, the Galerkin method, finite elements (FE), enable such spatial discretizations via open-source as well as commercial software that produce ODEs with polynomial nonlinearities.

Autonomous systems of the form (1) are often analyzed around an equilibrium configuration or fixed point. In the presence of parameters, these fixed points may deviate from their nominal configuration. For instance, in a buckling problem, the trivial equilibrium of the system may bifurcate into a nontrivial equilibrium as the load parameter is varied. The influence of nonlinearities on the dynamics around the bifurcating equilibrium can be captured by a low-dimensional attracting invariant manifold attached to this equilibrium [31]. In the vibrations community, such invariant manifolds have been computed for decades, where they have been referred to as *nonlinear normal modes* (NNMs) [32, 33] and more recently, upon theoretical developments of their existence and properties, defined as *spectral submanifolds* (SSMs) [14, 27].

In fluid dynamics, the flow may bifurcate from a trivial state to a nontrivial flow pattern as the Reynolds number is varied. In such cases, the invariant manifold of interest is attached to the bifurcating flow, which also depends on parameters. For instance, the flow past a cylinder undergoes a Hopf bifurcation at a critical Reynolds number, where the trivial equilibrium bifurcates into a limit cycle that can be accurately captured via a center manifold reduction [1]. Practical computation of such manifolds often requires an explicit transformation of the governing equations to shift the origin to the bifurcating flow.

We now present a computational procedure for parameter-dependent invariant manifolds attached to nontrivial fixed points without shifting coordinates. We first compute the parameter-dependent fixed point $\mathbf{x}^\star(\boldsymbol{\mu})$ as a Taylor expansion in terms of the deviation $\boldsymbol{\delta} = \boldsymbol{\mu} - \boldsymbol{\mu}_0$ from the nominal parameter configuration $\boldsymbol{\mu}_0$. We then derive recursive expressions for computing the coefficients of the Taylor expansion of $\mathbf{x}^\star(\boldsymbol{\mu})$ and the associated invariant manifold and its reduced dynamics. The resulting expressions can be implemented

directly from the governing equations without any coordinate transformations. We summarize the notation used in the paper in Table 1.

For the ensuing computations, we require:

1. The autonomous system (1) has a fixed point $\mathbf{x}_0$ for some nominal parameter value $\boldsymbol{\mu}_0$, i.e.,

$$\mathbf{F}(\mathbf{x}_0; \boldsymbol{\mu}_0) = \mathbf{0}. \tag{2}$$

We denote the Jacobian of the right-hand side evaluated at $(\mathbf{x}_0; \boldsymbol{\mu}_0)$ as $\mathbf{A} \in \mathbb{R}^{N\times N}$, i.e.,

$$\mathbf{A} = \partial_{\mathbf{x}}\mathbf{F}(\mathbf{x}_0; \boldsymbol{\mu}_0). \tag{3}$$

2. The fixed point $\mathbf{x}_0$ smoothly persists upon perturbation of the parameter $\boldsymbol{\mu}_0$. This is guaranteed, for instance, by the implicit function theorem when $\mathbf{A}$ is invertible. This allows us to locally approximate the fixed point as a multivariate Taylor expansion in terms of the deviation $\boldsymbol{\delta} = \boldsymbol{\mu} - \boldsymbol{\mu}_0$ from the nominal parameter configuration as

$$\mathbf{x}^\star(\boldsymbol{\mu}) = \sum_{\boldsymbol{\ell}\in\mathbb{N}_0^m} \mathbf{x}^\star_{\boldsymbol{\ell}}\boldsymbol{\delta}^{\boldsymbol{\ell}}, \tag{4}$$

where the $\mathbf{x}^\star_{\boldsymbol{\ell}} \in \mathbb{R}^N$ is the expansion coefficient associated with the monomial $\boldsymbol{\delta}^{\boldsymbol{\ell}} = \delta_1^{\ell_1}\dots\delta_m^{\ell_m}$. Note that the coefficients $\mathbf{x}^\star_{\boldsymbol{\ell}}$ are a priori unknown except for $\boldsymbol{\ell} = \mathbf{0}$, i.e.,

$$\mathbf{x}^\star_{\mathbf{0}} = \mathbf{x}_0.$$

3. The right-hand side admits a *finite* Taylor expansion as

$$\mathbf{F}(\mathbf{x}; \boldsymbol{\mu}) = \sum_{j,k\in\mathbb{N}_0} \mathbf{F}_{j,k}(\underbrace{\mathbf{x}, \dots, \mathbf{x}}_{j \text{ times}}; \underbrace{\boldsymbol{\mu}, \dots, \boldsymbol{\mu}}_{k \text{ times}}), \tag{5}$$

where $\mathbf{F}_{j,k} \in \left(\mathbb{R}^N\right)^j \times (\mathbb{R}^m)^k \to \mathbb{R}^N$ are multilinear functions describing the polynomial dependence of the right-hand side on the state $\mathbf{x}$ and the parameters $\boldsymbol{\mu}$. Specifically, $\mathbf{F}_{j,k}$ has degree j in $\mathbf{x}$ and degree k in $\boldsymbol{\mu}$. Such representations are readily available in open-source finite-element model packages such as yaFEc [34]. For commercial packages, we discuss a nonintrusive construction of $\mathbf{F}_{j,k}$ by treating $\mathbf{F}$ as a black box in Sect. 4. We discuss in Appendix A.1 how this multilinear description for a polynomial function is generally not unique, but we always have a unique symmetric choice. This symmetric choice also reduces computational effort, as we show in Remark 2.

Next, we compute the coefficients $\mathbf{x}^\star_{\boldsymbol{\ell}}$ to determine how the fixed point $\mathbf{x}_0$ deviates when the parameter value $\boldsymbol{\mu}_0$ is perturbed.

2.1 Parameter-dependent fixed point

To determine the dependence of the fixed point $\mathbf{x}^\star$ on parameters, we need to solve the nonlinear system

$$\mathbf{F}(\mathbf{x}^\star(\boldsymbol{\mu}); \boldsymbol{\mu}) = \mathbf{0}. \tag{6}$$

One advantage of Taylor series representation (4) in systems with polynomial nonlinearities (5) is that the unknown coefficients $\mathbf{x}^\star_{\boldsymbol{\ell}}$ can be computed recursively by solving a set of *linear* equations. To this end, we first express the parameter $\boldsymbol{\mu}$ as an affine function of the deviation $\boldsymbol{\delta}$ as

$$\boldsymbol{\mu}(\boldsymbol{\delta}) = \boldsymbol{\mu}_0 + \boldsymbol{\delta} = \sum_{\boldsymbol{\ell}\in\mathbb{N}_0^m} \boldsymbol{\mu}_{\boldsymbol{\ell}}\boldsymbol{\delta}^{\boldsymbol{\ell}}, \tag{7}$$

where

$$\boldsymbol{\mu}_{\boldsymbol{\ell}} = \begin{cases} \boldsymbol{\mu}_0 & \boldsymbol{\ell} = \mathbf{0}, \\ \mathbf{e}_j & \boldsymbol{\ell} = \mathbf{e}_j, \quad j = 1, \dots, m, \\ \mathbf{0} & \text{otherwise.} \end{cases} \tag{8}$$

We then substitute the expansions (4) and (7) into the relation (6). Now, utilizing the expansion (5) and collecting coefficients of the monomial $\boldsymbol{\delta}^{\boldsymbol{\ell}}$ for any $|\boldsymbol{\ell}| > 0$, we obtain the linear system

$$\mathbf{A}\mathbf{x}^\star_{\boldsymbol{\ell}} = \mathbf{b}_{\boldsymbol{\ell}}, \tag{9}$$

where

$$\mathbf{b}_{\boldsymbol{\ell}} := \sum_{\substack{j,k\in\mathbb{N}_0,\,(j,k)\neq(0,0)\\ \boldsymbol{\ell}_1+\dots+\boldsymbol{\ell}_j+\boldsymbol{n}_1+\dots+\boldsymbol{n}_k=\boldsymbol{\ell},\\ \boldsymbol{\ell}_i\neq\boldsymbol{\ell},\forall i\in\{1,\dots,j\}}} -\mathbf{F}_{j,k}\left(\mathbf{x}^\star_{\boldsymbol{\ell}_1}, \dots, \mathbf{x}^\star_{\boldsymbol{\ell}_j}, \boldsymbol{\mu}_{\boldsymbol{n}_1}, \dots, \boldsymbol{\mu}_{\boldsymbol{n}_k}\right). \tag{10}$$

For deriving system (9), we have used the relation

$$\begin{aligned}\mathbf{A}\mathbf{x}^\star_{\boldsymbol{\ell}} &= \partial_{\mathbf{x}}\mathbf{F}(\mathbf{x}_0; \boldsymbol{\mu}_0)\mathbf{x}^\star_{\boldsymbol{\ell}} \\ &= \sum_{\substack{j,k\in\mathbb{N}_0,\,(j,k)\neq(0,0)\\ \boldsymbol{\ell}_1+\dots+\boldsymbol{\ell}_j=\boldsymbol{\ell},\\ \boldsymbol{\ell}_i=\boldsymbol{\ell},\ i\in\{1,\dots,j\}}} \mathbf{F}_{j,k}\left(\mathbf{x}^\star_{\boldsymbol{\ell}_1}, \dots, \mathbf{x}^\star_{\boldsymbol{\ell}_j}, \underbrace{\boldsymbol{\mu}_0, \dots, \boldsymbol{\mu}_0}_{k \text{ times}}\right).\end{aligned}$$

We note that right-hand side $\mathbf{b}_{\boldsymbol{\ell}}$ in system (9) depends only on the coefficients $\mathbf{x}^\star_{\boldsymbol{m}}$ with $|\boldsymbol{m}| < |\boldsymbol{\ell}|$. Hence, $\mathbf{x}^\star_{\boldsymbol{\ell}}$ can be determined by solving system (9) for arbitrary values of $\boldsymbol{\ell} \in \mathbb{N}^m$ in a recursive fashion with respect to increasing polynomial orders $|\boldsymbol{\ell}|$ (see Algorithm 2 in Appendix B).

Remark 1 (*Computations without shifting the origin*) The nonlinearity is expressed in arbitrary coordinates, and this recursive computation does not require a translation of the origin to the fixed point $(\mathbf{x}_0, \boldsymbol{\mu}_0)$. Thanks to the expansion (8), the coefficients with respect to the deviation $\boldsymbol{\delta}$ can be computed directly from the multilinear expansion for $\mathbf{F}$ up to arbitrary orders in any given coordinate system.

Remark 2 (*Exploiting symmetries in* $\mathbf{F}_{j,k}$) The summation (10) involves multiple evaluations of the multilinear functions $\mathbf{F}_{j,k}$, which is a computational bottleneck. For a symmetric construction of $\mathbf{F}_{j,k}$ (see Appendix A.1), we need to evaluate these functions only for unique combinations of the arguments, regardless of their permutations, thereby minimizing the number of function evaluations.

We will now discuss a similar recursive procedure to compute an invariant manifold of system (1), anchored to $\mathbf{x}^\star(\boldsymbol{\mu})$.

2.2 Parameter-dependent invariant manifold anchored to a nontrivial fixed point

We seek to compute a parameter-dependent invariant manifold $\mathcal{W}(\mathcal{E})$ of system (1), anchored at the fixed point $\mathbf{x}^\star(\boldsymbol{\mu})$ and tangent to an invariant subspace $\mathcal{E}$ of the linearized system,

$$\mathbf{B}\dot{\mathbf{x}} = \mathbf{A}\mathbf{x}, \tag{11}$$

at the nominal configuration $(\mathbf{x}_0, \boldsymbol{\mu}_0)$. By linearity, any invariant subspace of system (11) is spanned by some generalized eigenvectors defined by the eigenvalue problem

$$\left(\mathbf{A} - \lambda_j \mathbf{B}\right)\mathbf{v}_j = \mathbf{0}, \tag{12}$$

$$\bar{\mathbf{u}}_j^T\left(\mathbf{A} - \lambda_j \mathbf{B}\right) = \mathbf{0}, \quad j = 1, \ldots, N, \tag{13}$$

where $\lambda_j \in \mathbb{C}$ is an eigenvalue with the generalized left and right eigenvectors $\mathbf{u}_j, \mathbf{v}_j \in \mathbb{C}^N$. We pick an eigenvalue ordering such that $\mathcal{E} = \text{span}\{\mathbf{v}_1, \ldots, \mathbf{v}_M\}$ for some $M < N$, i.e., $\dim(\mathcal{E}) = M$.

Let $\mathbf{W} : \mathbb{C}^M \times \mathbb{R}^m \to \mathbb{R}^N$ be a mapping that parametrizes $\mathcal{W}(\mathcal{E})$ as a function of the coordinates $\mathbf{p} \in \mathbb{C}^M$ and system parameters $\boldsymbol{\mu}$. Then, $\mathbf{W}(\mathbf{p}, \boldsymbol{\mu})$ provides the coordinates of the manifold in the phase space of system (1), as shown in Fig. 1. For any trajectory $\mathbf{x}(t; \boldsymbol{\mu})$ on $\mathcal{W}(\mathcal{E})$, we have a *reduced dynamics* trajectory $\mathbf{p}(t; \boldsymbol{\mu})$ in the parametrization space such that

$$\mathbf{x}(t; \boldsymbol{\mu}) = \mathbf{W}(\mathbf{p}(t; \boldsymbol{\mu}); \boldsymbol{\mu}). \tag{14}$$

The evolution of this trajectory is governed by a low-dimensional, parameter-dependent ODE,

$$\dot{\mathbf{p}} = \mathbf{R}(\mathbf{p}; \boldsymbol{\mu}), \tag{15}$$

where $\mathbf{R} : \mathbb{C}^M \times \mathbb{R}^m \to \mathbb{C}^M$ is a parametrization for the reduced dynamics on $\mathcal{W}(\mathcal{E})$. Differentiating eq. (14) with respect to t, substituting the result into system (1) and utilizing eq. (15), we obtain the *invariance equation*

$$\mathbf{B}\left[\partial_{\mathbf{p}}\mathbf{W}(\mathbf{p}; \boldsymbol{\mu})\right]\mathbf{R}(\mathbf{p}; \boldsymbol{\mu}) = \mathbf{F}(\mathbf{W}(\mathbf{p}; \boldsymbol{\mu}); \boldsymbol{\mu}), \tag{16}$$

whose solution determines the parameterizations $\mathbf{W}$ and $\mathbf{R}$ required for model reduction.

We choose a Taylor ansatz to locally approximate $\mathbf{W}$ around $\mathbf{x}^\star(\boldsymbol{\mu})$ as

$$\mathbf{W}(\mathbf{p}; \boldsymbol{\mu}) = \sum_{\mathbf{m}\in\mathbb{N}_0^M, \boldsymbol{\ell}\in\mathbb{N}_0^m} \mathbf{w}_{\mathbf{m},\boldsymbol{\ell}}\mathbf{p}^{\mathbf{m}}\boldsymbol{\delta}^{\boldsymbol{\ell}}, \tag{17}$$

where $\mathbf{w}_{\mathbf{m},\boldsymbol{\ell}} \in \mathbb{C}^N$ are the coefficients associated with the scalar monomial $\mathbf{p}^{\mathbf{m}}\boldsymbol{\delta}^{\boldsymbol{\ell}}$. Similarly, we locally approximate $\mathbf{R}$ via a Taylor series as

$$\mathbf{R}(\mathbf{p}; \boldsymbol{\mu}) = \sum_{\mathbf{m}\in\mathbb{N}_0^M, \boldsymbol{\ell}\in\mathbb{N}_0^m} \mathbf{r}_{\mathbf{m},\boldsymbol{\ell}}\mathbf{p}^{\mathbf{m}}\boldsymbol{\delta}^{\boldsymbol{\ell}}, \tag{18}$$

where $\mathbf{r}_{\mathbf{m},\boldsymbol{\ell}} \in \mathbb{C}^M$ are the reduced dynamics coefficients associated with the monomial $\mathbf{p}^{\mathbf{m}}\boldsymbol{\delta}^{\boldsymbol{\ell}}$. Once again, thanks to the choice of a polynomial ansatz for $\mathbf{W}$ and $\mathbf{R}$, Eq. (16) simplifies to a set of *linear* equations in terms of the unknowns $\mathbf{w}_{\mathbf{m},\boldsymbol{\ell}}$, $\mathbf{r}_{\mathbf{m},\boldsymbol{\ell}}$ that can be solved via a nested recursion with respect to increasing polynomial orders $|\mathbf{m}|$ and $|\boldsymbol{\ell}|$, as shown in Algorithm 1.

Specifically, note that the leading order coefficients are a priori known due to the anchor point $\mathbf{x}^\star(\boldsymbol{\mu})$ and the eigenvectors associated with $\mathcal{E}$ as

$$\mathbf{w}_{\mathbf{0},\boldsymbol{\ell}} = \mathbf{x}^\star_{\boldsymbol{\ell}} \quad \forall \quad \boldsymbol{\ell} \in \mathbb{N}_0^m, \tag{19}$$

$$\mathbf{w}_{\mathbf{e}_j,\mathbf{0}} = \mathbf{v}_j \quad \forall j = 1, \ldots, M. \tag{20}$$

By construction, the parametrization $\mathbf{W}$ maps the origin $\mathbf{p} = \mathbf{0}$ to the fixed point $\mathbf{x}^\star$. Hence, the reduced dynamics (15) must satisfy $\mathbf{R}(\mathbf{0}, \boldsymbol{\mu}) \equiv \mathbf{0}$, i.e.,

$$\mathbf{r}_{\mathbf{0},\boldsymbol{\ell}} = \mathbf{0} \quad \forall \quad \boldsymbol{\ell} \in \mathbb{N}_0^m. \tag{21}$$

Furthermore, the eigenvalues associated with $\mathcal{E}$ determine the leading-order coefficients $\mathbf{R}$ at the nominal parameter configuration ($\boldsymbol{\ell} = \mathbf{0}$) as

$$\mathbf{r}_{\mathbf{e}_j,\mathbf{0}} = \lambda_j \mathbf{e}_j, \quad \forall j = 1, \ldots, M. \tag{22}$$

Finally, the remaining unknown coefficients $\mathbf{w}_{\mathbf{m},\boldsymbol{\ell}}, \mathbf{r}_{\mathbf{m},\boldsymbol{\ell}}$ are determined by collecting the coefficients of the monomial $\mathbf{p}^{\mathbf{m}}\boldsymbol{\delta}^{\boldsymbol{\ell}}$ in the invariance equation (16) for $|\mathbf{m}| > 0$ as (see Appendix C)

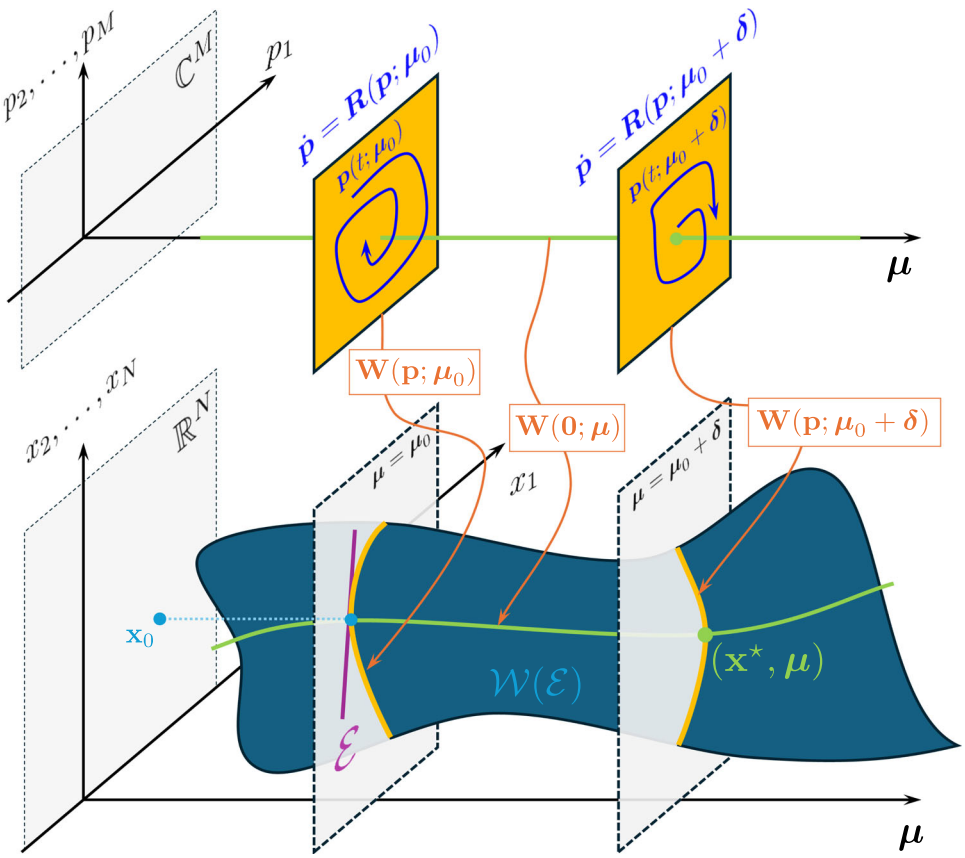

Fig. 1 $\mathcal{W}(\mathcal{E})$ is a parameter-dependent invariant manifold of system (1), tangent to the eigenspace $\mathcal{E}$ at the nominal parameter configuration $(\mathbf{x}_0, \boldsymbol{\mu}_0)$, and is anchored at the parameter-dependent equilibrium $\mathbf{x}^\star(\boldsymbol{\mu})$. The mapping $\mathbf{W} : \mathbb{C}^M \times \mathbb{R}^m \to \mathbb{R}^N$ parameterizes $\mathcal{W}(\mathcal{E})$ as a function of the coordinates $\mathbf{p} \in \mathbb{C}^M$ and parameters $\boldsymbol{\mu} \in \mathbb{R}^m$, and the function $\mathbf{R} : \mathbb{C}^M \times \mathbb{R}^m \to \mathbb{C}^M$ provides its parameter-dependent reduced dynamics. For a perturbed parameter value $\boldsymbol{\mu} = \boldsymbol{\mu}_0 + \boldsymbol{\delta}$, $\mathbf{W}$ maps the trajectories $\mathbf{p}(t; \boldsymbol{\mu})$ of the reduced system (15) onto $\mathcal{W}(\mathcal{E})$, and the origin $\mathbf{p} = \mathbf{0}$ to the fixed point $\mathbf{x}^\star(\boldsymbol{\mu})$ in the phase space of the full system

$$\underbrace{[\lambda_{\mathbf{m}}\mathbf{B} - \mathbf{A}]}_{\mathcal{L}_{\mathbf{m}}} \mathbf{w}_{\mathbf{m},\boldsymbol{\ell}} = \underbrace{\mathbf{s}_{\mathbf{m},\boldsymbol{\ell}} - \mathbf{D}\mathbf{r}_{\mathbf{m},\boldsymbol{\ell}}}_{\mathbf{b}_{\mathbf{m},\boldsymbol{\ell}}}, \tag{23}$$

where $\lambda_{\mathbf{m}} := m_1\lambda_1 + \cdots + m_M\lambda_M$, and $\mathbf{s}_{\mathbf{m},\boldsymbol{\ell}} \in \mathbb{C}^N$, $\mathbf{D} \in \mathbb{C}^{N\times M}$ are defined in Appendix C. Most importantly, $\mathbf{s}_{\mathbf{m},\boldsymbol{\ell}}$ depends only on lower-order coefficients $\mathbf{w}_{\mathbf{u},\boldsymbol{t}}, \mathbf{r}_{\mathbf{u},\boldsymbol{t}}$ with $|\mathbf{u}| < |\mathbf{m}|$ and $|\boldsymbol{t}| \le |\boldsymbol{\ell}|$. Now, $\mathbf{w}_{\mathbf{m},\boldsymbol{\ell}}, \mathbf{r}_{\mathbf{m},\boldsymbol{\ell}}$ are a priori determined for $|\mathbf{m}| = 0$ at all orders in $\boldsymbol{\ell}$ from eqs. (19),(21). And for $|\mathbf{m}| = 1$, the coefficients $\mathbf{w}_{\mathbf{m},\boldsymbol{\ell}}, \mathbf{r}_{\mathbf{m},\boldsymbol{\ell}}$ are known for $|\boldsymbol{\ell}| = 0$ from Eqs. (20) and (22). Hence, the coefficients $\mathbf{w}_{\mathbf{m},\boldsymbol{\ell}}, \mathbf{r}_{\mathbf{m},\boldsymbol{\ell}}$ can be determined up to any desired order in $\mathbf{m}$, $\boldsymbol{\ell}$ by solving the linear system (23) recursively (see Algorithm 1).

A symmetric construction of $\mathbf{F}_{j,k}$ is again computationally beneficial in evaluating $\mathbf{b}_{\mathbf{m},\boldsymbol{\ell}}$, as mentioned in Remark 2. In Appendix A.3, we discuss how conjugacies in the eigenvalues of $\mathcal{E}$ can be exploited to further reduce computational costs.

Remark 3 (*Nested recursion and parallelization*): The recursion with respect to $|\boldsymbol{\ell}|$ is nested inside the recursion with respect to $|\mathbf{m}|$, i.e., keeping $|\mathbf{m}|$ fixed, we first recursively solve system (23) up to desired order in $|\boldsymbol{\ell}|$, and then we increase $|\mathbf{m}|$. At a given pair of orders, $(|\mathbf{m}|,|\boldsymbol{\ell}|)$, the linear system (23) remains decoupled for each multi-index pair $(\mathbf{m}, \boldsymbol{\ell})$.

Algorithm 1 Nested recursion for solving the invariance Eq. (16)

$[\mathbf{W}, \mathbf{R}] =$ `compute_parametrization`$(\mathbf{x}_0, \boldsymbol{\mu}_0, \Lambda_{\mathcal{E}}, \mathbf{V}_{\mathcal{E}}, d_p, d_\mu)$

Input Nominal equilibrium configuration: $(\mathbf{x}_0, \boldsymbol{\mu}_0)$;
Eigenvalues $\lambda_1, \ldots, \lambda_M$ with eigenvectors $\mathbf{v}_1, \ldots, \mathbf{v}_M$ associated with $\mathcal{E}$;
Degrees of approximation d_p in $\mathbf{p}$ and d_μ in $\boldsymbol{\delta}$ for the parametrization (17) of $\mathcal{W}(\mathcal{E})$

`Setup` empty arrays for coefficients $\mathbf{w}_{\mathbf{m},\boldsymbol{\ell}} \in \mathbb{C}^N$ and $\mathbf{r}_{\mathbf{m},\boldsymbol{\ell}} \in \mathbb{C}^M$ for all $(\mathbf{m}, \boldsymbol{\ell}) \in \mathbb{N}_0^M \times \mathbb{N}_0^m : |\mathbf{m}| = 0, \ldots, d_p, |\boldsymbol{\ell}| = 0, \ldots, d_\mu$

`Assign` $\mathbf{w}_{\mathbf{0},\mathbf{0}} := \mathbf{x}_0, \mathbf{r}_{\mathbf{0},\mathbf{0}} := \mathbf{0}$;
$\mathbf{w}_{\mathbf{e}_j,\mathbf{0}} := \mathbf{v}_j, \mathbf{r}_{\mathbf{e}_j,\mathbf{0}} := \lambda_j \mathbf{e}_j \quad \forall j = 1, \ldots, M.$

`Setup` coefficients $\boldsymbol{\mu}_{\boldsymbol{\ell}} \in \mathbb{R}^m$ for the expansion (7) as $\boldsymbol{\mu}_{\boldsymbol{\ell}} := \begin{cases} \boldsymbol{\mu}_0 & \boldsymbol{\ell} = \mathbf{0}, \\ \mathbf{e}_j & \boldsymbol{\ell} = \mathbf{e}_j, \quad j = 1, \ldots, m, \\ \mathbf{0} & \text{otherwise.} \end{cases}$

for $k = 0, \ldots, d_p$
  for $l = 0, \ldots, d_\mu$
    if $(k, l) = (0, 0)$ **or** $(k, l) = (1, 0)$
      continue
    endif
    for $(\mathbf{m}, \boldsymbol{\ell}) \in \mathbb{N}_0^M \times \mathbb{N}_0^m : |\mathbf{m}| = k, |\boldsymbol{\ell}| = l$
      `Evaluate` $\mathbf{s}_{\mathbf{m},\boldsymbol{\ell}}$ using eq. (98), which requires $\mathbf{w}_{\mathbf{u},\boldsymbol{\ell}}, \mathbf{r}_{\mathbf{u},\boldsymbol{\ell}}$ with $|\mathbf{u}| < k$ and $|\boldsymbol{\ell}| \leq l$.
      `Solve` linear system (23) to obtain $\mathbf{w}_{\mathbf{m},\boldsymbol{\ell}}, \mathbf{r}_{\mathbf{m},\boldsymbol{\ell}}$ as discussed in Appendix D.
    endfor
  endfor
endfor

Output Coefficients $\mathbf{w}_{\mathbf{m},\boldsymbol{\ell}} \in \mathbb{C}^N, \mathbf{r}_{\mathbf{m},\boldsymbol{\ell}} \in \mathbb{C}^M$ for the expansions (17),(18) upto degrees d_p in $\mathbf{p}$ and d_μ in $\boldsymbol{\delta}$.

2.3 Choice of reduced dynamics

The linear system (23) is underdetermined as it contains N equations associated with the unknowns $\mathbf{w}_{\mathbf{m},\boldsymbol{\ell}} \in \mathbb{C}^N$, $\mathbf{r}_{\mathbf{m},\boldsymbol{\ell}} \in \mathbb{C}^M$, i.e., $N + M$ unknowns. This underdeterminacy allows for different *styles* of parameterization [25, 35], i.e., different solutions of $\mathbf{w}_{\mathbf{m},\boldsymbol{\ell}}$ for different choices of $\mathbf{r}_{\mathbf{m},\boldsymbol{\ell}}$. A trivial choice, i.e., $\mathbf{r}_{\mathbf{m},\boldsymbol{\ell}} = \mathbf{0}\ \forall\ |\mathbf{m}| \neq 1,\ \forall |\boldsymbol{\ell}| \geq 0$, is often possible and results in a linear expression for the reduced dynamics (15), i.e., linearized reduced dynamics. However, in the presence of (near-) resonances among the eigenvalues of $\mathcal{E}$, this trivial choice may no longer be (robustly) available, thereby resulting in nonlinear reduced dynamics associated with nonlinearizable phenomena [36]. Moreover, even when a complete linearization is formally possible, retaining near-resonant nonlinear terms is often desirable because these terms capture dynamically important effects and can increase the domain of convergence of the reduced dynamics expansions. Specifically, for an eigenvalue λ_j, a (near-) resonance of the form

$$\lambda_j \approx \lambda_{\mathbf{m}}, \quad j \in \{1, \ldots, N\} \tag{24}$$

results in the coefficient matrix $\boldsymbol{\mathcal{L}}_{\mathbf{m}}$ being (nearly) singular and the left eigenvector $\mathbf{u}_j \in \text{Ker}(\boldsymbol{\mathcal{L}}_{\mathbf{m}}^T)$; see [2] for a proof. To ensure (robust) solvability of system (23), $\mathbf{r}_{\mathbf{m},\boldsymbol{\ell}}$ must be chosen such that $\mathbf{b}_{\mathbf{m},\boldsymbol{\ell}}$ is in the range of $\boldsymbol{\mathcal{L}}_{\mathbf{m}}$.This choice is possible as long as $\lambda_j \in \text{Spec}(\mathcal{E})$, i.e., we have a (near) *inner* resonance among the eigenvalues of $\mathcal{E}$. Since $\text{Range}(\boldsymbol{\mathcal{L}}_{\mathbf{m}})$ is orthogonal to $\text{Ker}(\bar{\boldsymbol{\mathcal{L}}}_{\mathbf{m}}^T)$, we require

$$\langle \mathbf{u}_j, \mathbf{b}_{\mathbf{m},\boldsymbol{\ell}} \rangle = 0, \tag{25}$$

which imposes a constraint on the values of $\mathbf{r}_{\mathbf{m},\boldsymbol{\ell}}$ in the presence of a (near) inner resonance (24). For $\lambda_j \notin \text{Spec}(\mathcal{E})$, we have a (near) *outer* resonance, and system (23) is (ill-posed) unsolvable. Such an outer resonance can be converted into an inner resonance by augmenting the dimension of $\mathcal{E}$ by including any outer-resonant modes in it.

A *normal-form* style of parametrization is appealing in the presence of (near) inner resonances as it provide s a solution of system (23) that contains only the essential nonlinear monomials in the expression (18), producing a sparse expression for the reduced dynamics on $\mathcal{W}(\mathcal{E})$. We detail the implementation of the normal form and graph styles of parametrization in Appendix D.

Remark 4 (*Outer resonances and parameter dependence*): The existence of the manifold $\mathcal{W}(\mathcal{E})$ relies on the non-resonance condition between the spectrum within and outside $\mathcal{E}$. While this condition holds generically for a single parameter value, we assume it holds at $\boldsymbol{\mu} = \boldsymbol{\mu}_0$ and remains valid for $\boldsymbol{\mu} \approx \boldsymbol{\mu}_0$ to ensure Taylor expansion coefficients remain bounded. It is important to note that while an accumulation of resonances can occur, particularly across local bifurcations when overdamped modes are present, these effects typically affect higher-order terms [30]. Lower-order expansion coefficients typically persist through these transitions allowing truncated models to remain effective for parametric reduction, as demonstrated in Example 5.1.2.

2.4 A planar example

We consider the following planar system

$$\dot{x} = -x + \mu, \quad \dot{y} = -\sqrt{24}y + x^2 + x^3 + x^4 + x^5. \tag{26}$$

This system was originally studied in [14] for $\mu = 0$ without any parameter dependence, where the system was shown to have a unique analytic SSM tangent to the slowest spectral subspace (x-axis) at the origin. According to Theorem 3 in [14], this analytic SSM will persist under small perturbations in our parameter μ and will depend on these perturbations in an analytic fashion. Indeed, for $\mu \neq 0$ in system (26), the origin perturbs into a parameter-dependent equilibrium as

$$x_* = \mu, \quad y_* = \frac{\mu^2 + \mu^3 + \mu^4 + \mu^5}{\sqrt{24}}. \tag{27}$$

Next, we compute the slowest analytic SSM attached to the above equilibrium depending on μ via an analytical derivation and also via the algorithms we established in the previous sections. As we will see, these two methods yield the same results.

Classic calculation. For our analytical derivation, we first introduce a classical coordinate transformation $(x, y) \to (u, v)$ as

$$x = x_* + u, \quad y = y_* + v, \tag{28}$$

which shifts the equilibrium of system (26) to the origin, yielding

$$\begin{aligned}
\dot{u} &= -u,\\
\dot{v} &= -\sqrt{24}v + (5\mu^4 + 4\mu^3 + 3\mu^2 + 2\mu)u\\
&\quad + (10\mu^3 + 6\mu^2 + 3\mu + 1)u^2\\
&\quad + (10\mu^2 + 4\mu + 1)u^3 + (1 + 5\mu)u^4 + u^5
\end{aligned} \tag{29}$$

We observe that the two eigenvalues of the linearized system at $(u, v) = (0, 0)$ are $\lambda_1 = -1$ and $\lambda_2 = -\sqrt{24}$ indicating that the equilibrium is asymptotically stable for any value of μ. The corresponding eigenvectors are $\mathbf{v}_1 = \mathbf{e}_1$ and $\mathbf{v}_2 = \mathbf{e}_2$. We construct the slowest SSM as a parameter-dependent graph over $\mathbf{v}_1$ as

$$\begin{aligned}
v = h(u, \mu) &= a_{2,0}u^2 + a_{1,1}u\mu + a_{0,2}\mu^2 + a_{3,0}u^3\\
&\quad + a_{2,1}u^2\mu + a_{1,2}u\mu^2 + a_{0,3}\mu^3\\
&\quad + a_{4,0}u^4 + a_{3,1}u^3\mu + a_{2,2}u^2\mu^2\\
&\quad + a_{1,3}u\mu^3 + a_{0,4}\mu^4\\
&\quad + a_{5,0}u^5 + a_{4,1}u^4\mu + a_{3,2}u^3\mu^2\\
&\quad + a_{2,3}u^2\mu^3 + a_{1,4}u\mu^4 + a_{0,5}\mu^5 + \cdots,
\end{aligned} \tag{30}$$

where $a_{i,j}$ with $2 \le i \le 5$ and $0 \le j \le 5$ are the unknown coefficients in the Taylor expansion of h truncated at $\mathcal{O}(5)$. We substitute the expansion (30) into the state equation (29) and compare the coefficients of various monomials to obtain the unknown coefficients $a_{i,j}$ as shown in Appendix E.1.

Computation via Algorithms 1 & 2. We now perform the above computations, without shifting the origin, via the proposed algorithms. Expressing system (26) according to the notation of (1), we have

$$\begin{aligned}
&\mathbf{B} = \begin{pmatrix} 1 & 0 \\ 0 & 1 \end{pmatrix}, \ \mathbf{F}_{0,1}(\mu) = \begin{pmatrix} \mu \\ 0 \end{pmatrix},\\
&\mathbf{F}_{1,0}(\mathbf{x}) = \begin{pmatrix} -x \\ -\sqrt{24}y \end{pmatrix}, \ \mathbf{F}_{j,0}(\mathbf{x}_1, \ldots, \mathbf{x}_j) = \begin{pmatrix} 0 \\ x_1 x_2 \ldots x_j \end{pmatrix}
\end{aligned} \tag{31}$$

for $2 \le j \le 5$. We take the nominal equilibrium configuration as $(\mathbf{x}_0, \mu_0) = (\mathbf{0}, 0)$. Thus,

$$\mathbf{A} = \begin{pmatrix} -1 & 0 \\ 0 & -\sqrt{24} \end{pmatrix}. \tag{32}$$

Following Algorithm 2, we obtain the Taylor expansion for the parameter-dependent equilibrium as

$$\mathbf{x}^\star(\mu) = \begin{pmatrix} \delta \\ \frac{1}{\sqrt{24}}(\delta^2 + \delta^3 + \delta^4 + \delta^5) \end{pmatrix},$$

which agrees with our analytical calculation (27) since $\delta = \mu - \mu_0 = \mu$. Next, following Algorithm 1, we compute the parameter-dependent SSM $\mathcal{W}(\mathcal{E})$ with $\mathcal{E} = \text{span}\{\mathbf{e}_1\}$ to obtain as SSM parametrization $\mathbf{W}(p; \mu) : \mathbb{R} \times \mathbb{R} \to \mathbb{R}^2$ as

$$\begin{aligned}
w_1(p; \mu) &= p + \delta,\\
w_2(p; \mu) &\approx 0.204124(\delta^2 + \delta^3 + \delta^4 + \delta^5)\\
&\quad + 0.344949p^2 + 0.512955\delta p + 0.526599p^3\\
&\quad + 1.03485\delta p^2 + 0.769432\delta^2 p\\
&\quad + 1.11237p^4 + 2.10639\delta p^3 + 2.06969\delta^2 p^2\\
&\quad + 1.02591\delta^3 p\\
&\quad - 9.89898p^5 + 5.56186\delta p^4 + 5.26599\delta^2 p^3\\
&\quad + 3.44949\delta^3 p^2 + 1.28239\delta^4 p
\end{aligned} \tag{33}$$

and the reduced dynamics on the SSM as

$$\dot{p} = R(p; \mu) = -p, \tag{34}$$

which shows that the equilibrium $\mathbf{x}^\star(\mu)$ remains asymptotically stable for any parameter value, as expected. Since $\mathcal{E}$ is aligned with the x-axis, our parametrization coordinate p can be identified with the variable u in (28), and we observe

that the analytical coefficients in Appendix E.1 agree with the numerical results (33), which validates the effectiveness of our algorithms.

3 Nonautonomous systems with periodic/quasiperiodic time dependence

Weak periodic or quasiperiodic time dependence is common in many applications, such as mechanical systems under moderate external forcing, fluid flows under periodic excitation, and power grids under time-varying loads. In such systems, the role of a fixed point in the autonomous limit is replaced by a periodic or quasiperiodic steady state in the nonautonomous setting. These steady states typically emerge from the persistence of hyperbolic fixed points under weak or slow time-dependent forcing and depend smoothly on the parameters [37]. Invariant manifolds associated to the anchor fixed point also smoothly persist as periodic or quasiperiodic spectral submanifolds (SSMs) under appropriate nonresonance conditions that are generically satisfied [14]. In these systems, the nonautonomous invariant manifolds play a crucial role in reducing the system's response to time-dependent perturbations.

Prior efforts to compute such nonautonomous perturbations of autonomous invariant manifolds includes the computation of $\mathcal{O}(\epsilon)$-approximations of the nonautonomous SSMs in the presence of $\mathcal{O}(\epsilon)$-periodic/quasiperiodic forcing [2, 10, 38]. Another strategy for systems with harmonic forcing is to introduce the harmonic forcing function as an auxiliary variable to obtain an autonomous system in the extended phase space [33, 39]. This transformation enables the computation of invariant manifolds attached to periodic orbits by solving autonomous invariance equations. This trick has also been utilized to obtain higher order terms with respect to the harmonic forcing amplitude in manifold expansions [3]. Indeed, these higher-order terms are crucial for accurately capturing phenomena such as parametric and superharmonic resonances [3, 11]. However, these works do not take into account parameter dependence of nonautonomous systems.

We now extend our parametric algorithms from the autonomous setting to systems with periodic or quasiperiodic time dependence by introducing the Fourier basis function $\exp(\mathrm{i}\Omega t)$ associated with each independent frequency Ω as an independent variable in an augmented system. Specifically, we consider parametric systems with periodic/quasiperiodic time dependence as

$$\mathbf{B}\dot{\mathbf{x}} = \mathbf{F}(\mathbf{x}, \boldsymbol{\Omega} t; \boldsymbol{\mu}), \tag{35}$$

where $\boldsymbol{\Omega} \in \mathbb{R}^f$ contain f rationally incommensurate frequencies $\Omega_1, \ldots, \Omega_f > 0$. Similarly to the autonomous setting, we have the following requirements for our computations:

1. The nonautonomous system (35) has a fixed point $\mathbf{x}_0$ for some nominal parameter value $\boldsymbol{\mu}_0$, i.e.,

$$\mathbf{F}(\mathbf{x}_0, \boldsymbol{\Omega} t; \boldsymbol{\mu}_0) = \mathbf{0}, \quad \forall\, t \in \mathbb{R}. \tag{36}$$

   Furthermore, we assume that the Jacobian matrix $\partial_{\mathbf{x}}\mathbf{F}|_{(\mathbf{x}_0;\boldsymbol{\mu}_0)}$ is time-invariant and we denote it as $\mathbf{A}$, resulting in the linearization (11) around this configuration. In many applications with time-dependent forcing, such a fixed point $\mathbf{x}_0$ can be obtained by introducing the forcing amplitude as a parameter and selecting its nominal value in $\boldsymbol{\mu}_0$ to correspond to the unforced system, e.g., zero forcing amplitude. The fixed point $\mathbf{x}_0$ then coincides with the equilibrium of the unforced system. This construction is adopted.in the numerical examples considered later.
2. This fixed point $\mathbf{x}_0$ smoothly persists as a periodic/quasiperiodic trajectory $\mathbf{x}^\star(t; \boldsymbol{\mu})$ upon sufficiently small perturbation from $\boldsymbol{\mu}_0$. This allows us to express $\mathbf{x}^\star(t; \boldsymbol{\mu})$ as a Taylor-Fourier expansion in terms of the deviation $\boldsymbol{\delta} = \boldsymbol{\mu} - \boldsymbol{\mu}_0$ and the frequency $\boldsymbol{\Omega}$ as

$$\mathbf{x}^\star(t; \boldsymbol{\mu}) = \sum_{\boldsymbol{\ell} \in \mathbb{N}_0^m, \boldsymbol{\kappa} \in \mathbb{Z}^k} \mathbf{x}_{\boldsymbol{\kappa},\boldsymbol{\ell}} e^{\mathrm{i}\langle \boldsymbol{\kappa}, \boldsymbol{\Omega}\rangle t} \boldsymbol{\delta}^{\boldsymbol{\ell}}, \tag{37}$$

   where $\mathbf{x}_{\boldsymbol{\kappa},\boldsymbol{\ell}} \in \mathbb{R}^N$ denote the Taylor-Fourier expansion coefficients associated with the monomial $\boldsymbol{\delta}^{\boldsymbol{\ell}}$ and harmonic $e^{i\langle \boldsymbol{\kappa}, \boldsymbol{\Omega}\rangle t}$. Once again, these coefficients are a priori unknown except for $\boldsymbol{\ell} = \mathbf{0}$, i.e.,

$$\mathbf{x}_{\boldsymbol{\kappa},\mathbf{0}} = \begin{cases} \mathbf{x}_0 & \boldsymbol{\kappa} = \mathbf{0}, \\ \mathbf{0} & \text{otherwise.} \end{cases}$$

3. The right-hand side admits a finite Taylor-Fourier expansion in terms of its arguments as

$$\mathbf{F}(\mathbf{x}; \boldsymbol{\mu}, \boldsymbol{\Omega} t) = \sum_{j,k \in \mathbb{N}_0, \boldsymbol{\kappa} \in \mathbb{Z}^k} \mathbf{F}_{j,k,\boldsymbol{\kappa}}(\underbrace{\mathbf{x}, \ldots, \mathbf{x}}_{j \text{ times}}; \underbrace{\boldsymbol{\mu}, \ldots, \boldsymbol{\mu}}_{k \text{ times}}) e^{\mathrm{i}\langle \boldsymbol{\kappa}, \boldsymbol{\Omega}\rangle t}. \tag{38}$$

   where $\mathbf{F}_{j,k,\boldsymbol{\kappa}} \in \left(\mathbb{R}^N\right)^j \times (\mathbb{R}^m)^k \to \mathbb{R}^N$ are multilinear functions as in the autonomous setting.

We illustrate the above notation in the following example.

Example 5 We consider the periodically forced mechanical system

$$\ddot{y} + 2\zeta\omega_0\dot{y} + \omega_0^2 y = a + b\cos\Omega t, \tag{39}$$

with $\zeta, \omega_0 > 0$, written in the first-order form (35) as

$$\mathbf{x} = \begin{bmatrix} y \\ \dot{y} \end{bmatrix}, \quad \boldsymbol{\mu} = \begin{bmatrix} a \\ b \end{bmatrix},$$
$$\mathbf{F}(\mathbf{x}, \Omega t; \boldsymbol{\mu}) = \begin{bmatrix} x_2 \\ -2\zeta\omega_0 x_2 - \omega_0^2 x_1 + \mu_1 + \frac{\mu_2}{2}\left(e^{i\Omega t} + e^{-i\Omega t}\right) \end{bmatrix}.$$

For $\boldsymbol{\mu}_0 = (a_0, 0)^T$, we have the equilibrium $\mathbf{x}_0 = \left(\frac{a_0}{\omega_0^2}, 0\right)^T$ for system (39). In this linear setting, for any perturbation $\boldsymbol{\delta} = \boldsymbol{\mu} - \boldsymbol{\mu}_0$, i.e., $\delta_1 = a - a_0, \delta_2 = b$, system (39) has a unique periodic steady state. Indeed, substituting the ansatz (37) into (39) and comparing coefficients for $\boldsymbol{\ell} = \mathbf{e}_1, \mathbf{e}_2$ and $\kappa = -1, 0, 1$, we obtain (see Appendix E.2 for calculations)

$$\mathbf{x}^\star(\boldsymbol{\mu}, t) = \mathbf{x}_0 + \underbrace{\frac{1}{\omega_0^2}\begin{bmatrix} 1 \\ 0 \end{bmatrix}}_{\mathbf{x}_{0,\mathbf{e}_1}} \delta_1 + \underbrace{\frac{1}{-2\Omega^2 + \mathrm{i}4\zeta\omega_0\Omega + 2\omega_0^2}\begin{bmatrix} 1 \\ \mathrm{i}\Omega \end{bmatrix}}_{\mathbf{x}_{1,\mathbf{e}_2}} \delta_2 e^{\mathrm{i}\Omega t} + \underbrace{\frac{1}{-2\Omega^2 - \mathrm{i}4\zeta\omega_0\Omega + 2\omega_0^2}\begin{bmatrix} 1 \\ -\mathrm{i}\Omega \end{bmatrix}}_{\mathbf{x}_{-1,\mathbf{e}_2}} \delta_2 e^{-\mathrm{i}\Omega t}. \tag{40}$$

We now introduce new variables $\boldsymbol{\alpha}, \boldsymbol{\beta} \in \mathbb{T}^f$ as

$$\alpha_j = e^{\mathrm{i}\Omega_j t}, \beta_j = e^{-\mathrm{i}\Omega_j t}, j = 1, \ldots, f, \tag{41}$$

which allow us to express the Taylor-Fourier expansion (38) as a polynomial in the variables $\boldsymbol{\gamma} = (\boldsymbol{\alpha}, \boldsymbol{\beta}) \in \mathbb{T}^{2f}$ as

$$\mathbf{F}(\mathbf{x}; \boldsymbol{\mu}, \boldsymbol{\Omega} t) = \sum_{j,k \in \mathbb{N}_0, \boldsymbol{c} \in \mathbb{N}_0^{2f}} \mathbf{f}_{j,k,\boldsymbol{c}}(\underbrace{\mathbf{x}, \ldots, \mathbf{x}}_{j \text{ times}}; \underbrace{\boldsymbol{\mu}, \ldots, \boldsymbol{\mu}}_{k \text{ times}}) \boldsymbol{\gamma}^{\boldsymbol{c}}, \tag{42}$$

where $\mathbf{f}_{j,k,\boldsymbol{c}} \in \left(\mathbb{R}^N\right)^j \times (\mathbb{R}^m)^k \to \mathbb{R}^N$ are multilinear functions associated with the monomial $\boldsymbol{\gamma}^{\boldsymbol{c}} = \boldsymbol{\alpha}^{\boldsymbol{a}} \boldsymbol{\beta}^{\boldsymbol{b}} \in \mathbb{C}$ with the multi-indices $\boldsymbol{c} = (\boldsymbol{a}, \boldsymbol{b}) \in \mathbb{N}_0^{2f}$. Comparing the polynomial expression (42) with the Taylor-Fourier expression (38), we have $\mathbf{f}_{j,k,\boldsymbol{c}} = \mathbf{F}_{j,k,\boldsymbol{a}-\boldsymbol{b}}$. However, for a given $\boldsymbol{\kappa} \in \mathbb{Z}^f$ in expansion (38), there is generally no unique choice for $\boldsymbol{c} \in \mathbb{N}_0^{2f}$ in expansion (42). We discuss this redundancy and a canonical choice for $\boldsymbol{c} = (\boldsymbol{\kappa}^+, \boldsymbol{\kappa}^-)$ to resolve it in Appendix A.4.

Using the polynomial expansion (42), we transform the non-autonomous system (35) into an augmented autonomous form as

$$\mathbf{B}\dot{\mathbf{x}} = \mathbf{G}(\mathbf{z}; \boldsymbol{\mu}) \tag{43}$$
$$\dot{\boldsymbol{\alpha}} = \mathrm{i}\mathbf{D}\boldsymbol{\alpha}, \tag{44}$$
$$\dot{\boldsymbol{\beta}} = -\mathrm{i}\mathbf{D}\boldsymbol{\beta}, \tag{45}$$

with $\mathbf{z} = (\mathbf{x}, \boldsymbol{\alpha}, \boldsymbol{\beta})$, $\mathbf{D} = \mathrm{diag}(\Omega_1, \ldots, \Omega_f) \in \mathbb{R}^{f \times f}$, and the right-hand side $\mathbf{G}$ admits a Taylor expansion in terms of its arguments as

$$\mathbf{G}(\mathbf{z}; \boldsymbol{\mu}) = \sum_{j,k \in \mathbb{N}_0} \mathbf{G}_{j,k}(\underbrace{\mathbf{z}, \ldots, \mathbf{z}}_{j \text{ times}}; \underbrace{\boldsymbol{\mu}, \ldots, \boldsymbol{\mu}}_{k \text{ times}}), \tag{46}$$

where the multilinear functions $\mathbf{G}_{j,k} \in \left(\mathbb{R}^{N+2f}\right)^j \times (\mathbb{R}^m)^k \to \mathbb{R}^N$ are directly inferred from the polynomial expansion (42).

Remark 6 The augmented form (43)–(45) allows us to utilize the general expressions developed for computing autonomous invariant manifolds in computing periodic/quasiperiodic manifolds. As we will see in the numerical examples, these expressions also allow us to determine the dependence of these manifolds and their reduced dynamics on the frequency $\boldsymbol{\Omega}$, which appears as an independent linear parameter in (43)-(45).

Next, we determine how the fixed point $\mathbf{x}_0$ perturbs into the trajectory $\mathbf{x}^\star(t; \boldsymbol{\mu})$ under change of parameters, and at the same time, formally compute $\mathcal{W}(\mathcal{E})$, which is a parameter-dependent invariant manifold attached to $\mathbf{x}^\star(t; \boldsymbol{\mu})$ and serves as a nonlinear continuation of $\mathcal{E}$ at each time slice along $\mathbf{x}^\star(t; \boldsymbol{\mu})$.

3.1 Computing the parameter-dependent trajectory $\mathbf{x}^\star(t; \boldsymbol{\mu})$

We express the Taylor-Fourier expansion (37) using the variables $\boldsymbol{\gamma} = (\boldsymbol{\alpha}, \boldsymbol{\beta}) \in \mathbb{T}^{2f}$ as

$$\mathbf{x}^\star(t; \boldsymbol{\mu}) = \sum_{\boldsymbol{\ell} \in \mathbb{N}_0^m, \boldsymbol{c} \in \mathbb{N}_0^{2f}} \mathbf{x}^\star_{\boldsymbol{c},\boldsymbol{\ell}} \boldsymbol{\gamma}^{\boldsymbol{c}} \boldsymbol{\delta}^{\boldsymbol{\ell}}, \tag{47}$$

where $\mathbf{x}^\star_{\boldsymbol{c},\boldsymbol{\ell}} \in \mathbb{C}^N$ is the coefficient vector associated with the monomial $\boldsymbol{\gamma}^{\boldsymbol{c}} \boldsymbol{\delta}^{\boldsymbol{\ell}} = \boldsymbol{\alpha}^{\boldsymbol{a}} \boldsymbol{\beta}^{\boldsymbol{b}} \boldsymbol{\delta}^{\boldsymbol{\ell}} \in \mathbb{C}$ with the multi-indices $(\boldsymbol{c}, \boldsymbol{\ell}) \in \mathbb{N}_0^{2f} \times \mathbb{N}_0^m$. Similarly to the polynomial expansion (42), the elimination of redundancy in ansatz (47) compared to ansatz (37) is discussed in Appendix A.4.

Now, as $\mathbf{x}^\star(t; \boldsymbol{\mu})$ is a parameter-dependent solution trajectory it satisfies (35) or, equivalently, the augmented system (43), i.e,

$$\mathbf{B}\dot{\mathbf{x}}^\star = \mathbf{G}(\mathbf{z}^\star, \boldsymbol{\mu}), \tag{48}$$

where $\mathbf{z}^\star = (\mathbf{x}^\star, \boldsymbol{\alpha}, \boldsymbol{\beta})$. Collecting coefficients of the monomial $\boldsymbol{\delta}^{\boldsymbol{\ell}} \boldsymbol{\alpha}^{\boldsymbol{a}} \boldsymbol{\beta}^{\boldsymbol{b}}$ in Eq. (48), we obtain

$$\left[\mathrm{i}\langle \boldsymbol{a} - \boldsymbol{b}, \boldsymbol{\Omega} \rangle \mathbf{B} - \mathbf{A}\right] \mathbf{x}^\star_{\boldsymbol{c},\boldsymbol{\ell}} = \mathbf{b}_{\boldsymbol{c},\boldsymbol{\ell}}, \tag{49}$$

where the right-hand-side is defined as

$$\mathbf{b}_{\boldsymbol{c},\boldsymbol{\ell}} := \sum_{\substack{j,k\in\mathbb{N}_0,\,(j,k)\neq(0,0)\\ \boldsymbol{\ell}_1+\cdots+\boldsymbol{\ell}_j+\boldsymbol{n}_1+\cdots+\boldsymbol{n}_k=\boldsymbol{\ell},\\ \boldsymbol{c}_1+\cdots+\boldsymbol{c}_j=\boldsymbol{c},\\ (\boldsymbol{\ell}_i,\boldsymbol{c}_i)\neq(\boldsymbol{\ell},\boldsymbol{c}),\forall i\in\{1,\ldots,j\}.}} \mathbf{G}_{j,k}\left(\mathbf{z}^{\star}_{\boldsymbol{c}_1,\boldsymbol{\ell}_1},\ldots,\mathbf{z}^{\star}_{\boldsymbol{c}_j,\boldsymbol{\ell}_j},\boldsymbol{\mu}_{\boldsymbol{n}_1},\ldots,\boldsymbol{\mu}_{\boldsymbol{n}_k}\right). \tag{50}$$

Once again, $\mathbf{b}_{\boldsymbol{c},\boldsymbol{\ell}}$ depends only on lower-degree coefficients $\mathbf{x}^{\star}_{\boldsymbol{d},\boldsymbol{m}}$ with $|\boldsymbol{m}|<|\boldsymbol{\ell}|$ and $|\boldsymbol{d}|\leq|\boldsymbol{c}|$. Hence, $\mathbf{x}^{\star}_{\boldsymbol{c},\boldsymbol{\ell}}$ can be determined up to any desired order in $\mathbf{c},\boldsymbol{\ell}$ by solving the linear system (49) in a recursive fashion with respect to increasing polynomial orders $|\boldsymbol{\ell}|$ and $|\boldsymbol{c}|$, as shown in Algorithm 3 in Algorithm B.

Applying Algorithm 3 to the augmented form of Example 5 with

$$\mathbf{z}=[y,\dot{y},\alpha,\beta]^T,\quad \mathbf{G}(\mathbf{z};\boldsymbol{\mu})=\underbrace{\begin{bmatrix}0\\ \mu_1\end{bmatrix}}_{\mathbf{G}_{0,1}(\boldsymbol{\mu})}+\underbrace{\begin{bmatrix}z_2\\ -2\zeta\omega_0 z_2-\omega_0^2 z_1\end{bmatrix}}_{\mathbf{G}_{1,0}(\mathbf{z})}+\underbrace{\begin{bmatrix}0\\ \mu_2 z_3+\mu_2 z_4\end{bmatrix}}_{\mathbf{G}_{1,1}(\mathbf{z};\boldsymbol{\mu})},$$

we obtain the parameter-dependent periodic trajectory solution (47) by solving system (43) as

$$\mathbf{x}^{\star}(\boldsymbol{\mu},t)=\mathbf{x}_0+\underbrace{\frac{1}{\omega_0^2}\begin{bmatrix}1\\0\end{bmatrix}}_{\mathbf{x}^{\star}_{\mathbf{0},\mathbf{e}_1}}\delta_1+\underbrace{\frac{1}{-2\Omega^2+\mathrm{i}4\zeta\omega_0\Omega+2\omega_0^2}\begin{bmatrix}1\\ \mathrm{i}\Omega\end{bmatrix}}_{\mathbf{x}^{\star}_{\mathbf{e}_1,\mathbf{e}_2}}$$
$$\delta_2\alpha+\underbrace{\frac{1}{-2\Omega^2-\mathrm{i}4\zeta\omega_0\Omega+2\omega_0^2}\begin{bmatrix}1\\ -\mathrm{i}\Omega\end{bmatrix}}_{\mathbf{x}^{\star}_{\mathbf{e}_2,\mathbf{e}_2}}\delta_2\beta.$$

3.2 Parameter-dependent invariant manifold anchored to $\mathbf{x}^{\star}(t;\boldsymbol{\mu})$

We now compute a parameter-dependent periodic/quasiperiodic invariant manifold $\mathcal{W}(\mathcal{E})$ of system (35), anchored at the trajectory $\mathbf{x}^{\star}(t;\boldsymbol{\mu})$ and tangent to $\mathcal{E}$ at the nominal configuration $(\mathbf{x}_0,\boldsymbol{\mu}_0)$. We parametrize $\mathcal{W}(\mathcal{E})$ via the variables $\mathbf{q}=(\mathbf{p},\boldsymbol{\gamma})$, where $\mathbf{p}\in\mathbb{C}^M$ are the coordinatesalong $\mathcal{E}$ and $\boldsymbol{\gamma}\in\mathbb{T}^{2f}$ describe the periodic/quasiperiodic time dependence of $\mathcal{W}(\mathcal{E})$. Accordingly, we pick a Taylor ansatz for the parametrization $\mathbf{W}:\mathbb{C}^{M+2f}\times\mathbb{R}^m\to\mathbb{R}^N$

$$\mathbf{W}(\mathbf{q};\boldsymbol{\mu})=\sum_{\mathbf{n}\in\mathbb{N}_0^{M+2f},\boldsymbol{\ell}\in\mathbb{N}_0^m}\mathbf{w}_{\mathbf{n},\boldsymbol{\ell}}\mathbf{q}^{\mathbf{n}}\boldsymbol{\delta}^{\boldsymbol{\ell}}, \tag{51}$$

where $\mathbf{w}_{\mathbf{n},\boldsymbol{\ell}}\in\mathbb{C}^N$ are the coefficients associated with the monomial $\mathbf{q}^{\mathbf{n}}\boldsymbol{\delta}^{\boldsymbol{\ell}}=\mathbf{p}^{\mathbf{m}}\boldsymbol{\gamma}^{\boldsymbol{c}}\boldsymbol{\delta}^{\boldsymbol{\ell}}\in\mathbb{C}$ with the multi-index $(\mathbf{n},\boldsymbol{\ell})\in\mathbb{N}_0^{M+2f}\times\mathbb{N}_0^m$. We also parametrize the nonautonomous reduced dynamics on $\mathcal{W}(\mathcal{E})$ via the same Taylor ansatz as

$$\dot{\mathbf{p}}=\mathbf{R}(\mathbf{q};\boldsymbol{\mu})=\sum_{\mathbf{n}\in\mathbb{N}_0^{M+2f},\boldsymbol{\ell}\in\mathbb{N}_0^m}\mathbf{r}_{\mathbf{n},\boldsymbol{\ell}}\mathbf{q}^{\mathbf{n}}\boldsymbol{\delta}^{\boldsymbol{\ell}}, \tag{52}$$

where $\mathbf{r}_{\mathbf{n},\boldsymbol{\ell}}\in\mathbb{C}^M$ are the reduced dynamics coefficients associated with the monomial $\mathbf{q}^{\mathbf{n}}\boldsymbol{\delta}^{\boldsymbol{\ell}}$.

Substituting the parametrization (51) into system (43) for any trajectory $\mathbf{x}(t;\boldsymbol{\mu})=\mathbf{W}(\mathbf{q};\boldsymbol{\mu})$ on $\mathcal{W}(\mathcal{E})$ and utilizing its reduced dynamics (52) along with eqs (44)-(45), we obtain the invariance equation for $\mathcal{W}(\mathcal{E})$ as

$$\mathbf{B}\left(\left[\partial_{\mathbf{p}}\mathbf{W}\right]\mathbf{R}+\mathrm{i}\left[\partial_{\boldsymbol{\alpha}}\mathbf{W}\right]\boldsymbol{\Omega}-\mathrm{i}\left[\partial_{\boldsymbol{\beta}}\mathbf{W}\right]\boldsymbol{\Omega}\right)=\mathbf{G}((\mathbf{W},\boldsymbol{\alpha},\boldsymbol{\beta});\boldsymbol{\mu}). \tag{53}$$

We discuss the computational equivalence of the above invariance equation to an autonomous invariance equation in Appendix A.6. Similarly to the autonomous setting, the leading order coefficients in $\mathbf{W}$ are determined via the anchor trajectory $\mathbf{x}^{\star}(t;\boldsymbol{\mu})$ and the eigenvectors associated with $\mathcal{E}$ as

$$\mathbf{w}_{\mathbf{0},\mathbf{0}}=\mathbf{x}_0, \tag{54}$$

$$\mathbf{w}_{\mathbf{e}_j,\mathbf{0}}=\begin{cases}\mathbf{v}_j, & j=1,\ldots,M,\\ \mathbf{0}, & j=M+1,\ldots,M+2f,\end{cases} \tag{55}$$

The leading-order coefficients in $\mathbf{R}$ at the nominal parameter configuration ($\boldsymbol{\delta}=\mathbf{0}$) are determined via the eigenvalues associated with $\mathcal{E}$ as

$$\mathbf{r}_{\mathbf{0},\mathbf{0}}=\mathbf{0}, \tag{56}$$

$$\mathbf{r}_{\mathbf{e}_j,\mathbf{0}}=\begin{cases}\lambda_j\mathbf{e}_j, & j=1,\ldots,M,\\ \mathbf{0}, & j=M+1,\ldots,M+2f.\end{cases} \tag{57}$$

Upon collecting the coefficients of the monomial $\mathbf{q}^{\mathbf{n}}\boldsymbol{\delta}^{\boldsymbol{\ell}}$ in the invariance equation (53) for $|\mathbf{n}|>0$, we obtain the *linear* system

$$[\omega_{\mathbf{n}}\mathbf{B}-\mathbf{A}]\,\mathbf{w}_{\mathbf{n},\boldsymbol{\ell}}=\mathbf{s}_{\mathbf{n},\boldsymbol{\ell}}-\mathbf{D}\mathbf{r}_{\mathbf{n},\boldsymbol{\ell}}, \tag{58}$$

where $\mathbf{n} = (\mathbf{m}, \boldsymbol{a}, \boldsymbol{b}) \in \mathbb{N}_0^{M+2f}$, $\omega_{\mathbf{n}} = \lambda_{\mathbf{m}} + \mathrm{i}\,\langle \boldsymbol{a} - \boldsymbol{b}, \boldsymbol{\Omega}\rangle$, and $\mathbf{s}_{\mathbf{n},\boldsymbol{\ell}} \in \mathbb{C}^N, \mathbf{D} \in \mathbb{C}^{N\times M}$ are defined similarly to the autonomous setting by substituting $\mathbf{G}$ for $\mathbf{F}$ in Appendix C. Once again, $\mathbf{s}_{\mathbf{n},\boldsymbol{\ell}}$ depends only on lower-order coefficients, which allows us to determine the coefficients $\mathbf{w}_{\mathbf{n},\boldsymbol{\ell}}, \mathbf{r}_{\mathbf{n},\boldsymbol{\ell}}$ up to any desired order in $\mathbf{n}, \boldsymbol{\ell}$ by solving the linear system (58) recursively via Algorithm 1. Similarly to the autonomous setting, we discuss how conjugacies in $\boldsymbol{\gamma} = (\boldsymbol{\alpha}, \boldsymbol{\beta})$ can be exploited to further reduce computational costs in Appendix A.5.

4 Nonintrusive computations

The need for nonintrusive computations arises when we do not have comprehensive access to the governing equations, e.g., using commercial modeling software. In such cases, we can only evaluate the right-hand side $\mathbf{F}$ as a black-box function for any specified input $(\mathbf{x}; \boldsymbol{\mu})$. Non-intrusive or indirect methods interface with modeling packages with minimal access to their internal core and hence have a compelling use case. Projection-based model reduction literature has a rich collection of non-intrusive techniques such as the Stiffness Evaluation Procedure (STEP) [40], and its various enhancements (see, e.g., [41, 42]) in the data-free setting. For parameter-dependent systems, these techniques are enhanced by an appropriate interpolation among the bases for the projection subspaces at different parameter values [43]. In the data-driven setting as well, several nonintrusive techniques enable projection-based ROMs for parametric systems via proper orthogonal decomposition (POD) and its variants [44–46].

As model reduction via invariant manifolds has gained increasing attention due to their potential for rigourously capturing nonlinearizable phenomena, there is a growing interest in developing nonintrusive techniques for computing invariant manifolds and their reduced dynamics [27]. Invariant manifolds and their reduced dynamics have also been computed nonintrusively from governing equations via data-driven or data-assisted techniques [47–49]. The expressions developed in Ref. [4] enable data-free nonintrusive computation of invariant manifolds up to arbitrary polynomial orders in systems with up to cubic nonlinearities. We now show how this procedure extends to computing parameter-dependent invariant manifolds.

The expressions developed in the previous sections require explicit access to the multilinear functions $\mathbf{F}_{j,k}$ in the expansion (5). We discuss how these multilinear functions can be computed via black-box evaluations of $\mathbf{F}$. In particular, we will demonstrate that the nonintrusive procedure established in Ref. [4] can be extended to compute parameter-dependent invariant manifolds when $\mathbf{F}$ has an affine dependence on $\boldsymbol{\mu}$, i.e.,

$$\mathbf{F} = \sum_{j=0}^{3} \mathbf{F}_{j,0} + \sum_{j=0}^{3} \mathbf{F}_{j,1}, \tag{59}$$

where $\mathbf{F}_{j,0}$ and $\mathbf{F}_{j,1}$ are multilinear functions defined in the expansion (5). For our nonintrusive setup, we only require

(a) explicit access to the matrix $\mathbf{B}$ and the Jacobian matrices $\mathbf{A}$, $\mathbf{A}_0 := \partial_{\mathbf{x}}\mathbf{F}(\mathbf{0}, \mathbf{0})$, and $\mathbf{A}_i := \partial_{\mathbf{x}}\mathbf{F}(\mathbf{0}, \mathbf{e}_i) - \mathbf{A}_0, i = 1, \ldots, m$;
(b) a black-box evaluation of the function $\mathbf{F}$ for any specified input $(\mathbf{x}; \boldsymbol{\mu})$.

These requirements are typically satisfied even using commercial packages. We first aim for a nonintrusive evaluation of the multilinear components $\mathbf{F}_{1,0}(\mathbf{x})$, $\mathbf{F}_{2,0}(\mathbf{x}_1, \mathbf{x}_2)$ and $\mathbf{F}_{3,0}(\mathbf{x}_1, \mathbf{x}_2, \mathbf{x}_3)$ in (59). As we will see, our nonintrusive algorithm for the multilinear functions $\mathbf{F}_{j,0}$ directly extends to $\mathbf{F}_{j,1}$. To this end, we express the $\boldsymbol{\mu}-$dependence in (59) explicitly as

$$\mathbf{F}(\mathbf{x}; \boldsymbol{\mu}) = \mathbf{F}_0(\mathbf{x}) + \sum_{i=1}^{m} \mu_i \mathbf{F}_1^{(i)}(\mathbf{x}),$$

where $\mathbf{F}_0(\mathbf{x})$ denotes the component of $\mathbf{F}$ that is independent of $\boldsymbol{\mu}$ and $\mathbf{F}_1^{(i)}(\mathbf{x})$ is associated with linear dependence of $\mathbf{F}$ on μ_i. We note that these components can be computed via nonintrusive calls to $\mathbf{F}$ as

$$\mathbf{F}_0(\mathbf{x}) = \mathbf{F}(\mathbf{x}; \mathbf{0}) \tag{60}$$

$$\mathbf{F}_1^{(i)}(\mathbf{x}) = \mathbf{F}(\mathbf{x}; \mathbf{e}_i) - \mathbf{F}(\mathbf{x}; \mathbf{0}), \quad i = 1, \ldots, m. \tag{61}$$

Furthermore, $\mathbf{F}_0$ and $\mathbf{F}_1^{(i)}$'s can each have up to cubic dependence on $\mathbf{x}$. Specifically, for $\mathbf{F}_0(\mathbf{x})$ we have

$$\mathbf{F}_0(\mathbf{x}) = \mathbf{f}_0 + \mathbf{f}_1(\mathbf{x}) + \mathbf{f}_2(\mathbf{x}) + \mathbf{f}_3(\mathbf{x}), \tag{62}$$

where $\mathbf{f}_0, \mathbf{f}_1, \mathbf{f}_2$, and $\mathbf{f}_3$ denote the constant, linear, quadratic, and cubic components of $\mathbf{F}_0$. The nonintrusive algorithm involves two steps:

1. *Nonintrusive evaluation of* $\mathbf{f}_j(\mathbf{x})$. By separating the constant term $\mathbf{f}_0 = \mathbf{F}_0(\mathbf{0})$ and the linear term $\mathbf{f}_1(\mathbf{x}) = \mathbf{A}_0\mathbf{x}$, we evaluate the nonlinear part of $\mathbf{F}_0$ nonintrusively as

$$\mathbf{f}_{\mathrm{nl}}(\mathbf{x}) := \mathbf{f}_2(\mathbf{x}) + \mathbf{f}_3(\mathbf{x}) = \mathbf{F}_0(\mathbf{x}) - \mathbf{A}_0\mathbf{x} - \mathbf{F}_0(\mathbf{0}). \tag{63}$$

Using this nonintrusive evaluation of $\mathbf{f}_{\text{nl}}$, and using the fact that $\mathbf{f}_2$ is an even function and $\mathbf{f}_3$ is an odd function, we obtain a nonintrusive evaluation of $\mathbf{f}_2$ and $\mathbf{f}_3$ as

$$\mathbf{f}_2(\mathbf{x}) = \frac{\mathbf{f}_{\text{nl}}(\mathbf{x}) + \mathbf{f}_{\text{nl}}(-\mathbf{x})}{2}, \quad \mathbf{f}_3(\mathbf{x}) = \frac{\mathbf{f}_{\text{nl}}(\mathbf{x}) - \mathbf{f}_{\text{nl}}(-\mathbf{x})}{2}. \tag{64}$$

Hence, we can now evaluate $\mathbf{f}_0, \mathbf{f}_1, \mathbf{f}_2$ and $\mathbf{f}_3$ via nonintrusive function calls to $\mathbf{F}_0$, which can in turn be evaluated via nonintrusive calls to $\mathbf{F}$.

2. *Evaluation of multi-linear function* $\mathbf{F}_{j,0}(\mathbf{x}_1, \cdots, \mathbf{x}_j)$ *via* $\mathbf{f}_j$. We note that $\mathbf{F}_{0,0}, \mathbf{F}_{1,0}$ can be nonintrusively evaluated as $\mathbf{F}_{0,0} = \mathbf{f}_0$, $\mathbf{F}_{1,0}(\mathbf{x}) = \mathbf{f}_1(\mathbf{x})$. For the bilinear function $\mathbf{F}_{2,0}(\mathbf{x}_1, \mathbf{x}_2)$, we utilize the nonintrusive evaluation of $\mathbf{f}_2$ in the previous step to obtain

$$\mathbf{F}_{2,0}(\mathbf{x}_1, \mathbf{x}_2) = \frac{\mathbf{f}_2(\mathbf{x}_1 + \mathbf{x}_2) - \mathbf{f}_2(\mathbf{x}_1 - \mathbf{x}_2)}{4}. \tag{65}$$

When $\mathbf{x}_1 = \mathbf{x}_2$, the above formula reduces to $\mathbf{F}_{2,0}(\mathbf{x}_1, \mathbf{x}_1) = \mathbf{f}_2(\mathbf{x}_1)$, as expected from the definition (62) of $\mathbf{f}_2$. Similarly, we obtain a nonintrusive evaluation of $\mathbf{F}_{3,0}$ via $\mathbf{f}_3$ as

$$\mathbf{F}_{3,0}(\mathbf{x}_1, \mathbf{x}_2, \mathbf{x}_3) = \frac{\mathbf{f}_3(\mathbf{x}_1 + \mathbf{x}_2 + \mathbf{x}_3) + \mathbf{f}_3(\mathbf{x}_1) + \mathbf{f}_3(\mathbf{x}_2) + \mathbf{f}_3(\mathbf{x}_3)}{6} - \frac{\mathbf{f}_3(\mathbf{x}_1 + \mathbf{x}_2) + \mathbf{f}_3(\mathbf{x}_2 + \mathbf{x}_3) + \mathbf{f}_3(\mathbf{x}_1 + \mathbf{x}_3)}{6}. \tag{66}$$

Once again, in the special case that $\mathbf{x}_1 = \mathbf{x}_2 = \mathbf{x}_3$, the formula above is reduced as $\mathbf{F}_{3,0}(\mathbf{x}_1, \mathbf{x}_1, \mathbf{x}_1) = \mathbf{f}_3(\mathbf{x}_1)$. Thus, we can now evaluate $\mathbf{F}_{j,0}(\mathbf{x}_1, \cdots, \mathbf{x}_j)$ via nonintrusive calls to $\mathbf{f}_j$.

Replacing $\mathbf{F}_0$ by $\mathbf{F}_1^{(i)}$ in (62) and $\mathbf{A}_0$ by $\mathbf{A}_i$ in (63) for each $i = 1, \ldots, m$ and following the above two steps enables us to evaluate $\mathbf{F}_{j,1}(\mathbf{x}_1, \cdots, \mathbf{x}_j, \boldsymbol{\mu})$ nonintrusively.

5 Numerical examples

We consider a suite of examples to demonstrate the effectiveness of the proposed reduction approach. These examples are divided into three groups

(i) reduction on autonomous invariant manifolds;
(ii) reduction on nonautonomous invariant manifolds truncated at leading-order nonautonomous terms. This truncation saves computational cost and enables the transformation of periodic/quasi-periodic orbits of the full system into the fixed points/limit cycles of the associated reduced-order models;
(iii) reduction on nonautonomous invariant manifolds that take higher-order nonautonomous contributions into consideration. These higher-order contributions are essential to capture superharmonic and parametric resonances.

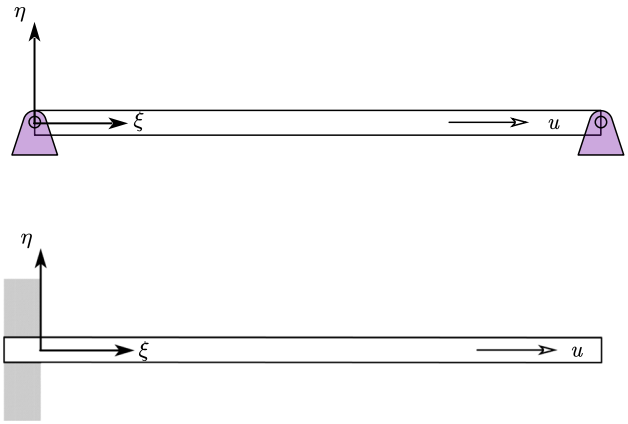

Fig. 2 A simply supported and a cantilevered pipe conveying fluid. Here u denotes flow velocity, ξ represents the dimensionless arc length, and $\eta(\xi, t)$ is the pipe deflection. The dashed lines mark the deformed configurations of the pipes

When illustrating results for periodic solutions, we will denote the maximal value of a periodic function over its period by $\| \bullet \|_\infty$.

5.1 Reduction on autonomous invariant manifolds

5.1.1 Slow manifold of a buckled pipe conveying fluid

We consider a simply-supported pipe conveying fluid shown in Fig. 2. This pipe system contains flow-induced gyroscopic forces and nonlinear damping. The straight pipe configuration will be buckled when the flow exceeds a critical value. Our goal is to perform model reduction via the SSM anchored at its nontrivial buckled configuration that depends on the flow velocity.

The dimensionless PDEs governing transverse oscillations of this simply-supported pipe, considering geometric nonlinearities and fluid flow at a constant velocity u, were discretized via the Galerkin method in [50]. We utilize the expressions in [50] to obtain a two-mode Galerkin model as

$$\begin{aligned}
&\ddot{y}_1 + \alpha\pi^4\dot{y}_1 - \frac{16}{3}\sqrt{\beta}u\dot{y}_2 + \pi^2(\pi^2 - u^2)y_1 \\
&\quad + \frac{\mu}{2}\pi^4 y_1\left(y_1^2 + 4y_2^2\right) + \alpha\mu\pi^4 y_1\left(y_1\dot{y}_1 + 4y_2\dot{y}_2\right) = 0, \\
&\ddot{y}_2 + \frac{16}{3}\sqrt{\beta}u\dot{y}_1 + 16\alpha\pi^4\dot{y}_2 + 4\pi^2(4\pi^2 - u^2)y_2 \\
&\quad + 2\mu\pi^4 y_2\left(y_1^2 + 4y_2^2\right) + 4\alpha\mu\pi^4 y_2\left(y_1\dot{y}_1 + 4y_2\dot{y}_2\right) = 0.
\end{aligned} \tag{67}$$

Here, y_i is the modal amplitude associated with the eigenfunction $\phi_j(\xi) = \sqrt{2}\sin(j\pi\xi)$, α is a dimensionless damping coefficient, β denotes a mass ratio, u is dimensionless flow velocity, and μ represents the slenderness of the pipe. This pipe is buckled in the first mode for $u \geq \pi$, and the associated nontrivial equilibria are given as

$$y_1^* = \pm\sqrt{\frac{2(u^2-\pi^2)}{\mu\pi^2}}, \quad y_2^* = 0. \tag{68}$$

Following the parameter dependence of equilibria in (68), we take $\boldsymbol{\mu} = (u, \mu)$ and compute the slowest SSM of the positive buckled configuration. We set $\boldsymbol{\mu}_0 = (3.6, 1000)$ such that the anchor point of SSM reduction is a nontrivial fixed point. This setup is different from the planar example in Sect. 2.4, where the anchor point is the origin. Moreover, the dimension of the slowest SSM in this example is two-dimensional, and hence, the dimension is reduced from four to two. Here, we compute the $\mathcal{O}(3, 1)$ approximation of the parameter-dependent equilibrium and its associated SSM, where $\mathcal{O}(n_p, n_\mu)$ denotes the truncation of the Taylor series at orders n_p and n_μ for the reduced coordinates $\mathbf{p}$ and the parameter deviation $\boldsymbol{\delta}$, respectively. The linear expansion in $\boldsymbol{\delta}$ allows us to extract the sensitivity of the equilibrium and of the SSM with respect to the parameters.

In the rest of the computations, we set $\alpha = 0.001$ and $\beta = 0.5$. Let $(x_1, x_2, x_3, x_4) = (y_1, y_2, \dot{y}_1, \dot{y}_2)$, we can rewrite the second-order ODEs (67) as the first-order form with $\mathbf{B} = \mathbf{I}_4$ and accordingly

$$\mathbf{A} = \begin{pmatrix} 0 & 0 & 1 & 0 \\ 0 & 0 & 0 & 1 \\ -\pi^2\left(\pi^2 - u^2 + 1.5\mu\pi^2(y_1^*)^2\right) & 0 & -\alpha\pi^4(1+\mu(y_1^*)^2) & \frac{16}{3}\sqrt{\beta}u \\ 0 & 4\pi^2\left(4\pi^2 - u^2 + 0.5\mu\pi^2(y_1^*)^2\right) & -\frac{16}{3}\sqrt{\beta}u & -16\alpha\pi^4 \end{pmatrix}. \tag{69}$$

The multilinear functions $\mathbf{F}_{j,k}$ can be directly inferred from (67) and are not listed here for brevity. The reduced dynamics on the parameter-dependent SSM is given as below (see (131) and (132))

$$\begin{aligned} \dot{\rho} &= (-0.0726771 - 0.0678322\delta_u)\rho \\ &\quad +(0.0409707 - 7.950881\delta_u + 4.097073\times 10^{-3}\delta_\mu)\rho^3, \\ \dot{\vartheta} &= 7.235509 + 8.090225\delta_u \\ &\quad -(6.187606 - 2.102311\times 10^3\delta_u + 0.6187606\delta_\mu)\rho^2, \end{aligned} \tag{70}$$

where we have used the notation $\boldsymbol{\delta} = (\delta_u, \delta_\mu)$ in this example. The expansion coefficients at the zeroth order in $\mathbf{p}$ are given as

$$\mathbf{w}_{\mathbf{0},\mathbf{0}} = \begin{pmatrix} 0.0250249 \\ \mathbf{0}_{3\times 1} \end{pmatrix}, \quad \mathbf{w}_{\mathbf{0},\mathbf{e}_1} = \begin{pmatrix} 0.0291515 \\ \mathbf{0}_{3\times 1} \end{pmatrix}, \quad \mathbf{w}_{\mathbf{0},\mathbf{e}_2} = \begin{pmatrix} -1.251244\times 10^{-5} \\ \mathbf{0}_{3\times 1} \end{pmatrix} \tag{71}$$

which are consistent with the parameter-dependent equilibrium in (68), namely, $y_1^* \approx 0.0250249$, $\partial_u y_1^* \approx 0.0291515$, and $\partial_\mu y_1^* \approx -1.251244 \times 10^{-5}$ at the nominal value of parameters.

We also present the sensitivity of the expansion coefficients at the cubic order in $\mathbf{p}$ in Appendix E.3. We also consider an alternative approach to obtain results above and validate the proposed algorithm's effectiveness. In particular, we solve the augmented invariance equation (see the computational note in Appendix A.6) to perform reduction on the parameter-dependent invariant manifold [15]. This technique involves the shift of equilibrium to the origin, the reformulation of nonlinearity due to the shift, and the extension of the phase space with the dummy variables. Thus, the dummy variable approach is cumbersome; relative to the proposed algorithm. More details about this approach can be found in Appendix E.3.

Computational results show that the dummy variable approach produces consistent results with the proposed algorithm. Specifically, the maximum relative error for the expansion coefficients shown in (70) is 1.6×10^{-3}, and the relative errors for the sensitivity in (115) and (116) are given as follows

$$\begin{aligned} &\mathrm{RelTol}(\mathbf{w}_{(3,0),\mathbf{e}_1}) \approx 2.2\times 10^{-15}, \quad \mathrm{RelTol}(\mathbf{w}_{(2,1),\mathbf{e}_1}) \approx 1.5\times 10^{-14}, \\ &\mathrm{RelTol}(\mathbf{w}_{(3,0),\mathbf{e}_2}) \approx 9.8\times 10^{-15}, \quad \mathrm{RelTol}(\mathbf{w}_{(2,1),\mathbf{e}_2}) \approx 52\times 10^{-14}. \end{aligned} \tag{72}$$

We note that the reduced phase space dimension in our approach is two, while that of the dummy variable approach is four because of the two dummy variables. Altogether, this suggests the accuracy and efficiency of the proposed algorithm.

5.1.2 Unstable manifold of a fluttered pipe conveying fluid

Now we consider a cantilevered pipe conveying fluid shown in Fig. 2. As the flow velocity exceeds a critical value, this

pipe undergoes flutter rather than the buckling observed in the simply supported configuration. Flutter is an instability associated with a Hopf bifurcation, where the asymptotically stable equilibrium becomes an unstable focus post flutter, and the trajectories approach a limit cycle along a two-dimensional unstable manifold. Here, we perform a flow velocity-dependent reduction along this unstable manifold.

Following [15], the equations of motion for such a cantilevered pipe system after a four-mode Galerkin discretization can be written as

$$\begin{aligned}\mathbf{M}\ddot{\mathbf{y}} + (\mathbf{C}^{(1)} + u\mathbf{C}^{(2)})\dot{\mathbf{y}} + (\mathbf{K}^{(1)} + u^2\mathbf{K}^{(2)})\mathbf{y} \\ +\mathbf{f}(u, \mathbf{y}, \dot{\mathbf{y}}) = \mathbf{0},\end{aligned} \tag{73}$$

where we have made the flow velocity explicit in the equations of motion to highlight the dependence on the flow velocity. Detailed expressions of these matrices and nonlinear functions can be found in [15]. Model reduction of this system along stable and unstable SSMs at *prescribed* flow velocities has been explored in [51]. Taking the flow velocity as a parameter, reduction on parameter-dependent unstable manifold has also been investigated via the dummy variable approach in [15].

Here, we use the proposed algorithm to perform reduction on a parameter-dependent unstable manifold in the post-flutter region. In contrast to [15], our algorithm does not introduce dummy variables and enables us to control the expansion orders in reduced coordinates and parameters independently.

With the phase space variables $\mathbf{x} = (\mathbf{y}, \dot{\mathbf{y}})$, the equations of motion (73) can be rewritten in the the first-order form (1) with $\mathbf{B} = \mathbf{I}_4$ and

$$\mathbf{F}(\mathbf{x}, u) = \begin{pmatrix} \dot{\mathbf{y}} \\ -\mathbf{M}^{-1}\Big((\mathbf{C}^{(1)}+u\mathbf{C}^{(2)})\dot{\mathbf{y}}+(\mathbf{K}^{(1)}+u^2\mathbf{K}^{(2)})\mathbf{y} \\ +\mathbf{f}(u, \mathbf{y}, \dot{\mathbf{y}})\Big) \end{pmatrix}. \tag{74}$$

We choose the system parameters as $\alpha = 0.001$, $\beta = 0.2$. The system undergoes a supercritical Hopf bifurcation at $u \approx 5.652$. We compute invariant manifolds that depend on the flow velocity u with the nominal value $u_0 = 6.4$ and perform reduction on the parameter-dependent unstable manifold in the post flutter regime. Therefore, the dimension of phase space is reduced from 8 to 2.

The pipe undergoes limit cycle oscillations in the post-flutter region. Such a limit cycle corresponds to a non-spurious fixed point ρ^* of the reduced dynamics (131) in polar coordinates. The period of this limit cycle can be computedvia (132). We map this limit cycle in reduced coordinates to the full system and then plot the amplitude and period of the limit cycle as a function of the flow velocity in Fig. 3. Here, w denotes the deflection at the free end of the pipe. We have fixed the expansion order in the reduced coordinate vector $\mathbf{p}$ to be 9 throughout this example in the computations because it is sufficient to yield converged solutions [51]. We gradually increase the truncation order in $\boldsymbol{\delta}$ and find that a cubic expansion in $\boldsymbol{\delta}$ is sufficient to yield converged solutions for $u \leq 7$ and the converged results match well with the reference solution obtained via a collocation method implemented in the continuation package COCO [52–54]. Here, the limited interval of convergence is attributed to the domain of analyticity of the Taylor expansion in $\boldsymbol{\delta}$.

We note that one can also select u_0 below the critical value where the Hopf bifurcation occurs and use the associated parameter-dependent SSM to perform model reduction. As shown in Fig. 13 and detailed in Appendix E.4, negative real eigenvalues appear only after the Hopf bifurcation; hence, the accumulation of outer resonances reported in [30] does not exist in this example. For $u_0 = 5.9$, the associated parametric ROM can also predict the limit cycle in the post-flutter regime, as illustrated in Fig. 14 and detailed in Appendix E.4. This is expected because the non-resonance condition holds through the Hopf bifurcation, which implies the persistence of SSM coefficients through the transition. We observe that this reduction predicts the limit cycle well for $u < 5.85$, which is a smaller range than the case of $u_0 = 6.4$ (cf. Fig. 3). Due to the limited domain of analyticity of the expansion in $\boldsymbol{\delta}$, a value of u_0 in the post-flutter regime is beneficial for enhancing the range of flow velocities over which limit cycles can be predicted.

We conclude this example by discussing the case of accumulated resonances [30]. When the damping coefficient is increased to $\alpha = 0.01$, two negative real eigenvalues appear before the Hopf bifurcation at $u = u_{\mathrm{HB}} \approx 5.978$ (see Fig. 15 and Appendix E.4). While this indicates the accumulation of resonances near the bifurcation [30], analysis in Appendix E.4 reveals that these resonances occur only at order 100 or higher. Since lower-order expansion coefficients persist through the bifurcation, we can successfully employ a lower-order truncated, parameter-dependent SSM for model reduction [30]. To demonstrate this, we perform the parametric SSM reduction by selecting $u_0 = 5.9$ and predict limit cycle oscillations in the post-flutter regime. As shown Fig. 16 and Appendix E.4, converged solutions are obtained for $u_{\mathrm{HB}} \leq u < 6.3$. Thus, the lower-order truncated ROM effectively predicts limit cycles in the post-flutter regime. Here, the limited domain of convergence arises not from accumulated resonances, but from a limited domain of analyticity of the expansion.

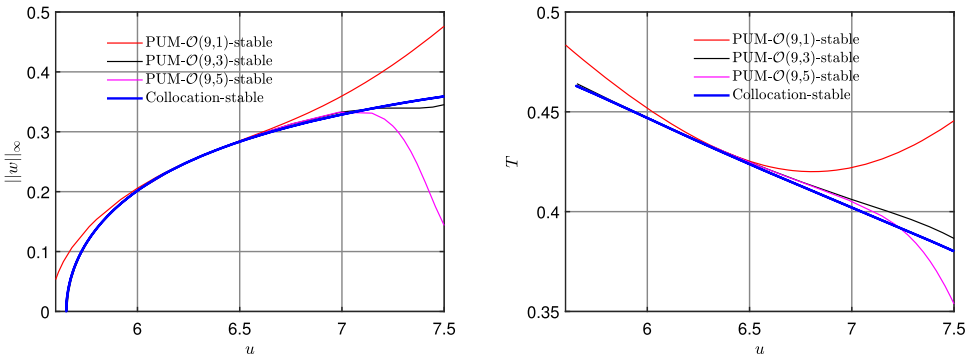

Fig. 3 Amplitude (left panel) and period (right panel) of limit cycle in the post-flutter region as functions of the flow velocity u. Here and throughout this paper, PUM denotes a parameter-dependent unstable manifold. Reference solutions obtained from the collocation method applied to the full system (73)

5.2 Leading-order nonautonomous reduction

As shown in previous studies of SSM reduction for harmonically forced mechanical systems, leading-order nonautonomous reduction is often sufficient to yield accurate predictions when the forcing frequency is near one of the natural frequencies. More importantly, this leading-order truncation enables simplification of the reduced dynamics. Specifically, periodic and quasi-periodic orbits of full systems are transformed into fixed points and limit cycles of the associated reduced-order models [55–57]. This simplification enables effective bifurcation analysis of the forced response of the mechanical systems. In this case, the equation of motion (35) is of the special form below

$$\mathbf{B}\dot{\mathbf{x}} = \mathbf{F}(\mathbf{x};\boldsymbol{\mu}) + \epsilon\mathbf{F}^{\text{ext}}(\Omega t) \tag{75}$$

We follow the same approach documented in [2, 55] to extract the leading-order nonautonomous contribution. As detailed in Appendix F, we can indeed extend the simplification into reduction on parameter-dependent invariant manifolds of mechanical systems.

5.2.1 A shallow shell with internal resonance

In this subsection, we consider a shallow shell structure with 1:2 internal resonance. This shell is simply supported at the two opposite edges aligned along the y-axis in Fig. 4. We tune the radius of curvature such that the natural frequencies of the first two modes admit a 1:2 internal resonance. Geometric and material properties of this structure can be found in [55]. We use flat facet shell finite elements to discretize the structure, resulting in a finite element model with 400 elements and 1,320 DOFs. The governing equations of this finite element model are listed below

$$\mathbf{M}\ddot{\mathbf{y}} + (\alpha\mathbf{M} + \beta E\mathbf{K}_e)\dot{\mathbf{y}} + E(\mathbf{K}_e\mathbf{y} + \mathbf{f}_e(\mathbf{y})) = \epsilon\mathbf{f}^{\text{ext}}\cos\Omega t. \tag{76}$$

Here, we have adopted Rayleigh damping and noted that the stiffness matrix and nonlinear internal force vector depend linearly on the Young's modulus E. In particular, $\mathbf{K}_e$ and $\mathbf{f}_e(\mathbf{z})$ are the system's stiffness matrix and nonlinear internal force vector when $E = 1$.

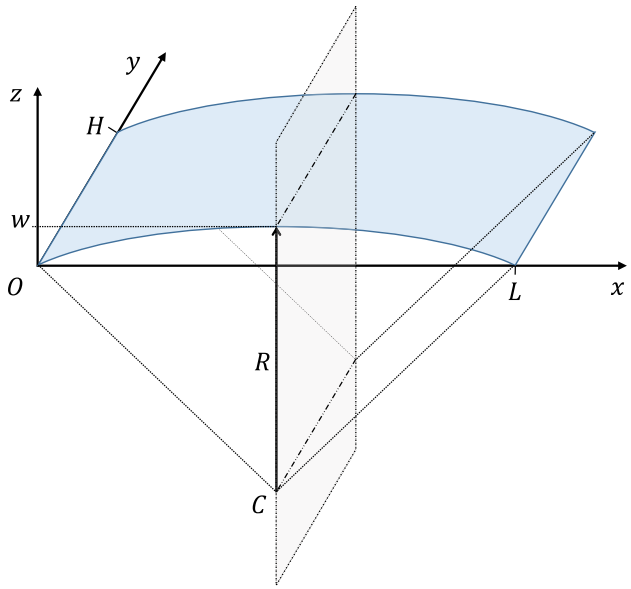

Fig. 4 The schematic of a shallow shell structure [2, 55]

In the next computations, we take the Young's modulus E as the parameter to perform model reduction on parameter-dependent SSMs in this high-dimensional finite element problem. The nominal value of the Young's modulus is given as $E_0 = 70 \times 10^9$ Pa. The constants α and β are chosen such that the damping ratios of the first two modes are 0.2% at $E = E_0$. Accordingly, the eigenvalues of the first two pairs of modes of the FE model are listed below [55]

$$\lambda_{1,2} = -0.30 \pm 149.22\text{i}, \quad \lambda_{3,4} = -0.60 \pm 298.78\text{i}. \tag{77}$$

Let $\mathbf{x} = (\mathbf{y}, \dot{\mathbf{y}})$, the equations of motion (76) at $\epsilon = 0$ can be rewritten in the form (75) with

$$\mathbf{B} = \begin{pmatrix} \alpha\mathbf{M} & \mathbf{M} \\ \mathbf{M} & \mathbf{0} \end{pmatrix},$$

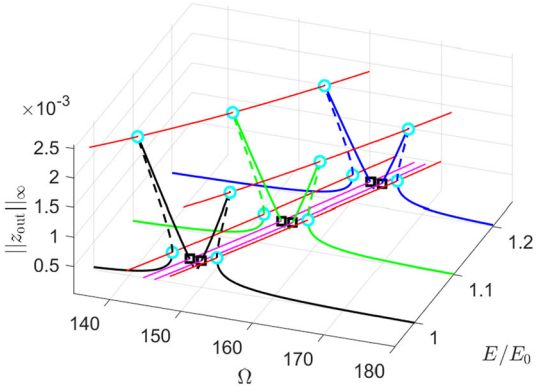

Fig. 5 A family of forced response curves with $E/E_0 \in \{1, 1.1, 1.2\}$ along with the four curves of saddle-node bifurcated periodic orbits (in red lines) and two curves of Neimark-Sacker bifurcated periodic orbits (in magenta lines) under the variations in E and Ω

$$\mathbf{F}(\mathbf{x}, E) = \begin{pmatrix} -E\left(\beta \mathbf{K}_e \dot{\mathbf{y}} + \mathbf{K}_e \mathbf{y} + \mathbf{f}_e(\mathbf{y})\right) \\ \mathbf{M}\dot{\mathbf{y}} \end{pmatrix},$$
$$\mathbf{F}^{\text{ext}}(\Omega t) = \begin{pmatrix} \mathbf{f}^{\text{ext}} \cos \Omega t \\ \mathbf{0} \end{pmatrix}. \tag{78}$$

We take the first two pairs of modes as the master subspace for model reduction. Thus, the phase space dimension is reduced from 2,640 to four. A concentrated load $\epsilon 100 \cos \Omega t$ in the $z-$ direction is applied at mesh node with $(x, y) = (0.25L, 0.5H)$. We then use the four-dimensional ROM (139) to study the forced response of the system in the parameter space (E, ϵ, Ω). In particular, we obtain a family of forced response curves with $E/E_0 \in \{1, 1.1, 1.2\}$ shown in Fig. 5. As expected, the peak amplitude of FRC decreases with increasing E. We observe that there are four saddle-node bifurcation points and two Neimark-Sacker bifurcation points on each of these FRCs. Such bifurcations have been observed and analyzed for systems with 1:2 internal resonance in Ref. [57]. Since they correspond to the saddle-node and Hopf bifurcated fixed points of the ROM (139), we use parameter continuation in COCO to extract the solution manifolds of these codimension-1 bifurcation points under the variations in (E, Ω) and obtain the bifurcation curves shown in Fig. 5.

We have used $\mathcal{O}(5, 3)$ expansion in the above computations. Indeed, as illustrated in [55], the forced response curve of this system converges well at $\mathcal{O}(5)$ approximation in the reduced coordinate vector $\mathbf{p}$. Next, we show that the cubic expansion in $\boldsymbol{\delta}$ is sufficient to generate converged solutions with increasing expansion orders in the parameter. Specifically, we compute the FRC at $E = 1.2E_0$ using $\mathcal{O}(5, 1)$, $\mathcal{O}(5, 2)$, and $\mathcal{O}(5, 3)$ expansions, and the obtained results are shown in the left panel of Fig. 6. We observe that the FRC at $\mathcal{O}(5, 1)$ is very different from that at $\mathcal{O}(5, 2)$, while the FRC at $\mathcal{O}(5, 2)$ is very close to that of $\mathcal{O}(5, 3)$. This suggests that the forced response converges at $\mathcal{O}(5, 3)$ expansion.

We further compare the predicted parameter-dependent FRC from with a direct SSM computation. Here, we construct a full system model at a prescribed value of the parameter and compute an SSM-based FRC for this model. We refer to this approach as *direct computation* in this paper. Such a direct reduction serves as a reference solution as it eliminates the truncation error in $\boldsymbol{\delta}$. We perform this direct comparison for Young's modulus $E = 1.2E_0$ as shown in the right panel of Fig. 6, where the reference solution from direct SSM computation matches well with that from our parameter-dependent SSM (PSSM) constructed around E_0.

5.2.2 An exhaust cover plate with geometric and damping nonlinearities modelled via COMSOL

As our next example, we consider the FE model of a cover plate shown in Fig. 7, which is a part of the exhaust system of a large diesel engine [58]. The welded boundary of this plate is modeled via a series of 80 linear springs in the radial direction, each having a stiffness of 650 N/m. The diameter and thickness of the plate are 317.5 mm and 1.5 mm. Other geometric parameters of the plate can be found in [58]. For material parameters, we consider the Young's modulus of 96 GPa, the Poisson ratio of 0.3, and the density of 5120 kg/m^3. We use a Kelvin-Voigt model of damping with the viscosity

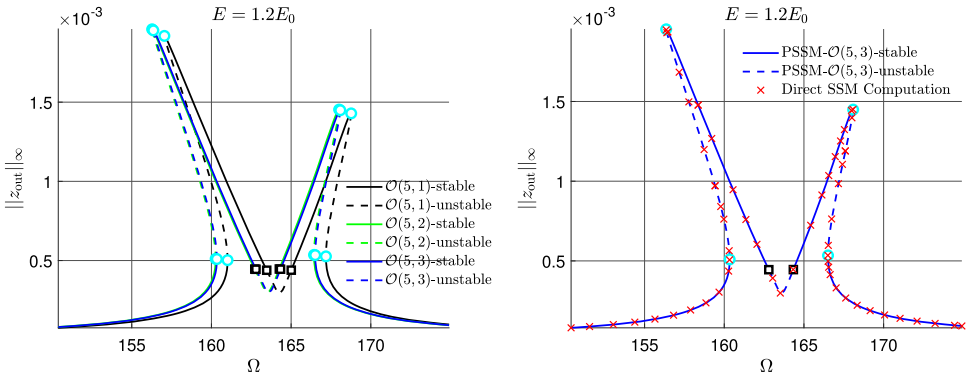

Fig. 6 (Left) Forced response curves of the shell at $E = 1.2E_0$, obtained via reduction on the parameter-dependent spectral manifold with various truncation orders. (Right) FRC obtained via $\mathcal{O}(5, 3)$ reduction PSSM along with reference solutions obtained from direct reduction on SSM at $E = 1.2E_0$

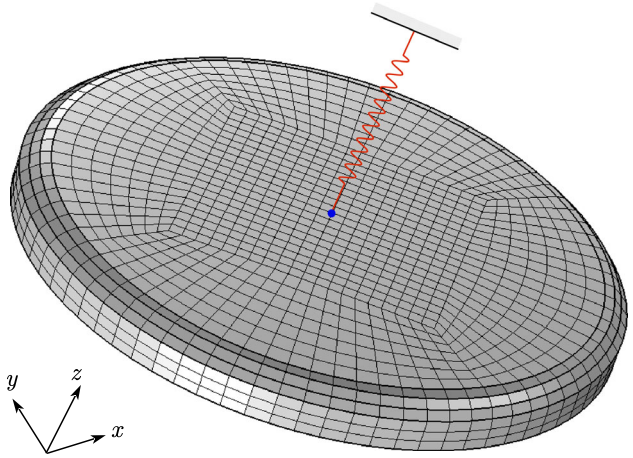

Fig. 7 A schematic plot of the mesh for the FE model of the cover plate with an attached cubic spring

parameter as 0.6 MPa. We note that this model results in damping nonlinearities in the equations of motion.

Model reduction of this finite element problem via SSMs has been performed in [4]. It was found that this system displays a softening-type behavior. Here, we revisit this problem but also attach a cubic spring at the center of the plate. With the added spring, we expect that the backbone curve of the system will display a more complex shape because the spring introduces hardening features. We take the spring stiffness k_3 as the parameter and perform a reduction on the associated parameter-dependent SSM. This finite element model is obtained via COMSOL Multiphysics, a commercial software supporting nonlinear force evaluations for generalized positions and velocities [4]. We use the nonintrusive technique detailed in Sect. 4 to compute a parameter-dependent SSM in this problem.

The equations of motion are of the form below

$$\mathbf{M}\ddot{\mathbf{y}} + \mathbf{C}\dot{\mathbf{y}} + \mathbf{K}\mathbf{y} + \mathbf{f}(\mathbf{y}, \dot{\mathbf{y}}, k_3) = \epsilon \mathbf{f}^{\text{ext}} \cos \Omega t. \tag{79}$$

For $\mathbf{x} = (\mathbf{y}, \dot{\mathbf{y}})$, the above equation can be rewritten in the form (75) with

$$\mathbf{B} = \begin{pmatrix} \mathbf{C} & \mathbf{M} \\ \mathbf{M} & \mathbf{0} \end{pmatrix}, \mathbf{F}(\mathbf{x}, k_3) = \begin{pmatrix} -\mathbf{C}\dot{\mathbf{y}} - \mathbf{f}(\mathbf{y}, \dot{\mathbf{y}}, k_3) \\ \mathbf{M}\dot{\mathbf{y}} \end{pmatrix},$$
$$\mathbf{F}^{\text{ext}}(\Omega t) = \begin{pmatrix} \mathbf{f}^{\text{ext}} \cos \Omega t \\ \mathbf{0} \end{pmatrix}. \tag{80}$$

This FE model has 7405 DOFs after boundary conditions are imposed. The first two natural frequencies of the system are $\omega_1 = 1272.0$ rad/s and $\omega_2 = 2065.8$ rad/s. We perform model reduction on the parameter-dependent SSM (PSSM) corresponding to the first (slowest) mode. In the rest of the computations, we set the nominal value for the cubic spring constant as $k_3 = 0$. We set the truncation order in the reduced coordinate vector $\mathbf{p}$ as five because it is the smallest order to capture the interplay between the softening and hardening mechanisms. In addition, as illustrated in [4], the results at $\mathcal{O}(5)$ truncation converge well. For the truncation order in $\boldsymbol{\delta}$, we found a quadratic expansion already showed convergence. Thus, we use an $\mathcal{O}(5, 2)$ expansion in this example.

In the autonomous case, we obtain the PSSM-based ROM (131) and (132), from which we can extract the backbone curve that depends on the parameter k_3. As seen in the left panel of Fig. 8, the softening backbone at $k_3 = 0$ tends to display hardening behavior at large response amplitudes when k_3 is increased to 6×10^9. This is expected because the hardening cubic spring will play a vital role when k_3 is large enough. Our PSSM-based ROM captures this transition accurately.

We further add a harmonic excitation $1.6 \cos \Omega t$ at the center point along the z-axis and consider the primary resonance of the first mode of the plate. Similar to the previous examples, we can use the PSSM-based ROM (139) to predict the forced response under the variations in k_3. In particular, we extract the forced response curves (FRCs) associated with the backbone curves and plot these FRCs in the right panel of Fig. 8. As expected, the peak response amplitude on FRC decreases with increasing k_3 because the cubic spring enhances the system's stiffness. Moreover, we observe that

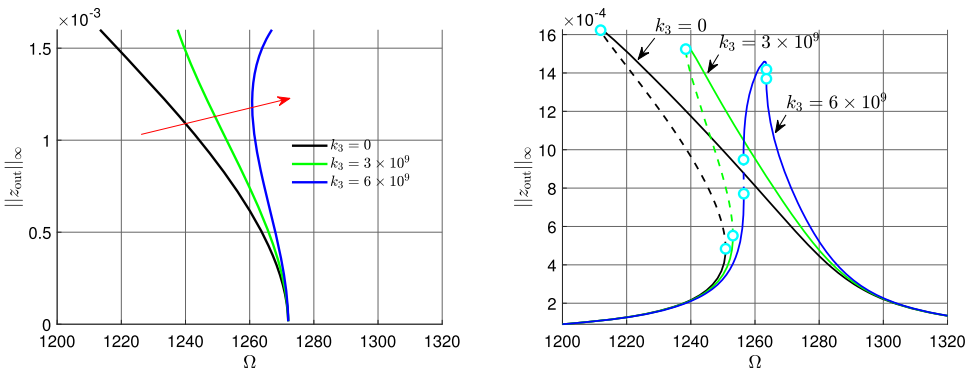

Fig. 8 Backbone curves (left panel) and forced response curves (right panel) of the cover plate linked by a cubic spring with various stiffness constants k_3. The red arrow in the left panel indicates the increasing direction of k_3. These curves are obtained via reduction on the parameter-dependent spectral manifold truncated at $\mathcal{O}(5, 2)$. In this example, z_{out} denotes the transverse deflection at the center of the plate

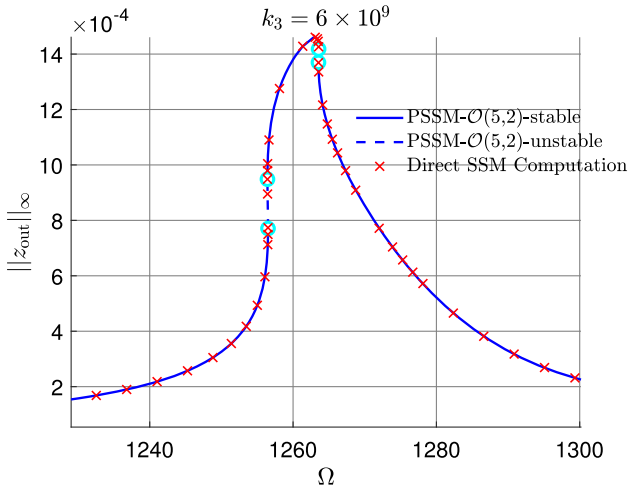

Fig. 9 Forced response curve of the cover plate predicted by PSSM-based ROM along with reference solutions obtained from direct reduction on SSM at $k_3 = 6 \times 10^9$

the FRCs are consistent with the backbone curves. In particular, at $k_3 = 6 \times 10^9$, the FRC softens at small response amplitudes but hardens at large response amplitudes.

We conclude this example with a comparison of our parameter-dependent ROM's predictions against the SSM-based ROM predictions on a system with a prescribed value for k_3. Specifically, we focus on the FRC at $k_3 = 6 \times 10^9$ that corresponds to the largest deviation from the nominal value of $k_3 = 0$. We follow the same approach as the previous example to validate the FRC predicted from $\mathcal{O}(5, 2)$ truncation. Specifically, we set $k_3 = 6 \times 10^9$ and compute the FRC via reduction on the updated system. As seen in Fig. 9, the reference solution via the direct computation matches well with that of the prediction of PSSM-based ROM at $\mathcal{O}(5, 2)$ truncation, which validates the effectiveness of the PSSM-based prediction.

5.3 Higher-order nonautonomous reduction

The leading-order nonautonomous reduction in Sec. 5.2 is unable to make prediction of superharmonic resonances or parametric resonances. By contrast, the higher-order nonautonomous reduction in Sec. 3.2 provides a unified framework for effective prediction of these two types of resonance. A key idea is to incorporate both the forcing frequency and amplitude into the parameter vector $\boldsymbol{\mu}$. Here, we use a few examples to illustrate the effectiveness of the proposed framework.

5.3.1 Superharmonic resonance of a shallow shell

We revisit the shallow shell structure shown in Fig. 4, but focus on the case of superharmonic resonance. In particular,the geometric and material parameters are listed in [2]. Here, the shell is not internally resonant, and hence we can perform reduction on the slowest two-dimensional SSM. Specifically, the first pair of eigenvalues with the largest real part (slowest decay) is given below

$$\lambda_{1,2} = -0.0029 \pm 147.45\mathrm{i}. \tag{81}$$

Next, we add a concentrated harmonic force $\epsilon 100 \cos \Omega t$ at the midpoint location $(x, y) = (L/4, H/2)$. We are interested in the superharmonic resonance at $\Omega \approx \mathrm{Im}(\lambda_1)/2$. With forcing frequency Ω and forcing amplitude ϵ treated as parameters, namely $\boldsymbol{\mu} = (\epsilon, \Omega)$, we perform reduction on a parameter-dependent two-dimensional SSM, and use this ROM to extract the forced response curve around the superharmonic resonance. Accordingly, we take $\boldsymbol{\mu}_0 = (0, \mathrm{Im}(\lambda_1)/2)$.

We obtain the FRC shown in Fig. 10. Indeed, as seen in the upper-left panel of Fig. 10, a leading-order truncation in $\boldsymbol{\delta}$ cannot capture the resonance at $\Omega \approx \mathrm{Im}(\lambda_1)/2$. In contrast, when the expansion order in $\boldsymbol{\delta}$ is increased to quadratic, the expected resonance is predicted, and the SSM-based prediction converges at the quadratic expansion. As seen in the upper-right and lower panels of Fig. 10, the SSM-based prediction converges at an $\mathcal{O}(5)$-truncation in $\mathbf{q}$, and a cubic expansion already gives an almost converged prediction.

We compare the SSM-based predictions with those obtained via the shooting method applied to the full system. Specifically, we use the shooting toolbox implemented in COCO [59] to obtain the FRC of the full system, where the Newmark scheme [60] is employed for time integration, and the pseudo-arclength method is adopted for parameter continuation. In the first trial, we set 200 integration steps per excitation period and obtained the results denoted by red circles in Fig. 10. We observe that the SSM-based prediction matches well with the Shooting-200 solution away from resonance, while slight discrepancies are found near the resonance peak. Given that the SSM-based prediction has converged, we infer that the discrepancies result from the error of the time integration. Indeed, upon increasing the number of integration steps per excitation period to 500, the obtained reference solution matches better with the SSM-based predictions, as shown in the lower panel of Fig. 10.

In terms of computational time, the SSM-based reduction takes less than 15 min for the $\mathcal{O}(7, 4)$ computation. In contrast, the shooting method with 200 steps per excitation period (Shooting-200) took approximately 19 h on the same machine. The computational gains from the SSM-based ROM is even more significant relative to Shooting-500, which took 41 h to extract the FRC of the full system.

5.3.2 Systems with parametric excitations

Parametric excitation occurs when a mechanical system is driven by temporal fluctuations of its internal parameters

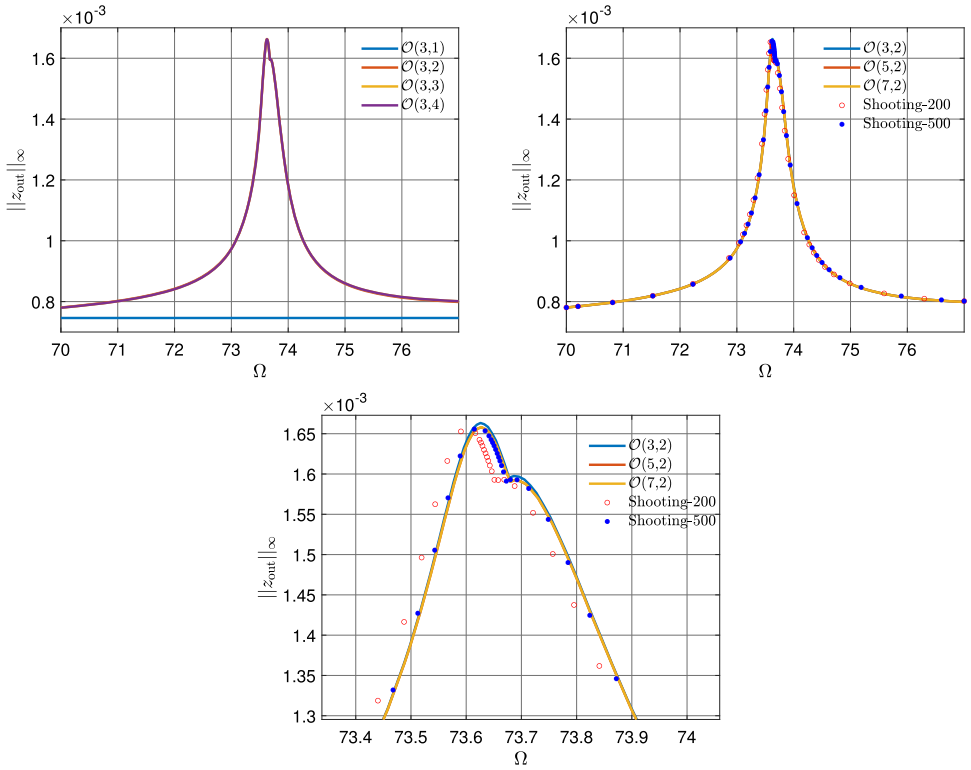

Fig. 10 Forced response curve for the superharmonic resonance of the shallow arc structure. In the upper-left panel, we show the SSM-based prediction truncated at cubic expansion in reduced coordinates but with various expansion orders in $\boldsymbol{\delta}$. In the upper-right panel, we fix quadratic expansion in $\boldsymbol{\delta}$ but vary the expansion order in the reduced coordinate vector $\mathbf{q}$. We also present the reference results obtained from the shooting method combined with parameter continuation. In particular, the legend "Shooting-200/500" refers to the excitation period, which is divided into 200/500 subintervals. The lower panel enlarges the upper-right panel near the resonance peak

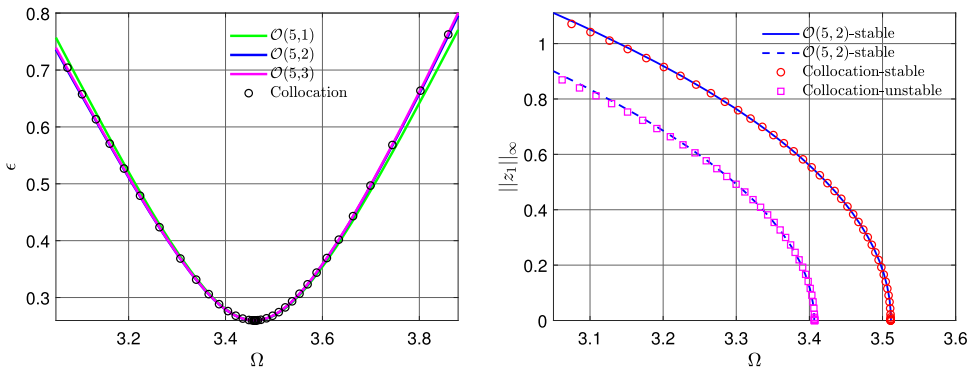

Fig. 11 Stability boundary of trivial solutions (left panel) forced response curves of nontrivial periodic orbits at $\epsilon = 0.275$ (right panel) for the system of two coupled Mathieu equations. Here, reference solutions of the full system are obtained via the po-toolbox of COCO, where periodic orbits are discretized by collocation methods, and are therefore labeled 'Collocation'

rather than by an external force. A system exhibits parametric resonance when its eigenfrequency and the parameter modulation frequency are rationally commensurate. A classic illustration is the periodic variation of the length of a pendulum at twice its natural frequency, which can destabilize an otherwise stable equilibrium.

Here, we consider two examples with parametric excitations to show that the proposed parameter-dependent SSM reduction can handle parametric resonance. In the first example, we consider a model of two oscillators described by two coupled Mathieu equations. We will use SSM reduction to extract the stability boundary of trivial solutions and the forced response curve of nontrivial periodic solutions. In the second example, we consider a model of a self-excited oscillator system with external and parametric excitation. We will use reduction on parameter-dependent SSM to extract the forced response curve of the system.

Coupled Mathieu equations. Consider a system of two oscillators described by coupled Mathieu equations [11]

$$m\ddot{y}_1 + 2c\dot{y}_1 - c\dot{y}_2 + 2ky_1 - ky_2 + \epsilon k\cos\Omega t(y_1 - y_2) + \kappa(-y_1^3 - (y_1 - y_2)^3) = 0, \quad (82)$$

$$m\ddot{y}_2 + 2c\dot{y}_2 - c\dot{y}_1 + 2ky_2 - ky_1 + \epsilon k\cos\Omega t(y_2 - y_1) + \kappa(-y_2^3 + (y_1 - y_2)^3) = 0. \quad (83)$$

Here we set $m = 1$, $k = 1$, $c = 0.05$, and $\kappa = 0.1$. The eigenvalues of the unforced system at $\epsilon = 0$ are obtained as

$\lambda_{1,2} = -0.025 \pm 0.9997\mathrm{i}$ and $\lambda_{3,4} = -0.075 \pm 1.7304\mathrm{i}$. We take the two-dimensional eigenspace associated with the second pair of eigenvalues as the master subspace for SSM-based model reduction. Similar to the previous example, we have $\boldsymbol{\mu} = (\epsilon, \Omega)$. Here we set $\boldsymbol{\mu}_0 = (0, 3.46)$ to study the parametric resonance at $\Omega \approx 2\mathrm{Im}(\lambda_3)$.

The system above admits trivial solutions which can become unstable for certain choices of (ϵ, Ω). Therefore, it is crucial to determine the stability boundary of the trivial solutions. We note that the trivial solution for $t \in [0, 2\pi/\Omega]$ is also a periodic orbit of the system. This trivial solution will undergo a periodic-doubling bifurcation (PD) when it crosses the stability boundary. Hence, we can track the bifurcation curve of PD points to extract the stability boundary. We follow this methodology and extract the stability boundary shown in the left panel of Fig. 11. Here, we fix $\mathcal{O}(5)$ truncation for the reduced coordinates (as in Ref. [11]) and vary the expansion order in $\boldsymbol{\delta}$. As seen in the figure, linear expansion in ϵ does not converge for large ϵ, necessitating a higher-order expansion in parameters. Indeed, a quadratic expansion converges and matches well with the reference solutions obtained from the po-toolbox of COCO. Therefore, our algorithm improves on the predictions obtained via the first-order formulas in ϵ proposed by [11] at larger values of the forcing amplitude ϵ.

We further extract the forced response curve of the nontrivial periodic solutions. Indeed, the system admits two PD points for $\epsilon \geq 0.26$, as seen in the left panel of Fig. 11. We fix $\epsilon = 0.275$ and then switch the continuation of periodic orbit with doubled period at each of these two PD points, yielding the two FRCs of nontrivial periodic solutions at the right panel of Fig. 11. Here, the periodic orbits born out of the left PD point are unstable, while those born out of the right PD point are stable. We again use the po-toolbox of COCO to extract the reference solutions of the full system. These full solutions match well with the ROM predictions, demonstrating the accuracy of the reduction on parameter-dependent invariant manifolds.

Self-excited oscillators with external and parametric forcing. We now consider a model of a self-excited oscillator system with simultaneous external and parametric excitation. The equations of motion of the system is given as [11]

$$\ddot{y}_1 + k(1 - \epsilon\cos 2\Omega t)(y_1 - y_2) + y_1 + \kappa y_1^3 = \epsilon\cos\Omega t, \quad (84)$$

$$\ddot{y}_2 - (c - \gamma\dot{y}_2^2)\dot{y}_2 - kM(1 - \epsilon\cos 2\Omega t)(y_1 - y_2) = 0. \quad (85)$$

Here, we set $k = 4$, $\kappa = 0.1$, $c = 0.01$, $\gamma = 0.05$, and $M = 0.5$. We again take the forcing frequency and amplitude as the parameters, namely, $\boldsymbol{\mu} = (\epsilon, \Omega)$. At $\epsilon = 0$, the eigenvalues associated with the linearized system are $\lambda_{1,2} = 0.0013 \pm 2.5887\mathrm{i}$ and $\lambda_{3,4} = 0.0037 \pm 0.5463\mathrm{i}$. We take the SSM associated with the first pair of eigenmodes to perform model reduction. In particular, we set $\boldsymbol{\mu}_0 = (0, 2.6)$ to study the primary and parametric resonances of the first mode.

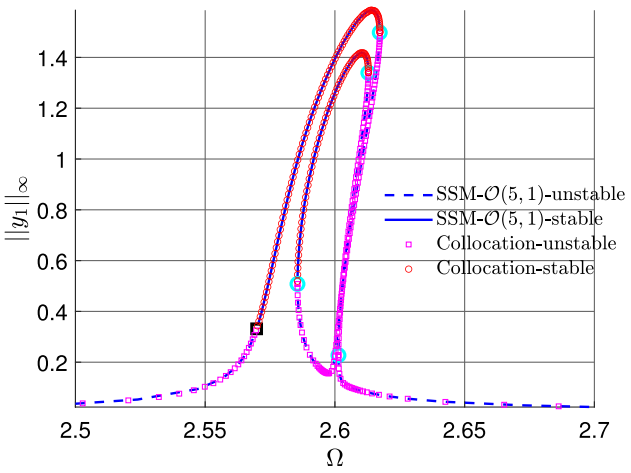

Fig. 12 Forced response curve of the self-excited oscillator at $\epsilon = 0.02$

We observe that an $\mathcal{O}(5, 1)$ truncation is sufficient to yield a converged solution. We extract the FRC at $\epsilon = 0.02$ and present it in Fig. 12. This FRC has a complex shape with a Neimark-Sacker bifurcation point and four saddle-node bifurcation points. We again use the po-toolbox of COCO to extract the reference solutions of these periodic orbits. The prediction via the reduction matches well with the full-system's result, illustrating the effectiveness of the proposed algorithm for systems subject combined to parametric and external excitations.

6 Conclusion

We have shown how invariant manifolds and their reduced dynamics can be efficiently computed in a parameter-dependent fashion from high-dimensional governing equations of physical systems. We have developed simplified expressions for these computations via multilinear function evaluations that can be readily interfaced with open-source modeling packages without coefficient-level knowledge of the governing equations (cf. [2]). When the modeling package is only available as a black box, we have shown how these computations can be performed nonintrusively for systems with up to cubic nonlinearities and affine parameter dependence.

While the proposed approach is theoretically equivalent to the classical shifting of the origin to a nominal configuration for manifold computations, rewriting the governing equations in a shifted frame is generally impractical, as it requires significant computational intrusion. The expressions developed here enable manifold and reduced-order model computations about nontrivial equilibria and parameter val-

ues without reformulating the governing equations in shifted coordinates.

We have demonstrated the effectiveness of these computations by constructing rigorous parameter-dependent reduced-order models across a range of numerical models based on open-source as well as commercial modeling packages. In particular, the resulting ROMs enable the analysis of local bifurcations with respect to parameters in diverse nonlinearizable phenomena, including buckling, flutter, period-doubling, internal resonances, and superharmonic and parametric resonances. Such analyses are typically infeasible at the full-system level due to prohibitive computational cost.

We expect parameter-dependent ROMs of this type to be especially valuable in design, optimization, and uncertainty-aware analysis, where repeated evaluations across parameter spaces are required. We believe this framework serves as a practical bridge between high-fidelity numerical models and advanced nonlinear dynamical analysis, enabling systematic exploration of stability, bifurcations, and nonlinear response in complex engineering systems.

A Computational notes

A.1 Unique symmetric choice of $\mathbf{F}_{j,k}$

For a homogeneous polynomial $\mathbf{p}(\mathbf{x};\boldsymbol{\mu})$ of degree j in $\mathbf{x}$ and degree k in $\boldsymbol{\mu}$, there is no unique choice for a multilinear function $\mathbf{F}_{j,k}$ such that $\mathbf{p}(\mathbf{x};\boldsymbol{\mu}) = \mathbf{F}_{j,k}(\mathbf{x},\ldots,\mathbf{x};\boldsymbol{\mu},\ldots,\boldsymbol{\mu})$ for $jk \geq 2$, but there is a unique symmetric candidate for $\mathbf{F}_{j,k}$ associated with $\mathbf{p}$ [62]. This is because any $j-$linear form $\mathbf{M}(\mathbf{a}_1,\ldots,\mathbf{a}_j)$ can be decomposed as $\mathbf{M} = \mathbf{S} + \mathbf{T}$, where

- $\mathbf{S}$ is symmetric: we have $\mathbf{M}(\mathbf{a}_1,\ldots,\mathbf{a}_j) = \mathbf{M}(P\{\mathbf{a}_1,\ldots,\mathbf{a}_j\})$ for any permutation $P\{\mathbf{a}_1,\ldots,\mathbf{a}_j\}$ of the arguments $\mathbf{a}_1,\ldots,\mathbf{a}_j$,
- $\mathbf{T}$ is skew-symmetric: It vanishes on the diagonal, i.e., $\mathbf{T}(\mathbf{x},\ldots,\mathbf{x}) = \mathbf{0}$ for any input $\mathbf{x}$.

For instance, the polynomial $F : \mathbb{R}^2 \times \mathbb{R} \to \mathbb{R}$ defined as $F(\mathbf{x},\mu) = 1 + (x_1+x_2)\mu + x_1^2\mu$ can be represented as $F(\mathbf{x},\mu) = F_0 + F_{1,1}(\mathbf{x},\mu) + F_{2,1}(\mathbf{x},\mathbf{x},\mu)$, where the degree zero term $F_0 = 1$,and the bilinear term $F_{1,1}(\mathbf{x},\mu) = (x_1+x_2)\mu$ are uniquely defined, but for $F_{2,1}$, we have infinitely many candidates. Indeed, $M_\alpha(\mathbf{a},\mathbf{b};\mu) = (a_1b_1 + \alpha a_2b_1 - \alpha a_1b_2)\mu$ is a valid candidate for $F_{2.1}$ because $M_\alpha(\mathbf{x},\mathbf{x};\mu) = x_1^2\mu\ \forall\alpha \in \mathbb{R}$. Note that $M_\alpha = S + T_\alpha$ where $S(\mathbf{a},\mathbf{b};\mu) = a_1b_1\mu$ is the symmetric candidate for $F_{2,1}$ and $T_\alpha = \alpha(a_2b_1 - \alpha a_1b_2)\mu$ is skew-symmetric. As we will see, this symmetric choice for computationally beneficial as it reduces the required number of function evaluations significantly.

A.2 The dummy-variable approach

We note that computing $\mathcal{W}(\mathcal{E})$ by solving (16) is equivalent to computing an $(M+m)$-dimensional invariant manifold $\tilde{\mathcal{W}}(\tilde{\mathcal{E}})$ in the extended system

$$\tilde{\mathbf{B}}\dot{\tilde{\mathbf{x}}} = \tilde{\mathbf{F}}(\tilde{\mathbf{x}}),\quad \tilde{\mathbf{B}} = \begin{bmatrix} \mathbf{B} & \\ & \mathbf{I}_m \end{bmatrix},\quad \tilde{\mathbf{F}}(\tilde{\mathbf{x}}) = [\mathbf{F}(\mathbf{x};\boldsymbol{\mu}),\mathbf{0}] \in \mathbb{R}^{N+m}, \tag{86}$$

where the parameters have been included as "dummy" variables in the phase space as $\tilde{\mathbf{x}} = (\mathbf{x},\boldsymbol{\mu})$. Here, $\tilde{\mathcal{W}}(\tilde{\mathcal{E}})$ is tangent to the subspace $\tilde{\mathcal{E}} = \mathcal{E} \oplus \text{span}\{\mathbf{e}_{N+1},\ldots,\mathbf{e}_{N+m}\}$ at the fixed point $\tilde{\mathbf{x}}_0 = (\mathbf{x}_0,\boldsymbol{\mu}_0)$, and the additional m dimensions take care of dependence on $\boldsymbol{\mu}$. Solving the extended invariance equation

$$\tilde{\mathbf{B}}\left[D\tilde{\mathbf{W}}\right]\tilde{\mathbf{R}}(\tilde{\mathbf{p}}) = \tilde{\mathbf{F}}(\tilde{\mathbf{W}}(\tilde{\mathbf{p}})),$$

where $\tilde{\mathbf{W}} : \mathbb{C}^{M+m} \to \mathbb{C}^{N+m}$, $\tilde{\mathbf{R}} : \mathbb{C}^{M+m} \to \mathbb{C}^{M+m}$ are the unknown parametrizations with parametrization coordinates $\tilde{\mathbf{p}} = (\mathbf{p},\boldsymbol{\delta})$, we obtain the solution $\tilde{\mathbf{W}}(\tilde{\mathbf{p}}) = [\mathbf{W}(\mathbf{p};\boldsymbol{\mu}),\boldsymbol{\mu}]$, $\tilde{\mathbf{R}}(\tilde{\mathbf{p}}) = [\mathbf{R}(\mathbf{p};\boldsymbol{\mu}),\mathbf{0}]$. However, the corresponding linear system has m additional equations and unknowns relative to system (23) and does not enable an independent control over the expansion orders in $\boldsymbol{\delta}$ and $\mathbf{p}$. Furthermore, the computational implementation of this approach is difficult even via open-source modeling software since it mixes the state variables with parameters.

A.3 Exploiting conjugacy in Spec($\mathcal{E}$)

When the spectrum of $\mathcal{E}$ contains non-real eigenvalues, the computational cost for determining the coefficients in the expansions (17), (18), can be cut in half relative to the general setting. Specifically, suppose we have $2c$ complex-conjugate eigenvalues $\lambda_{2j-1} = \bar{\lambda}_{2j}$ with eigenvectors $\mathbf{v}_{2j} = \bar{\mathbf{v}}_{2j-1}$ $(j = 1,\ldots,c)$, and $\lambda_{2c+1},\ldots,\lambda_M \in \mathbb{R}$. Then, the parametrization coordinates also exhibit this conjugacy pattern, i.e., $p_{2j} = \bar{p}_{2j-1}$ and $p_{2c+1},\ldots,p_M \in \mathbb{R}$ by construction. Now for any $\mathbf{m} \in \mathbb{N}_0^M$, we have

$$\begin{aligned}\overline{\mathbf{p}^{\mathbf{m}}} &= \overline{p_1^{m_1}\bar{p}_1^{m_2}\cdots p_{2c-1}^{m_{2c-1}}\bar{p}_{2c-1}^{m_{2c}}p_{2c+1}^{m_{2c+1}}\cdots p_M^{m_M}} \\ &= p_1^{m_2}\bar{p}_1^{m_1}\cdots p_{2c-1}^{m_{2c}}\bar{p}_{2c-1}^{m_{2c-1}}p_{2c+1}^{m_{2c+1}}\cdots p_M^{m_M} = \mathbf{p}^{\tilde{\mathbf{m}}},\end{aligned}$$

where $\tilde{\mathbf{m}} = (m_2,m_1,\ldots,m_{2c},m_{2c-1},m_{2c+1},\ldots,m_M)$. Hence, this conjugacy carries over to the monomials in the expansions (17), (18) as $\mathbf{p}^{\tilde{\mathbf{m}}}\boldsymbol{\delta}^{\boldsymbol{\ell}} = \overline{\mathbf{p}^{\mathbf{m}}\boldsymbol{\delta}^{\boldsymbol{\ell}}}$. Since $\mathbf{W}(\mathbf{p};\boldsymbol{\mu})$ maps into the real space $\mathbb{R}^N$, we have $\mathbf{w}_{\tilde{\mathbf{m}},\boldsymbol{\ell}} = \bar{\mathbf{w}}_{\mathbf{m},\boldsymbol{\ell}}$. Furthermore, since $\dot{p}_{2j-1} = \dot{\bar{p}}_{2j}$ $(j = 1,\ldots,c)$, we have for any $\mathbf{m} \in \mathbb{N}_0^M, \boldsymbol{\ell} \in \mathbb{N}_0^m$: if $\mathbf{r}_{\mathbf{m},\boldsymbol{\ell}} = (r_1,,\ldots r_M)$, then $\mathbf{r}_{\tilde{\mathbf{m}},\boldsymbol{\ell}} = (\bar{r}_2,\bar{r}_1,\ldots,\bar{r}_{2c-1},\bar{r}_{2c},r_{2c+1},\ldots,r_M)$. Thus, $\mathbf{w}_{\tilde{\mathbf{m}},\boldsymbol{\ell}}$, $\mathbf{r}_{\tilde{\mathbf{m}},\boldsymbol{\ell}}$ can be inferred directly from $\mathbf{w}_{\mathbf{m},\boldsymbol{\ell}}$, $\mathbf{r}_{\mathbf{m},\boldsymbol{\ell}}$.

A.4 Redundancy in expansions (42) and (47)

Every vector $\boldsymbol{\kappa} = (\kappa_1, \ldots, \kappa_f) \in \mathbb{Z}^f$ can be expressed as a difference $\boldsymbol{\kappa} = \boldsymbol{a} - \boldsymbol{b}$, with $\boldsymbol{a}, \boldsymbol{b} \in \mathbb{N}_0^n$. However, such a decomposition is not unique. For example,

$$\boldsymbol{\kappa} = (3, -2, 0) = \underbrace{(3, 0, 0)}_{\boldsymbol{a}_1} - \underbrace{(0, 2, 0)}_{\boldsymbol{b}_1} = \underbrace{(4, 5, 0)}_{\boldsymbol{a}_2} - \underbrace{(1, 7, 0)}_{\boldsymbol{b}_2}.$$

This decomposition can be made unique if we require the disjoint support condition: $a_i b_i = 0$ for each i. The canonical choice for this unique decomposition is defined by vectors containing the coordinatewise positive and negative parts as

$$\boldsymbol{\kappa}^+ := (\max(\kappa_1, 0), \ldots, \max(\kappa_f, 0)),$$
$$\boldsymbol{\kappa}^- := (\max(-\kappa_1, 0), \ldots, \max(-\kappa_f, 0)).$$

The unique decomposition is $\boldsymbol{\kappa} = \boldsymbol{\kappa}^+ - \boldsymbol{\kappa}^-$. Examples:

1. $\boldsymbol{\kappa} = (3, -2, 0)$ Canonical decomposition: $\boldsymbol{\kappa}^+ = (3, 0, 0)$, $\boldsymbol{\kappa}^- = (0, 2, 0)$. Other decomposition include $(3, -2, 0) = (4, 5, 0) - (1, 7, 0)$.
2. $\boldsymbol{\kappa} = (0, -4, 2, -1)$; Canonical decomposition: $\boldsymbol{\kappa}^+ = (0, 0, 2, 0)$, $\boldsymbol{\kappa}^- = (0, 4, 0, 1)$. Other decomposition include $(0, -4, 2, -1) = (3, 1, 2, 2) - (3, 5, 0, 3)$.

A.5 Exploiting conjugacy in $\boldsymbol{\gamma} = (\boldsymbol{\alpha}, \boldsymbol{\beta})$

The coefficients $\mathbf{x}^\star_{\boldsymbol{c},\ell}$ in the expansion (47) have a conjugacy relationship due to their association with the complex exponential $\boldsymbol{\gamma}^{\boldsymbol{c}} = e^{i\langle \boldsymbol{a}, \boldsymbol{\Omega}\rangle t} e^{-i\langle \boldsymbol{b}, \boldsymbol{\Omega}\rangle t}$, i.e., $e^{i\langle \boldsymbol{a}, \boldsymbol{\Omega}\rangle t} e^{-i\langle \boldsymbol{b}, \boldsymbol{\Omega}\rangle t} = \overline{e^{i\langle \boldsymbol{b}, \boldsymbol{\Omega}\rangle t} e^{-i\langle \boldsymbol{a}, \boldsymbol{\Omega}\rangle t}}$. Since $\mathbf{x}^\star(t; \boldsymbol{\mu})$ represents a trajectory in the real space $\mathbb{R}^N$, we must have $\mathbf{x}^\star_{(\boldsymbol{a},\boldsymbol{b}),\ell} = \bar{\mathbf{x}}^\star_{(\boldsymbol{b},\boldsymbol{a}),\ell}$. As a result, we need to solve (49) only for unordered pairs $(\boldsymbol{a}, \boldsymbol{b}) \in \mathbb{N}_0^{2f}$, which cuts the computational burden by half relative to the general setting.

A.6 Computational equivalence of Eq. (53) to an autonomous invariance equation

Computing $\mathcal{W}(\mathcal{E})$ by solving Eq. (53) is equivalent to computing an autonomous invariant manifold of the augmented system (43)–(45) attached to the fixed point $\mathbf{z}_0 = (\mathbf{x}_0, \mathbf{0}, \mathbf{0})$ at $\boldsymbol{\mu} = \boldsymbol{\mu}_0$ and tangent to the subspace $\tilde{\mathcal{E}} = \mathcal{E} \oplus \text{span}\{\mathbf{e}_{N+1}, \ldots, \mathbf{e}_{N+2f}\}$. The corresponding invariance equation is given as (cf. [3, 39])

$$\tilde{\mathbf{B}}\left[\partial_{\mathbf{q}}\tilde{\mathbf{W}}(\mathbf{q}; \boldsymbol{\mu})\right]\tilde{\mathbf{R}}(\mathbf{q}; \boldsymbol{\mu}) = \tilde{\mathbf{G}}(\tilde{\mathbf{W}}(\mathbf{q}; \boldsymbol{\mu}); \boldsymbol{\mu}), \tag{87}$$

where $\tilde{\mathbf{B}} = \begin{bmatrix} \mathbf{B} & \mathbf{0} \\ \mathbf{0} & \mathbf{I} \end{bmatrix} \in \mathbb{R}^{(N+2f)\times(N+2f)}$, $\tilde{\mathbf{W}} : \mathbb{C}^{M+2f} \to \mathbb{C}^{N+2f}$, $\tilde{\mathbf{R}} : \mathbb{C}^{M+2f} \to \mathbb{C}^{M+2f}$ and $\tilde{\mathbf{G}}(\mathbf{z}; \boldsymbol{\mu}) = [\mathbf{G}(\mathbf{q}; \boldsymbol{\mu}), i\mathbf{D}\boldsymbol{\alpha}, -i\mathbf{D}\boldsymbol{\beta}]$, to obtain the solution $\tilde{\mathbf{W}}(\mathbf{q}; \boldsymbol{\mu}) = [\mathbf{W}(\mathbf{q}; \boldsymbol{\mu}), \boldsymbol{\alpha}, \boldsymbol{\beta}]$, $\tilde{\mathbf{R}}(\mathbf{q}; \boldsymbol{\mu}) = [\mathbf{R}(\mathbf{q}; \boldsymbol{\mu}), i\mathbf{D}\boldsymbol{\alpha}, -i\mathbf{D}\boldsymbol{\beta}]$, but the corresponding linear system has a higher dimension relative to system (58).

B Anchor computation algorithms

Algorithm 2 Recursive computation of the expansion (4) for $\mathbf{x}^\star(\boldsymbol{\mu})$

$\mathbf{x}^\star(\boldsymbol{\mu}) =$ `compute_anchor`$(\mathbf{x}_0, \boldsymbol{\mu}_0, d_\mu)$

Input	Nominal equilibrium configuration: $(\mathbf{x}_0, \boldsymbol{\mu}_0)$;	
	Degree of approximation d_μ for the expansion (4)	
`Setup`	empty arrays for coefficients $\mathbf{x}^\star_{\boldsymbol{\ell}} \in \mathbb{R}^N$ for all $\boldsymbol{\ell} \in \mathbb{N}_0^m : \lvert\boldsymbol{\ell}\rvert = 0, \ldots, d_\mu$.	
`Assign`	$\mathbf{x}^\star_{\mathbf{0}} := \mathbf{x}_0$	
`Setup`	the coefficients $\boldsymbol{\mu}_{\boldsymbol{\ell}} \in \mathbb{R}^m$ for the expansion (7) as $\boldsymbol{\mu}_{\boldsymbol{\ell}} := \begin{cases} \boldsymbol{\mu}_0 & \boldsymbol{\ell} = \mathbf{0}, \\ \mathbf{e}_j & \boldsymbol{\ell} = \mathbf{e}_j, \quad j = 1, \ldots, m, \\ \mathbf{0} & \text{otherwise.} \end{cases}$	
for	$l = 1, \ldots, d_\mu$	
	for	$\boldsymbol{\ell} \in \mathbb{N}_0^m : \lvert\boldsymbol{\ell}\rvert = l$
	`Evaluate`	$\mathbf{b}_{\boldsymbol{\ell}}$ using eq. (10), which requires $\mathbf{x}^\star_{\boldsymbol{m}}$ for $\lvert\boldsymbol{m}\rvert < l$.
	`Solve`	linear system (10) to obtain $\mathbf{x}^\star_{\boldsymbol{\ell}}$.
	endfor	
endfor		
Output	Coefficients $\mathbf{x}^\star_{\boldsymbol{\ell}} \in \mathbb{R}^N$ for the expansion (4) upto degree d_μ.	

Algorithm 3 Nested recursion for computing the anchor trajectory $\mathbf{x}^\star(t; \boldsymbol{\mu})$ (47)

$[\mathbf{W}, \mathbf{R}] =$ `compute_anchor_trajectory`$(\mathbf{x}_0, \boldsymbol{\mu}_0, d_\mu, d_h)$

Input	Nominal equilibrium configuration: $(\mathbf{x}_0, \boldsymbol{\mu}_0)$;		
	Degrees of approximation d_h (harmonics) in $\boldsymbol{\gamma}$ and d_μ in $\boldsymbol{\delta}$ for the expansion (47) of $\mathbf{x}^\star(t; \boldsymbol{\mu})$.		
`Setup`	empty/zero arrays for coefficients $\mathbf{x}^\star_{\boldsymbol{c},\boldsymbol{\ell}} \in \mathbb{C}^N$ for all $(\boldsymbol{c}, \boldsymbol{\ell}) \in \mathbb{N}_0^{2f} \times \mathbb{N}_0^m : \lvert\boldsymbol{c}\rvert = 0, \ldots, d_h, \lvert\boldsymbol{\ell}\rvert = 0, \ldots, d_\mu$		
`Assign`	$\mathbf{x}^\star_{\boldsymbol{c},\mathbf{0}} := \mathbf{x}_0 \quad \forall \boldsymbol{\ell}$;		
`Setup`	coefficients $\boldsymbol{\mu}_{\boldsymbol{\ell}} \in \mathbb{R}^m$ for the expansion (7) as $\boldsymbol{\mu}_{\boldsymbol{\ell}} := \begin{cases} \boldsymbol{\mu}_0 & \boldsymbol{\ell} = \mathbf{0}, \\ \mathbf{e}_j & \boldsymbol{\ell} = \mathbf{e}_j, \quad j = 1, \ldots, m, \\ \mathbf{0} & \text{otherwise.} \end{cases}$		
for	$l = 1, \ldots, d_\mu$		
	for	$k = 0, \ldots, d_h$	
		for	$(\boldsymbol{c}, \boldsymbol{\ell}) \in \mathbb{N}_0^{2f} \times \mathbb{N}_0^m : \lvert\boldsymbol{c}\rvert = k, \lvert\boldsymbol{\ell}\rvert = l$
		`Evaluate`	$\mathbf{b}_{\boldsymbol{c},\boldsymbol{\ell}}$ using eq. (50), which requires $\mathbf{x}^\star_{\boldsymbol{d},\boldsymbol{m}}$ with $\lvert\boldsymbol{m}\rvert < l$ and $\lvert\boldsymbol{d}\rvert \le k$.
		`Solve`	linear system (49) to obtain $\mathbf{x}^\star_{\boldsymbol{c},\boldsymbol{\ell}}$.
		endfor	
	endfor		
endfor			
Output	Coefficients $\mathbf{x}^\star_{\boldsymbol{c},\boldsymbol{\ell}} \in \mathbb{C}^N$ for the expansion (47) upto degrees d_h in $\boldsymbol{\gamma}$ and d_μ in $\boldsymbol{\delta}$.		

C Derivation of system (23)

We collect coefficients of the monomial $\mathbf{p}^{\mathbf{m}}\boldsymbol{\delta}^{\boldsymbol{\ell}}$ in the invariance equation (16) as

$$\mathbf{B}\left(\left[\partial_{\mathbf{p}}\mathbf{W}\right]\mathbf{R}\right)_{\mathbf{m},\boldsymbol{\ell}} = [\mathbf{F} \circ \mathbf{W}]_{\mathbf{m},\boldsymbol{\ell}}. \tag{88}$$

These coefficients on the right-hand side of equation (88) can be expressed in terms of $\mathbf{w}_{\mathbf{m},\boldsymbol{\ell}}$ and lower-order coefficients of $\mathbf{W}$ as

$$[\mathbf{F} \circ \mathbf{W}]_{\mathbf{m},\boldsymbol{\ell}} = \left[\mathbf{F}(\mathbf{W}(\mathbf{p}; \boldsymbol{\mu}); \boldsymbol{\mu})\right]_{\mathbf{m},\boldsymbol{\ell}} \tag{89}$$

$$= \sum_{\substack{j,k \in \mathbb{N}, \mathbf{m}_1 + \cdots + \mathbf{m}_j = \mathbf{m}, \\ \boldsymbol{\ell}_1 + \cdots + \boldsymbol{\ell}_j + \boldsymbol{n}_1 + \cdots + \boldsymbol{n}_k = \boldsymbol{\ell}}} \mathbf{F}_{j,k} \left(\mathbf{w}_{\mathbf{m}_1,\boldsymbol{\ell}_1}, \ldots, \mathbf{w}_{\mathbf{m}_j,\boldsymbol{\ell}_j}, \boldsymbol{\mu}_{\boldsymbol{n}_1}, \ldots, \boldsymbol{\mu}_{\boldsymbol{n}_k}\right) \tag{90}$$

$$= \mathbf{A}\mathbf{w}_{\mathbf{m},\boldsymbol{\ell}} + \mathbf{h}_{\mathbf{m},\boldsymbol{\ell}}, \tag{91}$$

where we have separated the terms depending on $\mathbf{w}_{\mathbf{m},\boldsymbol{\ell}}$ from the summation (90) and collected the remaining terms into $\mathbf{h}_{\mathbf{m},\boldsymbol{\ell}}$ in eq. (91). Similarly, the left-hand side of eq. (88) can be expressed in terms of $\mathbf{w}_{\mathbf{m},\boldsymbol{\ell}}$, $\mathbf{r}_{\mathbf{m},\boldsymbol{\ell}}$ and lower-order coefficients

of $\mathbf{W}$ and $\mathbf{R}$ as

$$\left(\left[\partial_{\mathbf{p}}\mathbf{W}\right]\mathbf{R}\right)_{\mathbf{m},\ell} = \sum_{\substack{\mathbf{a}+\mathbf{b}=\mathbf{m},\\ k+l=\ell,}} \left[\partial_{\mathbf{p}}\mathbf{W}\right]_{\mathbf{a},k}\mathbf{r}_{\mathbf{b},l}, \tag{92}$$

$$= \lambda_{\mathbf{m}}\mathbf{w}_{\mathbf{m},\ell} + \mathbf{k}_{\mathbf{m},\ell} + \mathbf{W}_1\mathbf{r}_{\mathbf{m},\ell}, \tag{93}$$

where

$$\mathbf{W}_1 = \left[\left(\mathbf{w}_{\mathbf{e}_1,\mathbf{0}}\right), \ldots, \left(\mathbf{w}_{\mathbf{e}_M,\mathbf{0}}\right)\right] = \left[\mathbf{v}_1, \ldots, \mathbf{v}_M\right], \tag{94}$$

$$\mathbf{k}_{\mathbf{m},\ell} = \sum_{\substack{\mathbf{a}+\mathbf{b}=\mathbf{m},\\ k+l=\ell,\\ (\mathbf{a},k)\neq(\mathbf{0},0)\\ (\mathbf{b},l)\neq(\mathbf{e}_j,0)}} \left[\partial_{\mathbf{p}}\mathbf{W}\right]_{\mathbf{a},k}\mathbf{r}_{\mathbf{b},l}, \quad j = 1, \ldots, M, \tag{95}$$

and

$$\left[\partial_{\mathbf{p}}\mathbf{W}\right]_{\mathbf{m},\ell} = \left[\left((m_1+1)\mathbf{w}_{\mathbf{m}+\mathbf{e}_1,\ell}\right), \ldots, \left((m_M+1)\mathbf{w}_{\mathbf{m}+\mathbf{e}_M,\ell}\right)\right]. \tag{96}$$

Finally, substituting eqs. (91), (93) into eq. (88), we obtain

$$\left[\lambda_{\mathbf{m}}\mathbf{B} - \mathbf{A}\right]\mathbf{w}_{\mathbf{m},\ell} = \mathbf{s}_{\mathbf{m},\ell} - \mathbf{D}\mathbf{r}_{\mathbf{m},\ell}, \tag{97}$$

where

$$\mathbf{s}_{\mathbf{m},\ell} = \mathbf{h}_{\mathbf{m},\ell} - \mathbf{B}\mathbf{k}_{\mathbf{m},\ell}, \tag{98}$$

$$\mathbf{D} = \mathbf{B}\mathbf{W}_1. \tag{99}$$

D Solving the linear system (23)

We normalize the eigenvectors with respect to the matrix $\mathbf{B}$ such that

$$\bar{\mathbf{u}}_j^T\mathbf{B}\mathbf{v}_k = \delta_{jk}, \forall j, k = 1, \ldots, M, \tag{100}$$

where δ_{jk} is the Kronecker delta.

D.1 Normal-form style parametrization

Now, for any $\mathbf{m} \in \mathbb{N}^M$, we arrange the eigenvalues of $\mathcal{E}$ such that the first r eigenvalues are in resonance with $\lambda_{\mathbf{m}}$ without loss of generality, i.e.,

$$\lambda_j \approx \lambda_{\mathbf{m}}, \quad j = 1, \ldots, r, \tag{101}$$

where $0 \leq r \leq M$; $r = 0$ corresponds to no resonance. These (near) inner resonances, result in the constraints (25) on the solution choices for $\mathbf{r}_{\mathbf{m},\ell}$ as

$$\langle \mathbf{u}_j, \mathbf{s}_{\mathbf{m},\ell} - \mathbf{D}\mathbf{r}_{\mathbf{m},\ell}\rangle = 0, \quad j = 1, \ldots, r \tag{102}$$

$$\implies \langle \mathbf{u}_j, \mathbf{D}\mathbf{r}_{\mathbf{m},\ell}\rangle = \langle \mathbf{u}_j, \mathbf{s}_{\mathbf{m},\ell}\rangle, \quad j = 1, \ldots, r. \tag{103}$$

Thanks to the normalization (100), the left-hand side of eq. (103) can be simplified as

$$\langle \mathbf{u}_j, \mathbf{D}\mathbf{r}_{\mathbf{m},\ell}\rangle = \bar{\mathbf{u}}_j^T\mathbf{D}\mathbf{r}_{\mathbf{m},\ell} = \bar{\mathbf{u}}_j^T\mathbf{B}\mathbf{W}_1\mathbf{r}_{\mathbf{m},\ell}$$
$$= \bar{\mathbf{u}}_j^T\mathbf{B}\left[\mathbf{v}_1, \ldots, \mathbf{v}_M\right]\mathbf{r}_{\mathbf{m},\ell} = \mathbf{e}_j^T\mathbf{r}_{\mathbf{m},\ell},$$

and we obtain an explicit value for the j^{th}element of $\mathbf{r}_{\mathbf{m},\ell}$ due to constraint (103) as

$$r^j_{\mathbf{m},\ell} = \bar{\mathbf{u}}_j^T\mathbf{s}_{\mathbf{m},\ell}, \quad j = 1, \ldots, r. \tag{104}$$

The remaining coefficients are free to take any value and we make the trivial choice in accordance with the normal-form style as

$$\mathbf{r}_{\mathbf{m},\ell} = \begin{bmatrix} \bar{\mathbf{u}}_1^T\mathbf{s}_{\mathbf{m},\ell} \\ \vdots \\ \bar{\mathbf{u}}_r^T\mathbf{s}_{\mathbf{m},\ell} \\ 0 \\ \cdots \\ 0 \end{bmatrix}. \tag{105}$$

Substituting the solution (102) into(23), we pick the minimum-norm solution for $\mathbf{w}_{\mathbf{m},\ell}$ as

$$\mathbf{w}_{\mathbf{m},\ell} = \mathcal{L}_{\mathbf{m}}^{\dagger}[\mathbf{s}_{\mathbf{m},\ell} - \mathbf{D}\mathbf{r}_{\mathbf{m},\ell}].$$

The normalization (100) may not be possible when $\mathbf{B}$ is singular. In that case, the coordinate-wise simplification (104) is not feasible. We then construct a bordered system along with the constraint to simultaneously solve for $\mathbf{w}_{\mathbf{m},\ell}, \mathbf{r}_{\mathbf{m},\ell}$ as

$$\underbrace{\begin{bmatrix} \mathcal{L}_{\mathbf{m}} & \mathbf{D} \\ \mathbf{0} & \bar{\mathbf{U}}_r^T\mathbf{D} \end{bmatrix}}_{\mathcal{N}_{\mathbf{m}}} \begin{bmatrix} \mathbf{w}_{\mathbf{m},\ell} \\ \mathbf{r}_{\mathbf{m},\ell} \end{bmatrix} = \begin{bmatrix} \mathbf{s}_{\mathbf{m},\ell} \\ \bar{\mathbf{U}}_r^T\mathbf{s}_{\mathbf{m},\ell} \end{bmatrix},$$

where $\mathcal{N}_{\mathbf{m}} \in \mathbb{C}^{(N+r)\times(N+M)}$, $\mathbf{U}_r = [\mathbf{u}_1, \ldots, \mathbf{u}_r]$. The minimum norm solution for $\mathbf{w}_{\mathbf{m},\ell}, \mathbf{r}_{\mathbf{m},\ell}$ is then determined simultaneously as

$$\begin{bmatrix} \mathbf{w}_{\mathbf{m},\ell} \\ \mathbf{r}_{\mathbf{m},\ell} \end{bmatrix} = \begin{cases} \mathcal{N}_{\mathbf{m}}^{\dagger}\begin{bmatrix} \mathbf{s}_{\mathbf{m},\ell} \\ \bar{\mathbf{U}}_r^T\mathbf{s}_{\mathbf{m},\ell} \end{bmatrix}, & \mathbf{m} \in \mathbb{N}^m : \text{resonance (101) occurs} \\ \begin{bmatrix} \mathcal{N}_{\mathbf{m}}^{\dagger}\mathbf{s}_{\mathbf{m},\ell} \\ \mathbf{0} \end{bmatrix}, & \text{otherwise.} \end{cases}.$$

D.2 Graph style parametrization

In a graph style of parametrization, for each $\mathbf{m} \in \mathbb{N}^M$, we impose the constraints

$$\langle \mathbf{u}_j, \mathbf{s}_{\mathbf{m},\boldsymbol{\ell}} - \mathbf{D}\mathbf{r}_{\mathbf{m},\boldsymbol{\ell}} \rangle = 0, \quad j = 1, \ldots, M,$$

on the solution choice for $\mathbf{r}_{\mathbf{m},\boldsymbol{\ell}}$, regardless of the presence of (near) resonances in $\mathrm{Spec}(\mathcal{E})$. Similarly to the discussion in section D.1, the above constraints provide an explicit solution for $\mathbf{r}_{\mathbf{m},\boldsymbol{\ell}}$ via the normalization (100) as

$$\mathbf{r}_{\mathbf{m},\boldsymbol{\ell}} = \bar{\mathbf{U}}^T \mathbf{s}_{\mathbf{m},\boldsymbol{\ell}}, \quad \forall \mathbf{m} \in \mathbb{N}^M, \boldsymbol{\ell} \in \mathbb{N}_0^m,$$

where

$$\mathbf{U} = \left[\mathbf{u}_1, \ldots, \mathbf{u}_M \right] \in \mathbb{C}^{N \times M}.$$

Furthermore, in the absence of normalization (100), we construct the bordered system

$$\underbrace{\begin{bmatrix} \mathcal{L}_{\mathbf{m}} & \mathbf{D} \\ \mathbf{0} & \bar{\mathbf{U}}^T \mathbf{D} \end{bmatrix}}_{\mathcal{G}_{\mathbf{m}}} \begin{bmatrix} \mathbf{w}_{\mathbf{m},\boldsymbol{\ell}} \\ \mathbf{r}_{\mathbf{m},\boldsymbol{\ell}} \end{bmatrix} = \begin{bmatrix} \mathbf{s}_{\mathbf{m},\boldsymbol{\ell}} \\ \bar{\mathbf{U}}^T \mathbf{s}_{\mathbf{m},\boldsymbol{\ell}} \end{bmatrix},$$

to simultaneously compute $\mathbf{w}_{\mathbf{m},\boldsymbol{\ell}}$, $\mathbf{r}_{\mathbf{m},\boldsymbol{\ell}}$ as

$$\begin{bmatrix} \mathbf{w}_{\mathbf{m},\boldsymbol{\ell}} \\ \mathbf{r}_{\mathbf{m},\boldsymbol{\ell}} \end{bmatrix} = \mathcal{G}_{\mathbf{m}}^{\dagger} \begin{bmatrix} \mathbf{s}_{\mathbf{m},\boldsymbol{\ell}} \\ \bar{\mathbf{U}}^T \mathbf{s}_{\mathbf{m},\boldsymbol{\ell}} \end{bmatrix}, \quad \forall \mathbf{m} \in \mathbb{N}^M, \boldsymbol{\ell} \in \mathbb{N}_0^m.$$

E Supplementary analysis of examples

E.1 Example 2.4

Here we present a detailed derivation yielding the expansion coefficients in (30). We take the time derivative of (30) and obtain

$$\dot{v} = (\partial_u h)\dot{u} + (\partial_\mu h)\dot{\mu} = -u\partial_u h(u, \mu) \tag{106}$$

where we have used $\dot{u} = -u$ shown in (29). We then substitute (106) and (30) into the second differential equation in (29), yielding

$$\begin{aligned}
&-\Big(2a_{20}u + a_{11}\mu + 3a_{30}u^2 + 2a_{21}u\mu + a_{12}\mu^2 + 4a_{40}u^3 \\
&\quad + 3a_{31}u^2\mu + 2a_{22}u\mu^2 + a_{13}\mu^3 \\
&\quad + 5a_{50}u^4 + 4a_{41}u^3\mu + 3a_{32}u^2\mu^2 + 2a_{23}u\mu^3 + a_{14}\mu^4 + \cdots\Big)u \\
&= -\sqrt{24}\Big(a_{20}u^2 + a_{11}u\mu + a_{02}\mu^2 + a_{30}u^3 + a_{21}u^2\mu \\
&\quad + a_{12}u\mu^2 + a_{03}\mu^3 \\
&\quad + a_{40}u^4 + a_{31}u^3\mu + a_{22}u^2\mu^2 + a_{13}u\mu^3 + a_{04}\mu^4 \\
&\quad + a_{50}u^5 + a_{41}u^4\mu + a_{32}u^3\mu^2 + a_{23}u^2\mu^3 + a_{14}u\mu^4 + a_{05}\mu^5\Big) \\
&\quad + (5\mu^4 + 4\mu^3 + 3\mu^2 + 2\mu)u + (10\mu^3 + 6\mu^2 + 3\mu + 1)u^2 \\
&\quad + (10\mu^2 + 4\mu + 1)u^3 + (1 + 5\mu)u^4 + u^5.
\end{aligned} \tag{107}$$

By matching the coefficients of monomials, we obtain

$$\begin{aligned}
&\mathcal{O}(u^2) : -2a_{20} = -\sqrt{24}a_{20} + 1 \implies a_{20} = \frac{1}{\sqrt{24} - 2}, \\
&\mathcal{O}(u\mu) : -a_{11} = -\sqrt{24}a_{11} + 2 \implies a_{11} = \frac{2}{\sqrt{24} - 1}, \\
&\mathcal{O}(\mu^2) : 0 = -\sqrt{24}a_{02} \implies a_{02} = 0, \\
&\mathcal{O}(u^3) : -3a_{30} = -\sqrt{24}a_{30} + 1 \implies a_{30} = \frac{1}{\sqrt{24} - 3}, \\
&\mathcal{O}(u^2\mu) : -2a_{21} = -\sqrt{24}a_{21} + 3 \implies a_{21} = \frac{3}{\sqrt{24} - 2}, \\
&\mathcal{O}(u\mu^2) : -a_{12} = -\sqrt{24}a_{12} + 3 \implies a_{12} = \frac{3}{\sqrt{24} - 1}, \\
&\mathcal{O}(\mu^3) : 0 = -\sqrt{24}a_{03} \implies a_{03} = 0, \\
&\mathcal{O}(u^4) : -4a_{40} = -\sqrt{24}a_{40} + 1 \implies a_{40} = \frac{1}{\sqrt{24} - 4}, \\
&\mathcal{O}(u^3\mu) : -3a_{31} = -\sqrt{24}a_{31} + 4 \implies a_{31} = \frac{4}{\sqrt{24} - 3}, \\
&\mathcal{O}(u^2\mu^2) : -2a_{22} = -\sqrt{24}a_{22} + 6 \implies a_{22} = \frac{6}{\sqrt{24} - 2}, \\
&\mathcal{O}(u\mu^3) : -a_{13} = -\sqrt{24}a_{13} + 4 \implies a_{13} = \frac{4}{\sqrt{24} - 1}, \\
&\mathcal{O}(\mu^4) : 0 = -\sqrt{24}a_{04} \implies a_{04} = 0, \\
&\mathcal{O}(u^5) : -5a_{50} = -\sqrt{24}a_{50} + 1 \implies a_{50} = \frac{1}{\sqrt{24} - 5}, \\
&\mathcal{O}(u^4\mu) : -4a_{41} = -\sqrt{24}a_{41} + 5 \implies a_{41} = \frac{5}{\sqrt{24} - 4}, \\
&\mathcal{O}(u^3\mu^2) : -3a_{32} = -\sqrt{24}a_{32} + 10 \implies a_{32} = \frac{10}{\sqrt{24} - 3}, \\
&\mathcal{O}(u^2\mu^3) : -2a_{23} = -\sqrt{24}a_{23} + 10 \implies a_{23} = \frac{10}{\sqrt{24} - 2}, \\
&\mathcal{O}(u\mu^4) : -a_{14} = -\sqrt{24}a_{14} + 5 \implies a_{14} = \frac{5}{\sqrt{24} - 1}, \\
&\mathcal{O}(\mu^5) : 0 = -\sqrt{24}a_{05} \implies a_{05} = 0.
\end{aligned} \tag{108}$$

E.2 Example 5

Converting system (39) to first-order form with $\mathbf{x} = [y, \dot{y}]^T$ and $\mu = [a, b]^T$, we get

$$\dot{\mathbf{x}} = \begin{bmatrix} 0 & 1 \\ -\omega_0^2 & -2\zeta\omega_0 \end{bmatrix} \mathbf{x} + \begin{bmatrix} 0 \\ a + \frac{b}{2}(e^{i\Omega t} + e^{-i\Omega t}) \end{bmatrix} \tag{109}$$

The Taylor-Fourier ansatz for the unique periodic response is

$$\begin{aligned} \mathbf{x}^\star(\boldsymbol{\mu}, t) \; &= \mathbf{x}_0 + \mathbf{x}_{0,\mathbf{e}_1}\delta_1 + \mathbf{x}_{0,\mathbf{e}_2}\delta_2 \\ &\quad + \mathbf{x}_{1,\mathbf{e}_2}\delta_2 e^{i\Omega t} + \mathbf{x}_{-1,\mathbf{e}_2}\delta_2 e^{-i\Omega t} \end{aligned} \tag{110}$$

Substituting the above ansatz into system (109) and comparing coefficients for $\boldsymbol{\ell} = \mathbf{e}_1, \mathbf{e}_2$ and $\kappa = -1, 0, 1$, we get:

- $\boldsymbol{\ell} = \mathbf{e}_1, \kappa = 0$: Collecting coefficients of δ_1 gives:

$$\begin{bmatrix} 0 & 1 \\ -\omega_0^2 & -2\zeta\omega_0 \end{bmatrix} \mathbf{x}_{0,\mathbf{e}_1} + \begin{bmatrix} 0 \\ 1 \end{bmatrix} = \begin{bmatrix} 0 \\ 0 \end{bmatrix} \implies \mathbf{x}_{0,\mathbf{e}_1} = \frac{1}{\omega_0^2}\begin{bmatrix} 1 \\ 0 \end{bmatrix} \tag{111}$$

- $\boldsymbol{\ell} = \mathbf{e}_2, \kappa = 0$: Collecting coefficients of δ_2 gives:

$$\begin{bmatrix} 0 & 1 \\ -\omega_0^2 & -2\zeta\omega_0 \end{bmatrix} \mathbf{x}_{0,\mathbf{e}_2} = \begin{bmatrix} 0 \\ 0 \end{bmatrix} \implies \mathbf{x}_{0,\mathbf{e}_2} = [0\ 0]^T \tag{112}$$

- $\boldsymbol{\ell} = \mathbf{e}_1, \kappa = 1$: Collecting coefficients of $\delta_1 e^{i\Omega t}$ gives:

$$\begin{bmatrix} i\Omega & -1 \\ \omega_0^2 & i\Omega + 2\zeta\omega_0 \end{bmatrix} \mathbf{x}_{1,\mathbf{e}_1} = \begin{bmatrix} 0 \\ 0 \end{bmatrix} \implies \mathbf{x}_{1,\mathbf{e}_1} = \begin{bmatrix} 0 \\ 0 \end{bmatrix} \tag{113}$$

- $\boldsymbol{\ell} = \mathbf{e}_2, \kappa = 1$: Collecting coefficients of $\delta_2 e^{i\Omega t}$ gives:

$$\begin{bmatrix} i\Omega & -1 \\ \omega_0^2 & i\Omega + 2\zeta\omega_0 \end{bmatrix} \mathbf{x}_{1,\mathbf{e}_2} = \begin{bmatrix} 0 \\ 1/2 \end{bmatrix} \implies \mathbf{x}_{1,\mathbf{e}_2} = \frac{1}{-2\Omega^2 + i4\zeta\omega_0\Omega + 2\omega_0^2}\begin{bmatrix} 1 \\ i\Omega \end{bmatrix} \tag{114}$$

Due to conjugacy relations (see Computational note Appendix A.5), we have $\mathbf{x}_{-1,\mathbf{e}_1} = \bar{\mathbf{x}}_{1,\mathbf{e}_1}$ and $\mathbf{x}_{-1,\mathbf{e}_2} = \bar{\mathbf{x}}_{1,\mathbf{e}_2}$.

E.3 Example 5.1.1

The sensitivity with respect to u is given as

$$\mathbf{w}_{(3,0),\mathbf{e}_1} \approx \begin{pmatrix} -0.456715 + 5.304571\mathrm{i} \\ 0.964878 + 0.0691713\mathrm{i} \\ -91.803009 - 8.707063\mathrm{i} \\ -1.336599 + 16.413566\mathrm{i} \end{pmatrix},$$

$$\mathbf{w}_{(2,1),\mathbf{e}_1} \approx \begin{pmatrix} 0.694231 - 28.847972\mathrm{i} \\ 2.265520 - 0.00972369\mathrm{i} \\ -208.010438 - 3.731603\mathrm{i} \\ -1.233254 + 34.546931\mathrm{i} \end{pmatrix} \tag{115}$$

and the sensitivity with respect to μ is given as

$$\mathbf{w}_{(3,0),\mathbf{e}_2} \approx \begin{pmatrix} 8.933368 \times 10^{-5} - 9.583334 \times 10^{-4}\mathrm{i} \\ -1.861642 \times 10^{-4} - 1.389984 \times 10^{-5}\mathrm{i} \\ 2.078261 \times 10^{-2} + 2.148071 \times 10^{-3}\mathrm{i} \\ 3.423070 \times 10^{-4} - 4.037948 \times 10^{-3}\mathrm{i} \end{pmatrix},$$

$$\mathbf{w}_{(2,1),\mathbf{e}_2} \approx \begin{pmatrix} -1.361583 \times 10^{-4} + 5.708335 \times 10^{-3}\mathrm{i} \\ -4.426809 \times 10^{-4} + 8.677030 \times 10^{-6}\mathrm{i} \\ 4.092408 \times 10^{-2} + 8.174821 \times 10^{-4}\mathrm{i} \\ 3.082614 \times 10^{-4} - 1.043698 \times 10^{-2}\mathrm{i} \end{pmatrix}. \tag{116}$$

Dummy-variable approach We now present a detailed treatment for the dummy variable approach for the reduction on parameter-dependent invariant manifold of the buckled pipe conveying fluid. The first step is to shift the origin of phase space to the bucked configuration via a coordinate transformation. Specifically, let $y_1 = y_1^* + x_1$, $y_2 = y_2^* + x_2 = x_2$, we obtain the equations of motion in the new coordinates

$$\begin{aligned} &\ddot{x}_1 + \alpha\pi^4\left(1 + \mu(y_1^*)^2\right)\dot{x}_1 - \frac{16}{3}\sqrt{\beta}u\dot{x}_2 \\ &\quad + \pi^2\left(\pi^2 - u^2 + \frac{3}{2}\mu\pi^2(y_1^*)^2\right)x_1 \\ &\quad + \frac{\mu}{2}\pi^4\left(3y_1^*x_1^2 + x_1^3 + 4(y_1^* + x_1)x_2^2\right) \\ &\quad + \alpha\pi^4\mu\left((2y_1^*x_1 + x_1^2)\dot{x}_1 + 4(y_1^* + x_1)x_2\dot{x}_2\right) = 0, \\ &\ddot{x}_2 + \frac{16}{3}\sqrt{\beta}u\dot{x}_1 + 16\alpha\pi^4\dot{x}_2 + 4\pi^2(4\pi^2 - u^2 + 0.5\mu\pi^2(y_1^*)^2)x_2 \\ &\quad + 2\mu\pi^4 x_2\left(2y_1^*x_1 + x_1^2 + 4x_2^2\right) \\ &\quad + 4\alpha\pi^4\mu x_2\left(y_1^*\dot{x}_1 + x_1\dot{x}_1 + 4x_2\dot{x}_2\right) = 0. \end{aligned} \tag{117}$$

We take u and μ as parameters and compute the sensitivity of the SSM reduction. Let $u = u_0 + v$, $\mu = \mu_0 + \kappa$, we denote y_1^* and its derivatives with respect to u and μ evaluated at $(u, \mu) = (u_0, \mu_0)$ as q_0, q_u^*, and q_μ^*. We substitute them into (117) and truncate quadratic and higher order expansions in v and κ, yielding

$$\begin{aligned} &\ddot{x}_1 + \alpha\pi^4\left(1 + \mu_0 q_0^2 + 2\mu_0 q_0 q_u^* v\right)\dot{x}_1 - \frac{16}{3}\sqrt{\beta}(u_0 + v)\dot{x}_2 \\ &\quad + \pi^2\left(\pi^2 - (u_0^2 + 2u_0 v) + \frac{3\pi^2}{2}\left(\mu_0 q_0^2 + 2\mu_0 q_0 q_u^* v\right)\right)x_1 \\ &\quad + (\mu_0 + \kappa)\pi^4\left(\frac{x_1^3 + 4x_1x_2^2}{2} + \alpha(x_1^2\dot{x}_1 + 4x_1x_2\dot{x}_2)\right) \\ &\quad + (\mu_0 q_0 + \mu_0(q_u^* v + q_\mu^*\kappa) + \kappa q_0)\pi^4 \end{aligned}$$

$$\left(\frac{3x_1^2+4x_2^2}{2}+\alpha(2x_1\dot{x}_1+4x_2\dot{x}_2)\right)=0,$$
$$\ddot{x}_2+\frac{16}{3}\sqrt{\beta}(u_0+v)\dot{x}_1+16\alpha\pi^4\dot{x}_2 + 4\pi^2\left(4\pi^2-(u_0^2+2u_0v)+0.5\pi^2\left(\mu_0q_0^2+2\mu_0q_0q_u^*v\right)\right)x_2 + 2(\mu_0+\kappa)\pi^4\left(x_1^2x_2+4x_2^3+2\alpha(x_1\dot{x}_1x_2+4x_2^2\dot{x}_2)\right) + (\mu_0q_0+\mu_0(q_u^*v+q_\mu^*\kappa)+\kappa q_0)\pi^4(4x_1x_2+4\alpha\dot{x}_1x_2)=0, \tag{118}$$

where we have used the fact that $q_0^2+2\mu_0q_0q_\mu^*=0$ to simplify the derivation. Letting

$$z_1=x_1,\quad z_2=x_2,\quad z_3=\dot{x}_1,\quad z_4=\dot{x}_2,\quad z_5=v,\quad z_6=\kappa, \tag{119}$$

we can rewrite (118) as the first-order form. We note that the linear part of this extended system has two trivial eigenvalues because $\dot{z}_5=0$ and $\dot{z}_6=0$ are added to the extended system. Thus, we have a four-dimensional master subspace spanned by the eigenvectors corresponding to the two trivial eigenvalues and the pair of slowest decay eigenvalues associated with the buckled configuration. Then, we can use SSMTool [61] to perform the four-dimensional reduction, just as one did in [15]. In particular, we have $v\equiv p_3$ and $\kappa\equiv p_4$, and hence the expansion coefficients that are linear in p_3 and p_4 give the sensitivity we seek for.

E.4 Example 5.1.2

We present the spectrum of the linear part of (74) as a function of u in Fig. 13. We note that Hopf bifurcation occurs at $u=u_{\text{hb}}\approx 5.562$ and the pair of complex eigenvalues λ_5 and λ_6 is transformed into two real distinct eigenvalues at $u\approx 6.175$. Therefore, the system does not have real eigenvalues in the pre-flutter regime and the two real eigenvalues in the post-flutter regime are negative. Consequently, the resonance between $\lambda_{1,2}$ and real eigenvalues reported in [30] does not hold here.

Next, we take $u_0=5.4$ as the anchor point to perform reduction on parameter-dependent invariant manifold. In particular, we take the pair of modes associated with $\lambda_{1,2}$ as the master subspace of reduction. Thus, we perform reduction on parameter-dependent SSM. The obtained parametric ROM enables the prediction of limit cycle in the post-flutter regime, as seen in Fig. 14. Here, we gradually increase the truncation order in $\boldsymbol{\delta}$ and find that a cubic expansion in $\boldsymbol{\delta}$ is sufficient to yield converged solutions for $u_{\text{hb}}\le u<5.85$. In contrast, we can obtain converged solutions for $u_{\text{hb}}\le u<7$ when we choose $u_0=6.4$, as seen in Fig. 3. Therefore, one should take u_0 in the post-flutter regime to perform reduction if one aims at predicting limit cycle born out of Hopf bifurcation. This is consistent with our expectation because the Taylor expansion in $\boldsymbol{\delta}$ has a limited domain of convergence.

Now we increase the damping coefficient to $\alpha=0.01$ such that the system admits negative, real eigenvalues before Hopf bifurcation. Indeed, as seen in Fig. 15, the Hopf bifurcation occurs at $u=u_{\text{HB}}\approx 5.978$ and the transition of a pair of complex conjugate pair eigenvalues into real eigenvalues occurs at $u=u_{\text{C2R}}\approx 5.821$. Thus, we have two negative real eigenvalues between the two critical flow velocities, which suggests the accumulation of resonances when u approaches the Hopf bifurcation [30]. We note that $\text{Re}(\lambda_1)\sim O(0.1)$ and $\lambda_{3,4}\sim O(10)$ generally hold for $u\in(u_{\text{C2R}},u_{\text{HB}})$. Thus, the outer resonances accumulated at the Hopf bifurcation [30] will be at or higher than $O(100)$.

Since lower-order SSM expansion coefficients persists through the Hopf bifurcation [30], we can use parameter-dependent invariant manifold with lower-order truncation to perform model reduction through the bifurcation. This idea has been demonstrated in a data-driven setting via interpolation of lower-order expansion coefficients [30]. As mentioned in Sect. 5.1.2, we fix the expansion order in $\boldsymbol{p}$ to be 9 given it is sufficient. Thus, the corresponding lower-order Taylor expansion coefficients persist because the resonances are at the order of 100 or higher. We take $u_0\in(u_{\text{C2R}},u_{\text{HB}})$, perform parameter-dependent reduction and then predict the limit cycle oscillation in post-flutter regime. With $\alpha=0.01$ and $u_0=5.9$, we obtain the predicted results along with reference solutions from the collocation method in Fig. 16. We observe that the converged solutions of limit cycles are obtained for $u<6.3$, suggesting that the lower-order truncated ROM can indeed predict limit cycle in the post-flutter regime. We note that limited domain of convergence is not resulted from the resonances but indicates the fact that these lower-order expansion coefficients themselves have limited domain of analyticity.

F Reduced dynamics for underdamped master subspace

In this section, we present the explicit reduced dynamics on underdamped SSMs. Such explicit reduced dynamics enables us to extract backbone curves and limit cycles of autonomous systems. As for full systems subject to harmonic excitations, the explicit reduced dynamics transform forced periodic (quasi-periodic) orbits of full systems as fixed points (limit cycles) of the associated reduced-order models.

We consider the following M-dimensional *master* spectral subspace

$$\mathcal{E}=\text{Span}\{\mathbf{v}_1^{\mathcal{E}},\bar{\mathbf{v}}_1^{\mathcal{E}},\cdots,\mathbf{v}_{M/2}^{\mathcal{E}},\bar{\mathbf{v}}_{M/2}^{\mathcal{E}}\}, \tag{120}$$

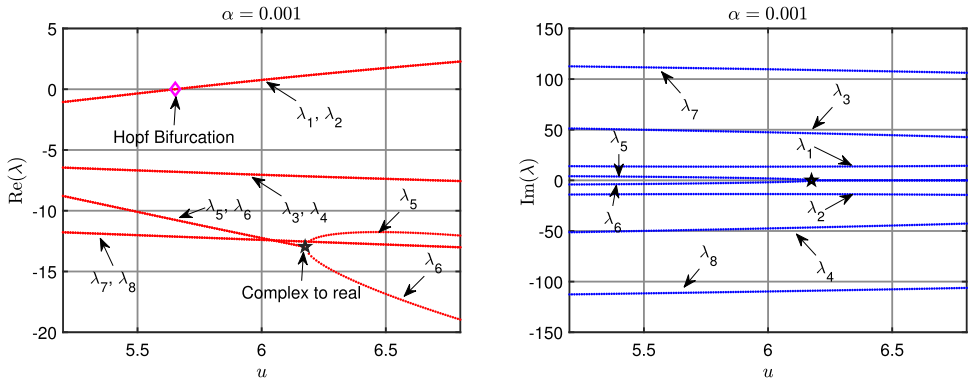

Fig. 13 Spectrum of the linear vibration of the cantilerved pipe (74) as a function of the flow velocity. Here, $\alpha = 0.001$ and $\beta = 0.2$. The magenta diamond marks Hopf bifurcation, and the black pentagram denotes the transition of a pair of complex eigenvalues into two real eigenvalues

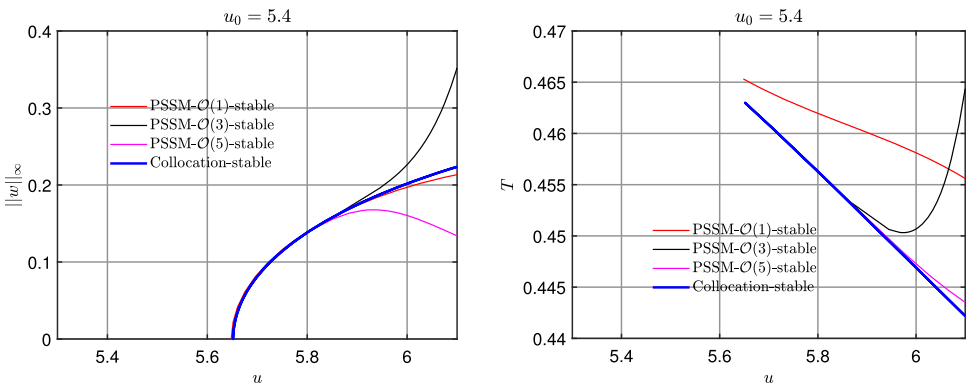

Fig. 14 Amplitude (left panel) and period (right panel) of limit cycle in the post-flutter region as functions of the flow velocity u. Here, we take $u_0 = 5.4$ in the pre-flutter regime as the nominal value to perform reduction. The damping coefficient $\alpha = 0.001$, which is the same as in Fig. 3

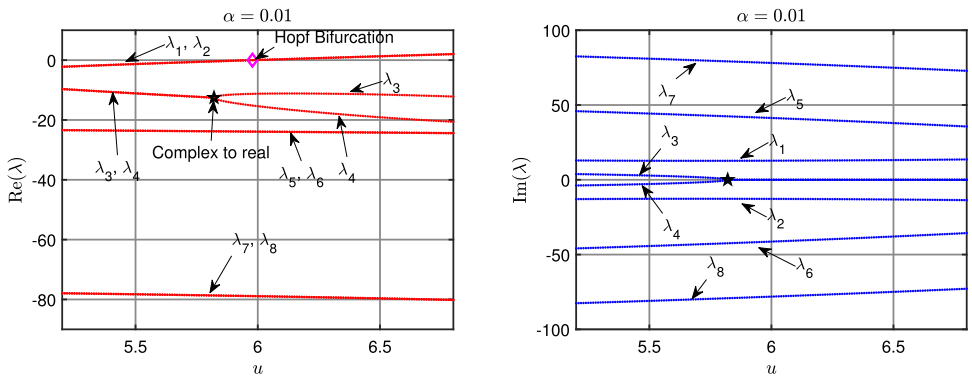

Fig. 15 Spectrum of the linear vibration of the cantilerved pipe (74) as a function of the flow velocity. Here, $\alpha = 0.01$ and $\beta = 0.2$. The magenta diamond marks Hopf bifurcation, and the black pentagram denotes the transition of a pair of complex eigenvalues into two real eigenvalues

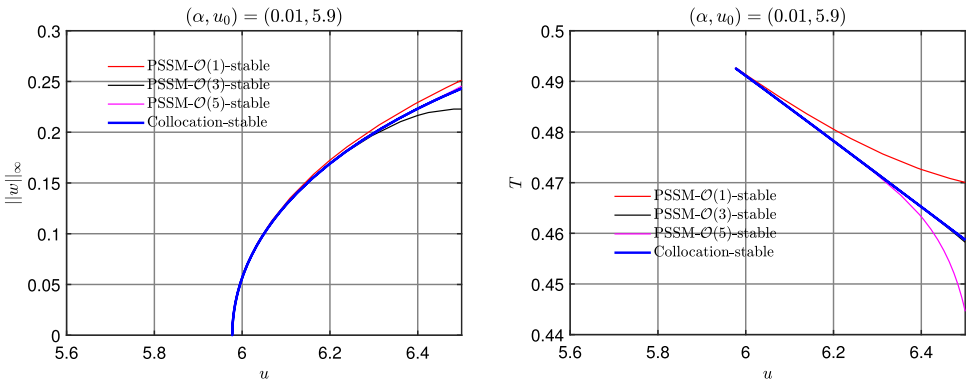

Fig. 16 Amplitude (left panel) and period (right panel) of limit cycle in the post-flutter region as functions of the flow velocity u. Here, $\alpha = 0.01$ and we take $u_0 = 5.9$ as the nominal value to perform reduction

and its spectrum is given as follows

$$\text{spect}(\mathcal{E}) = \{\lambda_1^{\mathcal{E}}, \bar{\lambda}_1^{\mathcal{E}}, \cdots, \lambda_{M/2}^{\mathcal{E}}, \bar{\lambda}_{M/2}^{\mathcal{E}}\} \tag{121}$$

with $\text{Im}(\lambda_j^{\mathcal{E}}) \neq 0$ for $j = 1, \cdots, M/2$. We expect the spectral subspace $\mathcal{E}$ to be composed of internally resonant modes of the system. In particular, we allow for the following type

of (near) *inner* resonances

$$\lambda_i^{\mathcal{E}} \approx \mathbf{m}_1 \cdot \lambda^{\mathcal{E}} + \mathbf{m}_2 \cdot \bar{\boldsymbol{\lambda}}^{\mathcal{E}}, \quad \bar{\lambda}_i^{\mathcal{E}} \approx \mathbf{m}_2 \cdot \lambda^{\mathcal{E}} + \mathbf{m}_1 \cdot \bar{\boldsymbol{\lambda}}^{\mathcal{E}} \quad (122)$$

for some $i \in \{1, \cdots, M/2\}$, where $\mathbf{m}_1, \mathbf{m}_2 \in \mathbb{N}_0^{M/2}$, $|\mathbf{m}_1 + \mathbf{m}_2| := \sum_{k=1}^{M/2}(m_{1,k} + m_{2,k}) \geq 1$, and

$$\boldsymbol{\lambda}^{\mathcal{E}} = (\lambda_1^{\mathcal{E}}, \cdots, \lambda_{M/2}^{\mathcal{E}}). \quad (123)$$

F.1 Autonomous dynamics

Now, let the autonomous part of the vector field of the reduced dynamics be arranged in complex conjugate blocks as follows

$$\mathbf{R}(\mathbf{p}.\boldsymbol{\mu}) = \begin{pmatrix} \mathbf{R}_1(\mathbf{p}, \boldsymbol{\delta}) \\ \vdots \\ \mathbf{R}_{M/2}(\mathbf{p}, \boldsymbol{\delta}) \end{pmatrix}, \quad (124)$$

where $\mathbf{R}_i(\mathbf{p}, \boldsymbol{\delta}) \in \mathbb{C}^2$ contains the complex conjugate components of the autonomous part of the vector field associated to the i-th pair of master mode $(\boldsymbol{v}_i^{\mathcal{E}}, \bar{\boldsymbol{v}}_i^{\mathcal{E}})$. Under the (near) inner resonances given by (122), we define a set containing the corresponding monomial multi-indices as

$$\mathcal{R}_i = \{(\boldsymbol{m}_1, \boldsymbol{m}_2) : \lambda_i^{\mathcal{E}} \approx \boldsymbol{m}_1 \cdot \boldsymbol{\lambda}^{\mathcal{E}} + \boldsymbol{m}_2 \cdot \bar{\boldsymbol{\lambda}}^{\mathcal{E}}\}. \quad (125)$$

We note that the parameterization coordinates $\mathbf{p}$ are $M/2$ pairs of complex conjugate coordinates, namely,

$$\mathbf{p} = (s_1, \bar{s}_1, \cdots, s_{M/2}, \bar{s}_{M/2}), \quad (126)$$

where s_i and $\bar{s}_i$ denote the parameterization coordinates corresponding to $\mathbf{v}_i^{\mathcal{E}}$ and $\bar{\mathbf{v}}_i^{\mathcal{E}}$, respectively. As a generalization of the results in [55], the normal-form-style parameterization of the autonomous reduced dynamics is given by

$$\mathbf{R}_i(\mathbf{p}, \boldsymbol{\delta}) = \sum_{(\mathbf{m}_1, \mathbf{m}_2) \in \mathcal{R}_i, \boldsymbol{\ell}} \begin{pmatrix} \gamma(\mathbf{m}_1, \mathbf{m}_2, \boldsymbol{l}) \mathbf{s}^{\mathbf{m}_1} \bar{\mathbf{s}}^{\mathbf{m}_2} \boldsymbol{\delta}^{\boldsymbol{\ell}} \\ \bar{\gamma}(\mathbf{m}_1, \mathbf{m}_2, \boldsymbol{\ell}) \mathbf{s}^{\mathbf{m}_2} \bar{\mathbf{s}}^{\boldsymbol{m}_1} \boldsymbol{\delta}^{\boldsymbol{\ell}} \end{pmatrix}. \quad (127)$$

We further follow the derivation in [55] to derive the above reduced dynamics in the form of polar coordinates. In particular, let

$$s_i = \rho_i e^{\mathrm{i}\vartheta_i}, \bar{s}_i = \rho_i e^{-\mathrm{i}\vartheta_i}, \quad (128)$$

the reduced dynamics in *polar* coordinates $(\boldsymbol{\rho}, \boldsymbol{\vartheta}) \in \mathbb{R}^{M/2} \times \mathbb{T}^{M/2}$ is given by

$$\begin{pmatrix} \dot{\rho}_i \\ \dot{\vartheta}_i \end{pmatrix} = \sum_{(\mathbf{m}_1, \mathbf{m}_2) \in \mathcal{R}_i, \boldsymbol{\ell}} \boldsymbol{\rho}^{\mathbf{m}_1 + \mathbf{m}_2} \boldsymbol{\delta}^{\boldsymbol{\ell}} \mathbf{Q}(\rho_i, \varphi_i(\mathbf{m}_1, \mathbf{m}_2)) \begin{pmatrix} \mathrm{Re}(\gamma(\mathbf{m}_1, \mathbf{m}_2, \boldsymbol{\ell})) \\ \mathrm{Im}(\gamma(\mathbf{m}_1, \mathbf{m}_2, \boldsymbol{\ell})) \end{pmatrix} \quad (129)$$

for $i = 1, \cdots, M/2$. Here,

$$\varphi_i(\mathbf{m}_1, \mathbf{m}_2) = \langle \mathbf{m}_1 - \mathbf{m}_2 - \mathbf{e}_i, \boldsymbol{\vartheta} \rangle,$$
$$\mathbf{Q}(\rho, \theta) = \begin{pmatrix} \cos\theta & -\sin\theta \\ \frac{1}{\rho}\sin\theta & \frac{1}{\rho}\cos\theta \end{pmatrix}, \quad (130)$$

where $\mathbf{e}_i \in \mathbb{R}^{M/2}$ is the unit vector aligned along the i-th axis

In the special case that $M = 2$, we have $m_1 = m_2 + 1$ and hence $\varphi_1(m_1, m_2) \equiv 0$. The reduced dynamics (129) becomes

$$\dot{\rho} = a(\rho) = \sum_{m_2 \geq 0, \boldsymbol{\ell}} \rho^{2m_2+1} \boldsymbol{\delta}^{\boldsymbol{\ell}} \mathrm{Re}(\gamma(m_2 + 1, m_2, \boldsymbol{\ell})), \quad (131)$$

$$\dot{\vartheta} = b(\rho) = \sum_{m_2 \geq 0, \boldsymbol{\ell}} \rho^{2m_2} \boldsymbol{\delta}^{\boldsymbol{\ell}} \mathrm{Im}(\gamma(m_2 + 1, m_2, \boldsymbol{\ell})). \quad (132)$$

It follows that we can extract parameter-dependent backbone curves from (132). In addition, a nonspurious fixed point ρ^* in the dynamics of ρ corresponds to a limit cycle of the full system. The period of the limit cycle is given as $T = 2\pi/b(\rho^*)$.

F.2 Leading-order non-autonomous dynamics

With the addition of harmonic forcing $\mathbf{F}^{\mathrm{ext}}(\Omega t)$, the reduced dynamics takes the form

$$\dot{\mathbf{p}} = \mathbf{R}(\mathbf{p}, \boldsymbol{\mu}) + \epsilon \mathbf{S}_0(\Omega t) + \mathcal{O}(\epsilon|\mathbf{p}|, \epsilon|\boldsymbol{\delta}|). \quad (133)$$

As in (124), we arrange the non-autonomous part of the vector field of reduced dynamics in complex conjugate blocks as follows [55]

$$\mathbf{S}_0(\Omega t) = \begin{pmatrix} \mathbf{S}_{0,1}(\Omega t) \\ \vdots \\ \mathbf{S}_{0,M/2}(\Omega t) \end{pmatrix}, \quad (134)$$

where $\mathbf{S}_{0,i}(\Omega t) \in \mathbb{C}^2$ contains the complex conjugate components of the leading-order non-autonomous part of the vector field associated with the i-th pair of master modes, $(\mathbf{v}_i^{\mathcal{E}}, \bar{\mathbf{v}}_i^{\mathcal{E}})$. Let

$$\mathbf{F}^{\mathrm{ext}}(\Omega t) = \mathbf{F}^{\mathrm{a}} e^{\mathrm{i}\Omega t} + \bar{\mathbf{F}}^{\mathrm{a}} e^{-\mathrm{i}\Omega t}, \quad (135)$$

where the forcing amplitude vector $\mathbf{F}^{\mathrm{a}} \in \mathbb{C}^{2n}$ with superscript 'a' stands for 'amplitude'. It follows that [55]

$$\mathbf{S}_{\mathbf{0},i}(\Omega t) = \begin{pmatrix} f_i e^{\mathrm{i}\Omega t} \\ \bar{f}_i e^{-\mathrm{i}\Omega t} \end{pmatrix}, \quad i = 1, \cdots, M/2, \quad (136)$$

with

$$f_i = \begin{cases} (\mathbf{u}_i^{\mathcal{E}})^* \mathbf{F}^{\mathrm{a}} & \text{if } \lambda_i^{\mathcal{E}} \approx \mathrm{i}\Omega \\ 0 & \text{otherwise} \end{cases}. \tag{137}$$

In polar coordinates, we let $\vartheta_i = \theta_i + r_i \Omega t$, i.e.,

$$s_i = \rho_i e^{\mathrm{i}(\theta_i + r_i \Omega t)}, \bar{s}_i = \rho_i e^{-\mathrm{i}(\theta_i + r \Omega t)}. \tag{138}$$

We follow the derivation in [55] to derive the vector field for (ρ_i, θ_i), yielding

$$\begin{pmatrix} \dot{\rho}_i \\ \dot{\theta}_i \end{pmatrix} = \begin{pmatrix} 0 \\ -r_i \Omega \end{pmatrix} + \sum_{(\mathbf{m}_1, \mathbf{m}_2) \in \mathcal{R}_i, \boldsymbol{\ell}} \boldsymbol{\rho}^{\mathbf{m}_1 + \mathbf{m}_2} \boldsymbol{\delta}^{\boldsymbol{\ell}} \mathbf{Q}(\rho_i, \varphi_i(\mathbf{m}_1, \mathbf{m}_2)) \begin{pmatrix} \mathrm{Re}(\gamma(\mathbf{m}_1, \mathbf{m}_2, \boldsymbol{\ell})) \\ \mathrm{Im}(\gamma(\mathbf{m}_1, \mathbf{m}_2, \boldsymbol{\ell})) \end{pmatrix} + \epsilon \mathbf{Q}(\rho_i, -\theta_i) \begin{pmatrix} \mathrm{Re}(f_i) \\ \mathrm{Im}(f_i) \end{pmatrix}. \tag{139}$$

Due to the transformation (138), a fixed point of (139) corresponds to a forced periodic orbit of the full system. It follows that we can infer bifurcation of periodic orbits of the full system via that of the fixed points of (139) [55]. Moreover, the limit cycle of (139) gives a two-dimensional torus on which the quasi-periodic orbit of the full system stays [55]. We use parameter continuation in the extended parameter space $(\epsilon, \Omega, \boldsymbol{\delta})$ to investigate the forced response and its bifurcations. In particular, we use a publicly available package, COCO [52–54] to perform the parameter continuation.

Acknowledgements The authors are grateful to the anonymous reviewers of this manuscript for their careful reading and insightful comments, which significantly improved the quality of the manuscript. ML acknowledges financial support from National Natural Science Foundation of China (No. 12572010).

Author Contributions SJ conceptualized the research, developed the mathematical expressions and computational tools, and led the writing of the manuscript. ML supported the conceptualization, contributed to the development of the corresponding sections of the manuscript. Both authors reviewed and edited the manuscript, and approved its final draft.

Funding ML was supported by National Natural Science Foundation of China (No. 12572010).

Data Availability The results and analysis are based on the governing equations and not on any datasets. The numerical examples presented in this work are openly available in the SSMTool repository [54]. The numerical parameters and the algorithms used to generate the results are included in the manuscript. A software implementation of these algorithms will be made available upon publication.

Declarations

Conflict of interest The authors declare no conflict of interest.

References

1. Carini, M., Auteri, F., Giannetti, F.: Centre-manifold reduction of bifurcating flows. J. Fluid Mech. **767**, 109–145 (2015)
2. Jain, S., Haller, G.: How to compute invariant manifolds and their reduced dynamics in high-dimensional finite element models. Nonlinear Dyn. **107**(2), 1417–1450 (2022)
3. Vizzaccaro, A., Gobat, G., Frangi, A., Touzé, C.: Direct parametrisation of invariant manifolds for non-autonomous forced systems including superharmonic resonances. Nonlinear Dyn. **112**(8), 6255–6290 (2024)
4. Li, M., Thurnher, T., Xu, Z., Jain, S.: Data-free non-intrusive model reduction for nonlinear finite element models via spectral submanifolds. Comput. Methods Appl. Mech. Eng. **434**, 117590 (2025)
5. Pozzi, M., Marconi, J., Jain, S., Braghin, F.: Backbone curve tailoring via lyapunov subcenter manifold optimization. Nonlinear Dyn. **112**, 15719–15739 (2024)
6. Pozzi, M., Marconi, J., Jain, S., Li, M., Braghin, F.: Topology optimization of nonlinear structural dynamics with invariant manifold-based reduced order models. Struct. Multidiscip. Optim. **68**, 72 (2025)
7. Liang, H., Pozzi, M., Marconi, J., Jain, S., Li, M.: Topology optimization of nonlinear forced response curves via reduction on spectral submanifolds. Nonlinear Dyn. **114**, 713 (2026)
8. Li, M.: Explicit sensitivity analysis of spectral submanifolds of mechanical systems. Nonlinear Dyn. **112**, 16733–16770 (2024)
9. Pozzi, M., Marconi, J., Jain, S., Li, M., Braghin, F.: Adjoint sensitivities for the optimization of nonlinear structural dynamics via spectral submanifolds. Proc. R. Soc. A: Math. Phys. Eng. Sci. **481**(2328), 20250244 (2025)
10. Ponsioen, S., Jain, S., Haller, G.: Model reduction to spectral submanifolds and forced-response calculation in high-dimensional mechanical systems. J. Sound Vib. **488**, 115640 (2020)
11. Thurnher, T., Haller, G., Jain, S.: Nonautonomous spectral submanifolds for model reduction of nonlinear mechanical systems under parametric resonance. Chaos Interdiscip. J. Nonlinear Sci. **34**(7), 073145 (2024)
12. Guckenheimer, J., Holmes, P.: Nonlinear Oscillations, Dynamical Systems, and Bifurcations of Vector Fields. Applied Mathematical Sciences, vol. 42. Springer, New York (1983)
13. Kelley, A.: The stable, center-stable, center, center-unstable, unstable manifolds. J. Differ. Equ. **3**(4), 546–570 (1967)
14. Haller, G., Ponsioen, S.: Nonlinear normal modes and spectral submanifolds: existence, uniqueness and use in model reduction. Nonlinear Dyn. **86**(3), 1493–1534 (2016)
15. Li, M., Wang, L.: Parametric model reduction for a cantilevered pipe conveying fluid via parameter-dependent center and unstable manifolds. Int. J. Non-Linear Mech. **160**, 104629 (2024)
16. Irwin, M.C.: On the stable manifold theorem. Bull. Lond. Math. Soc. **2**, 196–198 (1970)
17. Hirsch, M.W., Pugh, C.C., Shub, M.: Invariant Manifolds. Lecture Notes in Mathematics, vol. 583. Springer, Berlin (1977)
18. Irwin, M.C.: A new proof of the pseudostable manifold theorem. J. Lond. Math. Soc. **s2–21**, 557–566 (1980)

19. de la Llave, R., Wayne, C.E.: On irwin's proof of the pseudostable manifold theorem. Math. Z. **219**, 301–321 (1995)
20. Kelley, A.: Analytic two-dimensional subcenter manifolds for systems with an integral. Pac. J. Math. **29**(2), 335–350 (1969)
21. Cabré, X., Fontich, E., de la Llave, R.: The parameterization method for invariant manifolds I: manifolds associated to non-resonant subspaces. Indiana Univ. Math. J. **52**(2), 283–328 (2003)
22. Cabré, X., Fontich, E., de la Llave, R.: The parameterization method for invariant manifolds II: regularity with respect to parameters. Indiana Univ. Math. J. **52**(2), 329–360 (2003)
23. Cabré, X., Fontich, E., de la Llave, R.: The parameterization method for invariant manifolds III: overview and applications. J. Differ. Equ. **218**(2), 444–515 (2005)
24. Castelli, R., Lessard, J.-P., Mireles James, J.D.: Parameterization of invariant manifolds for periodic orbits I: efficient numerics via the floquet normal form. SIAM J. Appl. Dyn. Syst. **14**(1), 132–167 (2015)
25. Haro, A., Canadell, M., Figueras, J.-L., Luque, A., Mondelo, J.-M.: The Parameterization Method for Invariant Manifolds: From Rigorous Results to Effective Computations. Applied Mathematical Sciences, vol. 195. Springer, Berlin (2016)
26. Haller, G., Kaszás, B., Liu, A., Axas, J.: Nonlinear model reduction to fractional and mixed-mode spectral submanifolds. Chaos Interdiscip. J. Nonlinear Sci. **33**(6), 063138 (2023)
27. Haller, G.: Modeling Nonlinear Dynamics from Equations and Data—with Applications to Solids, Fluids, and Controls. Society for Industrial and Applied Mathematics (2025)
28. Morsy, A.A., Tiso, P.: Model reduction for systems with random parameters using spectral submanifolds. Nonlinear Dyn. **113**, 24141–24157 (2025)
29. Abbasciano, G., Endresz, B., Stepan, G., Haller, G.: Data-driven modeling of global bifurcations and chaos in a mechanical system under delayed and quantized control. J. Sound Vib. **628**, 119660 (2026)
30. King, J., Kaszás, B., Buza, G., Jussiau, W., Haller, G.: Parametric spectral submanifolds across hopf bifurcations with applications to fluid dynamics (Submitted to Chaos) (2026). arXiv:2603.19079v2
31. Habib, G., Cenedese, M., Rega, G.: Spectral submanifold reduction of high dimensional nonlinear systems for dynamical integrity analysis. Nonlinear Dyn. **113**, 28983–29005 (2025)
32. Shaw, S., Pierre, C.: Normal modes for non-linear vibratory systems. J. Sound Vib. **164**, 85–124 (1993)
33. Shaw, S.W., Pierre, C., Pesheck, E.: Modal analysis-based reduced-order models for nonlinear structures-an invariant manifold approach. Shock Vib. Dig. **31**, 3–16 (1999)
34. Jain, S., Marconi, J., Tiso, P.: YetAnotherFECode v1.1.1 (2020)
35. Murdock, J.: Normal Forms and Unfoldings for Local Dynamical Systems. Springer Monographs in Mathematics, Springer, New York (2003)
36. Cenedese, M., Axas, J., Bauerlein, B., Avila, K., Haller, G.: Data-driven modeling and prediction of non-linearizable dynamics via spectral submanifolds. Nat. Commun. **13**, 872 (2022)
37. Haller, G., Kaundinya, R.: Nonlinear model reduction to temporally aperiodic spectral submanifolds. Chaos Interdiscip. J. Nonlinear Sci. **34**, 4 (2024)
38. Breunung, T., Haller, G.: Explicit backbone curves from spectral submanifolds of forced-damped nonlinear mechanical systems. Proc. R. Soc. A Math. Phys. Eng. Sci. **474**(2213), 20180083 (2018)
39. Jiang, D., Pierre, C., Shaw, S.W.: Nonlinear normal modes for vibratory systems under harmonic excitation. J. Sound Vib. **288**(4–5), 791–812 (2005)
40. Muravyov, A.A., Rizzi, S.A.: Determination of nonlinear stiffness with application to random vibration of geometrically nonlinear structures. Comput. Struct. **81**, 1513–1523 (2003)
41. Mahdiabadi, M.K., Tiso, P., Brandt, A., Rixen, D.J.: A non-intrusive model-order reduction of geometrically nonlinear structural dynamics using modal derivatives. Mech. Syst. Signal Process. **147**, 107126 (2021)
42. Lin, J., Wang, X., Wainwright, B., Mignolet, M.P.: Improved identification of stiffness coefficients of non intrusive nonlinear geometric reduced order models of structures. Int. J. Non-Linear Mech. **152**, 104380 (2023)
43. Amsallem, D., Farhat, C.: Interpolation method for adapting reduced-order models and application to aeroelasticity. AIAA J. **46**, 1803–1813 (2008)
44. Hajisharifi, A., Romano, F., Girfoglio, M., Beccari, A., Bonanni, D., Rozza, G.: A non-intrusive data-driven reduced order model for parametrized cfd-dem numerical simulations. J. Comput. Phys. **491**, 112355 (2023)
45. Hesthaven, J., Ubbiali, S.: Non-intrusive reduced order modeling of nonlinear problems using neural networks. J. Comput. Phys. **363**, 55–78 (2018)
46. Oulghelou, M., Allery, C.: Non intrusive method for parametric model order reduction using a bi-calibrated interpolation on the grassmann manifold. J. Comput. Phys. **426**, 109924 (2021)
47. Kaszas, B., Cenedese, M., Haller, G.: Dynamics-based machine learning of transitions in couette flow. Phys. Rev. Fluids **7**, L082402 (2022)
48. Cenedese, M., Marconi, J., Haller, G., Jain, S.: Data-assisted non-intrusive model reduction for forced nonlinear finite elements models. Nonlinear Dyn. **113**, 6465–6489 (2025)
49. Morsy, A.A., Xu, Z., Tiso, P., Haller, G.: Data-driven reduction of the finite-element model of a tribomechadynamics benchmark problem. Nonlinear Dyn. **113**, 24539–24555 (2025)
50. Li, M., Yan, H., Wang, L.: Data-driven model reduction for pipes conveying fluid via spectral submanifolds. Int. J. Mech. Sci. **277**, 109414 (2024)
51. Li, M., Yan, H., Wang, L.: Nonlinear model reduction for a cantilevered pipe conveying fluid: a system with asymmetric damping and stiffness matrices. Mech. Syst. Signal Process. **188**, 109993 (2023)
52. Dankowicz, H., Schilder, F.: Recipes for Continuation. Society for Industrial and Applied Mathematics (2013)
53. Schilder, F., Dankowicz, H., Li, M.: Continuation core and toolboxes (COCO) (2025). https://sourceforge.net/projects/cocotools. Accessed 18 Feb 2025
54. Ahsan, Z., Dankowicz, H., Li, M., Sieber, J.: Methods of continuation and their implementation in the COCO software platform with application to delay differential equations. Nonlinear Dyn. **107**(4), 3181–3243 (2022)
55. Li, M., Jain, S., Haller, G.: Nonlinear analysis of harmonically excited mechanical systems with internal resonance using spectral submanifolds, part i: periodic response and forced response curves. Nonlinear Dyn. **110**(2), 1005–1043 (2022)
56. Li, M., Jain, S., Haller, G.: Nonlinear analysis of forced mechanical systems with internal resonance using spectral submanifolds, part II: bifurcation and quasi-periodic response. Nonlinear Dyn. **110**(2), 1045–1083 (2022)
57. Liang, H., Jain, S., Li, M.: Bifurcation analysis of quasi-periodic orbits of mechanical systems with 1:2 internal resonance via spectral submanifolds. Nonlinear Dyn. **113**(11), 12609–12640 (2025)
58. Ehrhardt, D.A., Allen, M.S., Beberniss, T.J., Neild, S.A.: Finite element model calibration of a nonlinear perforated plate. J. Sound Vib. **392**, 280–294 (2017)
59. Li, M., Dankowicz, H.: A COCO-based shooting toolbox for dynamical systems (2021). https://github.com/mingwu-li/forward. Accessed 1 Sept 2024

60. Newmark, N.M.: A method of computation for structural dynamics. ASCE J. Eng. Mech. Div. **85**(3), 67–94 (1959)
61. Jain, S., Li, M., Thurnher, T., Haller, G.: SSMTool 2.6: computation of invariant manifolds in high-dimensional mechanics problems (2024). https://doi.org/10.5281/zenodo.13909795
62. Greub, W.: Multilinear Algebra. Springer, New York (1978)